SEDIMENTOLOGY, SEQUENCE STRATIGRAPHY, CHEMOSTRATIGRAPHY, AND DIAGENESIS OF THE CYRENAICAN MIOCENE, AL-JABAL AL-KHDAR UPLIFT AND SOLUQ TROUGH, NE LIBYA

A Dissertation

by

KHALED SALEH AMROUNI

Submitted to the Office of Graduate and Professional Studies of
Texas A&M University
in partial fulfilment of the requirements for the degree of

DOCTOR OF PHILOSOPHY

Chair of Committee,	Michael C. Pope
Committee Members,	Ernest A. Mancini
	Yuefeng Sun
	Debbie Thomas
Head of Department,	Rick Giardino

August 2015

Major Subject: Geology

ABSTRACT

This study established the sequence stratigraphic framework of the Cyrenaican Miocene through the integration of the sedimentology, stratigraphy, gamma-ray logs, chemostratigraphy, and diagenesis. Carbon-isotope curves and gamma-ray logs with sedimentologically described measured stratigraphic rock sections of the Ar-Rajmah Group were implemented to define facies depositional models and their sequence stratigraphic patterns within a high resolution timeframe.

The Ar-Rajmah Group of the Cyrenaican Miocene includes the Benghazi Formation and Wadi-al-Qattarah in the Al-Jabal al-Khdar north, and its equivalent Msus and Sceleidima formations in the Soluq Trough south. The Cyrenaican Miocene is made up of two 2nd-oreder sequences (SS1-SS2) that includes six 3rd-order sequences (S1-S6), and at least 20 parasequences.

The 3rd-order sequences S1 and S2 represent the Early Miocene and are dominated by open marine bioclastic packstone and red algal packstone facies. The Early Miocene SS1 is separated from the Middle and Late Miocene SS2 by a major unconformity surface. The Middle Miocene is represented by the 3rd-order sequence S3 that dominated a mixture of oolitic grainstone, microbialites, and bioclastic packstone, red algal packstone, with evaPorites, sandstone and green shale. The 3rd-order sequences S4-S6 represent that Late Miocene sequences and dominated by oolitic grainstone, microbialites, with evaPorites and some bioclastic packstone and red algal packstone facies.

The correlation between the Cyrenaican stratigraphic record and the regional Mediterranean and global Miocene isotope records, and global sea level curve indicates that the 3rd-order depositional sequences of the Cyrenaican platform were affected by a tectonic signature besides the eustatic sea level fluctuations. The Cyrenaican Miocene sea level curve does not show a great similarity with the global sea level curve due to the tectonic influence.

Microscopic analysis, stable isotope data, and trace elements were implemented to define the diagenetic events. Cross-cutting relationships were applied to define the paragenetic sequence of the diagenetic events within the stratigraphic framework of the Cyrenaican Miocene succession. The Ar-Rajmah Group carbonate rocks were affected by 18 diagenetic events caused by six diagenetic processes including the meteoric water diagenesis.

DEDICATION

To my late father, to my family, and to you.

ACKNOWLEDGMENTS

This PhD work has been done under the supervision of Dr. Mike Pope. I gratefully acknowledge my committee chair, Dr. Michael Pope, and my committee members Dr. Earnest Mancicni, Dr. Yuefeng Sun, and Dr. Debbie Thomas for their guidance and support throughout the course of the study.

My sincere gratitude and deep thanks must go to my family for their unlimited logistic and financial support for my field work, and throughout the course of my study. I would like to express my gratitude Prof. Ali A. El-Arnauti and Prof. Ahmed S. El-Hawat for their support and advice as knowledgeable local experts in the geology of Cyrenaican.

My thanks extend to Dr. Saad El-Ebaidi the chairman of the Earth Sciences Department, Garyounis University, and to the Lab personnel of the Arab Gulf Oil Company (AGOCO) for their support. Thanks are due to my previous students at Garyounis University for their field assistance. Finally, I would like to record my gratitude to everyone who helped during the preparation of this work.

TABLES OF CONTENTS

Page

ABSTRACT ii

DEDICATION iv

ACKNOWLEDGMENTS v

TABLES OF CONTENTS vi

LIST OF FIGURES x

LIST OF TABLES xvi

CHAPTER I INTRODUCTION 1

CHAPTER II SEDIMENTOLOGY AND SEQUENCE STRATIGRAPHY OF THE CYRENAICAN MIOCENE STRATA, Al-JABAL Al-KHDAR UPLIFT AND SOLUQ TROUGH, NE LIBYA 4

- Overview 4
- Introduction 5
- Geological Setting 6
- Methods 14
- Results 16
  - Depositional Facies of the Cyrenaican Miocene Ar-Rajmah Group 16
    - Peritidal facies 16
      - Evaporite 16
      - Microbialite 23
      - Pelletal wackestone/packstone 24
      - Bioclastic Porites reefs 24
      - Quartz sandstone facies 25
      - Green shale 25
    - Ramp crest facies 26
      - Oolitic grainstone 26
    - Shallow subtidal facies 26

Bioclastic mudstone /packstone 26
Reworked bioclastic packstone 27
Coralline red algal reefs 28
Reworked red algae 28
Sequence Stratigraphy of the Cyrenaican Miocene Ar-Rajmah Group 29
3rd-order sequence S1 36
3rd-order sequence S2 36
3rd-order sequence S3 37
3rd-order sequence S4 39
3rd-order sequence S5 40
3rd-order sequence S6 40
Palaeocurrents Data Analysis of the Cyrenaican Miocene Ar-Rajmah Group 41
Discussion 46
Stratigraphic Chart and Chemostratigraphic Constrains on the Cyrenaican Miocene 46
Depositional Model and Shoreline Progradation of the Cyrenaican Miocene Ar-Rajmah Group 48
The Depositional Models of the Mediterranean Region 51
Miocene Sequence Stratigraphic Framework of the Mediterranean Region, 2nd-Order Sequences 51
Miocene Sequence Stratigraphic Framework of the Cyrenaican Ar-Rajmah Group, Regionally Correlative 2nd -and 3rd-Order Sequences 54
Paleogeographic maps with palaeocurrents analysis of the Cyrenaican Miocene Ar-Rajmah Group 57
The Miocene palaeography of the Mediterranean region 57
Paleoclimate of the Cyrenaican Miocene Ar-Rajmah Group 58
The Miocene Paleoclimate of the Mediterranean Region 58
Conclusions 60
CHAPTER III STABLE ISOTOPE CHEMOSTRATIGRAPHY OF THE CYRENAICAN MIOCENE AR-RAJMAH GROUP, AL-JABAL AL-KHDAR UPLIFT AND SOLUQ TROUGH, NE LIBYA 61
Overview 61
Introduction 63

Geological Setting 64
Methods/Data 71
Results 73
Depositional Facies of the Cyrenaican Miocene Ar-Rajmah Group 73
Peritidal facies 73
Evaporite 73
Microbialite 77
Pelletal wackestone/packstone 78
Bioclastic Porites reefs 78
Quartz sandstone 79
Green Shale 79
Ramp crest facies 80
Oolitic grainstone 80
Shallow subtidal facies 80
Bioclastic mudstone /packstone 80
Re-worked bioclastic packstone/grainstone 81
Coralline red algal reefs 82
Re-worked red algae 82
Sequence Stratigraphy 82
Carbon and Oxygen Isotopes 85
Carbon Isotope Record 89
Discussion 90
Ramp Geometry 90
Climate 90
The global Miocene paleoclimate 90
The Mediterranean region Miocene paleoclimate 91
The Cyrenaican Ar-Rajmah Group Miocene paleoclimate 93
Cyrenaican Stable Isotope Patterns, Interpretations, and Comparison with Regional and Global Coevals 94
Isotopes and Depositional Facies 96
Isotope Correlation and Relative Sea-Level Changes 96
Cyrenaican Miocene events 99
Conclusions 100

CHAPTER IV SEQUENCE STRATIGRAPHY AND DIAGENESIS IN THE CYRENAICAN MIOCENE CARBONATE SUCCESSIONS, AL-JABAL AL-KHDAR UPLIFT AND SOLUQ TROUGH, NR LIBYA 102

Overview 102
Introduction 103
Geological Setting 105
Methods/Data 108
Results 109
Discussion 127
Conclusions 132

CHAPTER V CONCLUSIONS 134

REFERENCES 137

APPENDIX 156

LIST OF FIGURES

Page

Figure 1. (A) Location map of the study area in northeastern Libya. (B) Landsat image of NE Libya showing the geological boundaries of Cretaceous- Tertiary rocks. The geological boundaries are based on the IRCs sheet-Benghazi (Klen, 1974) and sheet-Soluq (Francis and Issawi, 1977) that were later modified by (El-Hawat et al., 1987). 8

Figure 2. Land-sat false-colored TM© image of the main tectonic provinces of Cyrenaica: Al-Jabal Al-Khdar Uplift; Cyrenaica Platform, Soluq Trough and Marmarica Trough (From El-Hawat, 2007). 9

Figure 3. Part of the surface stratigraphy chart of Cyrenaica (El-Hawat and Abdulsamad, 2004). The Miocene units of the proposed study are outlined in yellow. 12

Figure 4. Stratigraphic correlation chart of Cyrenaican Miocene units, a Middle Miocene age was thought for the entire sequence of Ar-Rajmah Group (modified by Amrouni K.S. from El-Hawat and Salem, 1987). Then, it was thought to be Middle and Late Miocene (El-Hawat and Abdulsamad, 2004). Now, Abdulsamad and El Zanati (2013) published a palaeontology based paper supports the presence of the whole Miocene section in the Soluq Trough area in Cyrenaica. This study has chemostratigraphy constrains supports the presence of the whole Miocene in the Cyrenaica in both the Al-Jabal Al-Khdar area and the Soluq Trough area. 13

Figure 5. Outcrops of the Peritidal Facies of the Cyrenaican Miocene: (A) Yellow Swallow tail selentic gypsum, (B) Microbial stromatolites, (C) White, very thick Pelletal wackestone to packstone, (D) White branched bioclastic Porites coral reefs, (E) Friable green shale, laminated at base, and (F) Whitish yellow friable fine to very fine quartz sandstone. 18

Figure 6. Thin sections of the Peritidal Facies of the Cyrenaican Miocene:(A) Chevron structure of yellow Swallow tail selentic

gypsum, (B) Microbial stromatolites of domal and laterally linked lamina, notice the angular silty size quartz grains (C) Pelletal wackestone to packstone, (D) branched bioclastic Porites coral reefs in a pelletal packstone background, (E) Friable green shale with gypsum crystals at base, and (F) friable fine to very fine quartz sandstone, the quartz grains are polycrystalline with some green shale matrix. 19

Figure 7. Outcrops of the Ramp Crest-Subtidal Facies of the Cyrenaican Miocene: (A) Oolitic grainstone unidirectional clinoforms, (B) Oolitic grainstone coarsening upwards into fenestral oolitic grapestone, (C) echinoid-rich bioclastic packstone, (D) Reworked marly bioclastic packstone, (E) Red algal packstone, and (F) Reworked red algal packstone.....21

Figure 8. Thin sections of the Ramp Crest-Subtidal Facies of the Cyrenaican Miocene: (A) Partially leached concentric oolitic grainstone, (B) oolitic grainstone mixed with oolitic grapestone, (C) Bioclastic packstone enriched in gastropods, bivalves, and forams, (D) Reworked marly bioclastic wackestone, (E) Red algal packstone, and (F) Reworked red algal packstone. 22

Figure 9. Ideal type section in the sequence stratigraphic context of the Cyrenaican Miocene carbonate platform, Ar-Rajmah Group: Stratigraphic log section F1, G-Ray profile, formations and sequence stratigraphic annotations. 30

Figure 10. Sequence stratigraphic framework of the Cyrenaican Miocene carbonate platform, Ar-Rajmah Group: inverted red triangles refer to the locations of the stratigraphic log section, G-Ray profile are thin black curves, Carbon stable isotope profiles are thick red curves, formations names, and sequence stratigraphic annotations. (modified from Amrouni et. al., 2013). 31

Figure 11. Wheeler chronostratigraphic diagram of the Cyrenaican Miocene carbonate platform, Ar-Rajmah Group. 32

Figure 12. Annotated field photographs for the Cyrenaican Miocene Carbonate Platform surfaces: (A) Maximum flooding surface (mfs), (B and C) The unconformity surface between the older 2nd - order supersequence (Early Miocene) and the younger 2nd-order

supersequence (Middle and Late Miocene), (D and E) the unconformity surface of around 35Ma duration between the Eocene and the Miocene. 33

Figure 13. The Cyrenaican sequences shoreline aggradation /progradation curve throughout the Miocene time. 34

Figure 14. Palaeocurrents data analysis of the Cyrenaican Miocene carbonate platform, Ar-Rajmah Group. 42

Figure 15. Evolutionary depositional model of the Cyrenaican Miocene carbonate platform, Ar-Rajmah Group. 49

Figure 16. Depositional facies paleogeography and palaeocurrents of the Cyrenaican Miocene carbonate ramp, Ar-Rajmah Group. 50

Figure 17. (A) Location map of the study area in northeastern Libya. (B) Landsat image of NE Libya showing the geological boundaries of Cretaceous- Tertiary rocks. The geological boundaries are based on the IRCs sheet-Benghazi (Klen, 1974) and sheet-Soluq (Francis and Issawi, 1977) that were later modified by (El-Hawat et al., 1987). Measured sections are shown by colored bars, the yellow colored bars represent sections sampled for chemostratigraphy. 62

Figure 18. Sequence Stratigraphic framework of the Miocene, Ar-Rajmah Group, Cyrenaica, NE Libya (Amrouni et al., 2013). The locations of measured sections are marked at the top by inverted triangles. The blue triangles indicate sections sampled for chemostratigraphy .Thin black curves are gamma ray, and the thick red curves are carbon isotopes curves. 65

Figure 19. Chemostratigraphic correlation between carbon stable isotope curves of the Cyrenaican Miocene carbonate sequence, Ar-Rajmah Group. 66

Figure 20. Chemostratigraphic comparison between the Ar-Rajmah Group Cyrenaican Miocene and the global carbon curves, besides the comparison between the Ar-Rajmah Cyrenaican Miocene and the global and sea level. Global events listed in this figure are

defined in (A) Zachos et al. (2001), (B) John et al. (2003), (C) Halfar and Mutti (2005), and (D) Vincent and Berger (1985). 67

Figure 21. Comparison between the Ar-Rajmah Group Cyrenaican, Mediterranean, Indian Ocean, and the global carbon Miocene curves. 68

Figure 22. Simplified 2D evolutionary depositional models of the Miocene Cyrenaican carbonate platform, Ar-Rajmah Group, NE Libya.....75

Figure 23. Age based oxygen and carbon cross-plot of the Cyrenaican Miocene carbonate platform, Ar-Rajmah group, NE Libya.....87

Figure 24. Facies based oxygen and carbon cross-plot of the Cyrenaican Miocene carbonate platform, Ar-Rajmah group, NE Libya.....88

Figure 25. (A) Location map of the study area in northeastern Libya. (B) Landsat image of NE Libya showing the geological boundaries of Cretaceous- Tertiary rocks. The geological boundaries are based on the IRCs sheet-Benghazi (Klen, 1974) and sheet-Soluq (Franci Francis and Issawi, 1977) that were later modified by (El-Hawat et al., 1987).....104

Figure 26. Paragenetic sequence of the Ar-Rajmah Group carbonate platform, Cyrenaica, NE Libya. 110

Figure 27. Photomicrographs of the micritization (A) Micrite envelopes around the forma fossils in pelletal-bioclastic grainstone, (f) forams and (p) pellets. (B) Micritized grains in red algal facie, (r) red algae fragments. 112

Figure 28. Photomicrographs of symmetrical asymmetrical rim cements. (A) Fibrous symmetrical rim cement in bioclastic grainstone facies. (B) Dogtooth symmetrical rim cement in oolitic grainstone facies.....113

Figure 29. Photomicrographs of asymmetrical rim cements. (A) Meniscus asymmetrical rim cement in oolitic grainstone facies. (B) Gravity/Pendant asymmetrical rim cement in bioclastic facies. 114

Figure 30. Photomicrographs of the pore-filling cements. (A) Intergranular pore fill cement in oolitic grainstone facie. (B) Drusy and blocky cement in red algal facies.....115

Figure 31. Photomicrographs of the dolomite and silica fracture fill cements and Thick crust cements. (A) Dolomite cement filled vertical fracture and silica cement filled the horizontal fracture. (B) Thick cement layer show on the left side crust cement and on the right side a combination of fan-shape and botryoid cements in red algal facies, (c) crust cement, (f) fan shape cement, and (b) botryoid cement.....116

Figure 32. Photomicrographs of the secondary diagenetic pores. (A) Intercrystalline porosity in red algal facies. (B) Dolomoldic porosity in red algal facies. 117

Figure 33. Photomicrographs of the secondary diagenetic pores. (A) Oomoldic porosity and geopetal dissolution structure in oolitic grainstone facies. (B) Biomoldic porosity bioclastic grainstone facies.....118

Figure 34. Photomicrographs of the secondary diagenetic pores. (A) Channel Porosity in red algal facies. (B) Vuggy porosity in red algal facies.....119

Figure 35. Photomicrographs of the recrystallization and 1st compaction phase. (A) Recrystallization of the mud matrix caused crystals growth in microbialite facies. (B) 1st Phase fractures were filled with microcrystalline quartz that was later leached at some places in oolitic grainstone facies. Later pores were filled with botryoid chalcedony.....120

Figure 36. Photomicrographs of the compaction types. (A) 2nd phase fractures are open and free of cement in red algal facies. (B) Dissolution seams in microbial facies occur due to chemical compaction and always associated with fractures.....121

Figure 37. Photomicrographs of the diagenetic replacement events. (A) Mixed Type-1 subhedral medium size mosaic dolomite and Type-2 coarse mosaic, cloudy core and clear rim dolomite in red algal

facies. (B) Type-2 coarse mosaic clear rim dolomite in red algal facies.....123

Figure 38. Photomicrographs of the diagenetic replacement events. (A) Type-3 coarse clear crystals dolomite in red algal facies. (B) Dedolomitization when dolomite replaced by calcite in red algal facies.....124

Figure 39. Photomicrographs of the diagenetic replacement events. (A) Quartz-rich thrombolite replaced by gypsum then by silica. (B) Gypsum crystal replaced by silica in siliciclastic facies. 125

Figure 40. Measured field section A1, two 2nd-order supersequences, six 3rd-order sequences, total Gamma Ray profile, Si wt% , Mg wt%, Mn wt%, and porosity% curves, and dolomite types plotted as columns. The time lines are delineated based on the $\delta^{18}O$ and δ13C stable isotopes correlation, the 2nd-order supersequence boundary is the denoted as S.B, and the maximum flooding zone is denoted as M.F.Z. 126

LIST OF TABLES

Page

Table 1. Peritidal Cyrenaican Miocene facies of the Ar-Rajmah Group. 17

Table 2. Ramp crest-subtidal Cyrenaican Miocene facies of the Ar-Rajmah Group. 20

Table 3. Summary of sequence stratigraphy of the Cyrenaican Miocene, Ar-Rajmah Group. 35

Table 4. Palaeocurrent data of the Cyrenaican Miocene Ar-Rajmah Group. 43

Table 5. Palaeocurrent data of Planar and trough cross bedding of the Cyrenaican Miocene Ar-Rajmah Group. 44

Table 6. Comparison between the Miocene reef builders types and platforms style in the Mediterranean region and the Cyrenaica, NE Libya. 52

Table 7. Synthesis of the Mediterranean Miocene three 2nd-order supersequences and the associated global events. 53

Table 8. Peritidal Cyrenaican Miocene facies of the Ar-Rajmah Group. 74

Table 9. Ramp crest-subtidal Cyrenaican Miocene facies of the Ar-Rajmah Group. 76

Table 10. Summary of sequence stratigraphy of the Cyrenaican Miocene, Ar-Rajmah Group. 83

Table 11. The Ar-Rajmah Group depositional facies ranges of the oxygen and carbon isotopic values of the Cyrenaican Miocene. 86

Table 12. The Ar-Rajmah Group ages ranges of the oxygen and carbon isotopic values of the Cyrenaican Miocene. 86

CHAPTER I

INTRODUCTION

Miocene carbonate platforms geology is a subject of great importance to the oil **industry, where oil reserves discovered in the Miocene reservoirs such as in the Middle** East. In addition, drastic changes in the Miocene rocks biota types and biota dominance reflect dramatic changes in the paleoclimate of the Mediterranean area. The Mediterranean is a land locked sea has a rock record of complex interaction between sea level fluctuations, sedimentation, tectonic, and climate controls.

The Cyrenaican Miocene carbonate platform is a ramp system produced a shallowing upward succession. It is represented by the Ar-Rajmah Group that includes Benghazi Formation, Wadi al-Qattarah Formation in Al-Jabal Al-Khdar north and its lateral equivalents Msus and Sceleidima formations in the Soluq Trough south. These Cyrenaican Miocene formations are diachronous rock units. The Cyrenaican platform is dominated by subtidal bioclastic and red algal associated with Porites coral facies in the Early Miocene, whereas the Middle Miocene is dominated by ramp crest-peritidal microbial oolitic grainstone associated with evaPorites, siliciclastics, bioclastic and red algal facies in, and the Late Miocene is dominated by ramp crest-peritidal microbial oolitic grainstones.

This study main target is to establish the sequence stratigraphic framework of the Cyrenaican Miocene carbonate platform through integration of the 29 high resolution field measured stratigraphic sections, 4 carbon-isotope curves, and 14 gamma-ray logs. By tying these elements together the high resolution chronostratigraphic model of the Ar-Rajmah group was developed. Furthermore, the diagenesis patterns and the paragenetic sequence of the Cyrenaican Miocene is incorporated within the sequence stratigraphic framework through the petrographic analysis of 503 samples, XRF-elements analysis, and oxygen and carbon stable isotopes patterns.

Chapters of this PhD dissertation have been written and organized systematically brick by brick to achieve goals this research seeking for. The main objectives of studying the Cyrenaican Miocene carbonate platform are: (1) to define depositional facies, sedimentary environments, depositional setting model, and to establish the high resolution sequence stratigraphic framework within a geochronological timeframe; (2) to establish the chemostratigraphic framework, deduce the paleoclimate and sea level control; (3) to define the diagenetic event and their environments, and establish the paragenetic sequence within the sequence stratigraphic framework.

Chapter two discusses the Cyrenaican Miocene detailed lithofacies description, their depositional environments, depositional model, and their sequence stratigraphic framework. Three evolutionary depositional models of the Cyrenaican ramp produced through time with their typical 3rd-order sequences. One detailed geochronologically controlled stratigraphic cross section were constructed for the Ar-Rajmah Group based on the integration of outcrop-based measured sections, gamma-ray profiles, and carbon isotope curves. Wheeler chronostratigraphic diagram, paleogeographic map, and shoreline aggradation/progradation curve, palaeocurrent azimuth analysis generated to illustrate the spatial facies distribution and their environmental development in the Cyrenaican Miocene succession through time.

Chapter three discusses the carbon and oxygen stable isotopes within the chemostratigraphic framework of the Cyrenaican Miocene carbonate succession. The chemostratigraphic framework of the Cyrenaican Miocene were established and integrated with the gamma-ray profiles and the sequence stratigraphic framework. The Cyrenaican oxygen and carbon stable isotopes curves compared with the regional Mediterranean, Indian Ocean, and global Miocene curves. The main local, regional, and global events were indicated and interpreted in the chemostratigraphic context of the Miocene. The chemostratigraphic changes through time and changes due to facies and depositional environments were investigated and discussed in details. In addition, the $CaCO_3$ dissolution events in the Ar-Rajmah Group are incorporated and discussed as global Miocene events.

Chapter four discusses the diagenetic events and the paragenetic sequence(s) of the Cyrenaican Miocene and its relation to the depositional facies, and the sequence stratigraphic context. The diagenesis study included thin section petrographic analysis, XRF-elemental study, and oxygen and carbon stable isotope data analysis. Concentrations of elements such as Mg, Mn, and SiO_2 are given a special attention in the diagenetic vents interpretations as supporters for the petrographic observations. In addition, cement types and generations are identified and put in a chronological order. Porosity types and their zones are defined and quantified as a major product of the diagenetic dissolution events.

CHAPTER II

SEDIMENTOLOGY AND SEQUENCE STRATIGRAPHY OF THE CYRENAICAN MIOCENE STRATA, Al-JABAL Al-KHDAR UPLIFT AND SOLUQ TROUGH, NE LIBYA

Overview

A sequence stratigraphic study of Miocene Ar-Rajmah Group rocks in the Cyrenaica carbonate platform, northeast Libya, extends from the north-western part of Al-Jabal Al-Khdar southwards to the Soluq Trough. This sequence stratigraphic study involves detailed regional facies relationships from 29 measured stratigraphic sections extending for over 130 km in a strike direction, 14 spectral gamma-ray profiles, annotated panoramic digital photomosaics, and petrographic analysis of 501 hand samples and their thin sections. The sequence stratigraphic framework includes correlation of stratigraphic surfaces, and vertical facies stacking patterns.

The Miocene Ar-Rajmah Group carbonate rocks record two 2^{nd}-order supersequences (97 m maximum thickness); six 3^{rd}-order sequences, and 20 regionally correlative parasequences (meter-scale cycles). The older 2^{nd}-order supersequence is not complete and contains only the shallowing upward highstand systems tract (HST), whereas the younger 2^{nd}-order supersequence is complete containing a deepening upward transgressive systems tract (TST), and the shallowing upward highstand systems tract (HST). A sharp disconformity surface separates the HST of the older 2^{nd}-order supersequence from the TST of the younger 2^{nd}-order supersequence. The HST of the older 2^{nd}-order supersequence the Early Miocene Benghazi Formation (46 m maximum thickness), the TST and HST of the younger 2^{nd}-order sequence is the Middle-Late Miocene Wadi Al-Qattarah Formation (26 m and 25m maximum thicknesses respectively).

The HST of the older 2nd-order sequence includes two 3rd-order sequences (S1 and S2), composed mainly of coral reefs, Porites, red algae (rhodoliths), and open marine skeletal packstone containing large bivalves, gastropods, oysters, and echinoids. The TST of the younger 2nd-order sequence records one 3rd-order sequence (S3) that has reworked red algae fragments at its base, shallowing upward into bioclastic grainstone, capped by interbedded cross-bedded oolitic grainstone, microbialite, and evaporite associated with pelletal mudstone/packstone. Fine to very fine quartz sandstone and green shale occur in the upper part of this 3rd-order sequence in the southern part of the field area. The HST of the younger 2nd order sequence includes three 3rd-order sequences (S4, S5, and S6), dominated by continuous bodies of oolitic grainstone and microbialite associated with some bioclastic carbonate, red algae, and pellets. Shallowing upward parasequences range in thickness from 1 m to more than 8.5 m. Peritidal-ramp crest facies are thicker in the south, whereas subtidal facies are thicker in the north. Also, peritidal-ramp crest facies are dominant in the younger sequences, whereas subtidal facies dominate the older sequences. This outcrop study of the Ar-Rajmah Group and its excellent 3-D exposure makes it an analogue for ooid grainstone carbonate reservoir in the subsurface within the Mediterranean region and globally.

Introduction

Understanding the Miocene carbonate platforms geology is a subject of great importance to the oil industry, where oil reserves discovered in the Miocene reservoirs such as in the Middle East. In addition, drastic changes in the Miocene biota types and abundance reflect dramatic changes in the paleoclimate of the Mediterranean area. The Mediterranean is a land locked sea, and a complex record of sedimentation, tectonism, and climate controls (Esteban, 1996). The sedimentological and stratigraphic study of the Cyrenaican Miocene ramp outcrops will be an excellent analogue for similar subsurface ramp reservoirs such as Jurassic Smackover Formation, Little Cedar Field, southwest Alabama (Tonietto and Pope, 2013; Al Haddad and Mancini, 2013; and

Benson and Mancini, 1984), and Permo-Triassic Khuff Formation, Ghawar Field, Saudi Arabia (Al-Dukhayyil, and Read, 2012).

The Cyrenaica Platform (Fig. 1) is located in northeastern Libya extends from the northwestern part of Al Jabal Al Khdar southwards to the Soluq Trough, between 31°-33° N Latitude and 19°-30'-21° E Longitude. The study area comprises both the IRC Benghazi (NI 34-14) and Soluq (NH 34-2) map sheets (Klen, 1974; Francis et al, 1977). The high-quality outcrops are exposed nearly continuously for greater than 130 km along the coastal escarpment. This paper documents the detailed sedimentology and 2nd- to 3rd-order sequence stratigraphy of the Miocene Ar-Rajmah Group in the Al-Jabal Al-Khdar and its equivalent in the Soluq Trough towards the south. In this work we will define the Ar-Rajmah Group depositional facies and their depositional environments, understand the vertical facies changes, construct the 2-D evolutionary depositional model(s), define the depositional cycles and construct the sequence stratigraphic framework, and create the paleogeographic maps with palaeocurrent data through time.

Geological Setting

The Cyrenaican platform (Fig. 2) in northeast Libya is a part of stable foreland basin in the Central Mediterranean region (Ziegler, 1988; and Esteban, 1996). Cyrenaica comprises two major tectonic provinces , Al-Jabal Al -Khdar Uplift in the north and the Cyrenaica Platform in the south, and two marginal troughs or indentations (Fig. 2) ,the Soluq Trough in the west and Marmarica Trough in the east (Hallett, 2002). The Cyrenaica Platform has a well preserved structure and stratigraphy because it was not subjected to severe tectonism after deposition, having formed within a splay wedge (Hallett, 2002).

Al Jabal Al-Khdar anticlinorium represents the southern portion of the Neo-Tethys basin that formed as an extensional trough or basin during the Middle Jurassic (El Hawat and Shelmani, 1993). Maximum subsidence of this area occurred during the Cretaceous; however, coincident with the opening of North Atlantic at the end of the

Cretaceous Al-Jabal Al-Khdar was in a dextral compressional duplex due to the persistent north-northwest movement of Africa towards Europe and the acceleration of the Alpine Orogeny. Later, subsidence of the Al-Jabal Al-Khdar trough ceased and it was inverted to form the Al-Jabal Al-Khdar uplifted anticlinorium (El Hawat and Shelmani, 1993).

The exposed surface rocks (Fig. 3) of the Cyrenaican Platform ranges from Cretaceous to Late Miocene (El-Hawat and Abdulsamad, 2004). The Eocene to Late Miocene rocks of Cyrenaica (Fig. 3) are sub-divided into five unconformity-bounded sequences (El Hawat and Shelmani, 1993; El-Hawat and Abdulsamad, 2004). The exposures of the Al-Jabal Al-Khdar, north Cyrenaica, are mainly shallow to deep marine carbonate rocks. However, Miocene mixed shallow marine carbonate and siliciclastic rocks exposed on the surface in Soluq Trough.

The Oligocene-Miocene boundary is an erosional surface everywhere in Libya (El Hawat and Shelmani, 1993). Subduction of the European plate under the African plate during the Late Oligocene-Early Miocene elevated a series of Cretaceous-Early Tertiary islands forming the Al-Jabal Al-Khdar anticlinorium during the Miocene (El Hawat and Shelmani, 1993). The Nummulite fichteli of the structurally uplifted Oligocene rocks were eroded and re-deposited as littoral to neritic Early Miocene rocks (El Hawat and Shelmani, 1993). The Early Miocene Al-Faidyah Formation is characterized by green glauconite at its basal contact overlain by marly wackestone to packstone (Pietersz, 1968; Rohlich, 1974; El-Hawat et al, 1993; Abdulsamad et al, 2009). Shallow marine facies of the Middle Miocene Benghazi Formation record a transgression that covered almost the entirety of the Cyrenaica Platform (El Hawat and Shelmani, 1993). Subsequently, a regional disconformity surface formed due to a major regression that coincided with the separation between the Tethys and the Paratethys, and the Messinian salinity crisis of the Mediterranean (El Hawat and Shelmani, 1993). The Late Miocene sequence of Al-Jabal Al-Khdar is composed primarily of Tortonian oolitic shoals overlain by Messinian restricted carbonate and evaporite rocks (El Hawat and Shelmani, 1993).

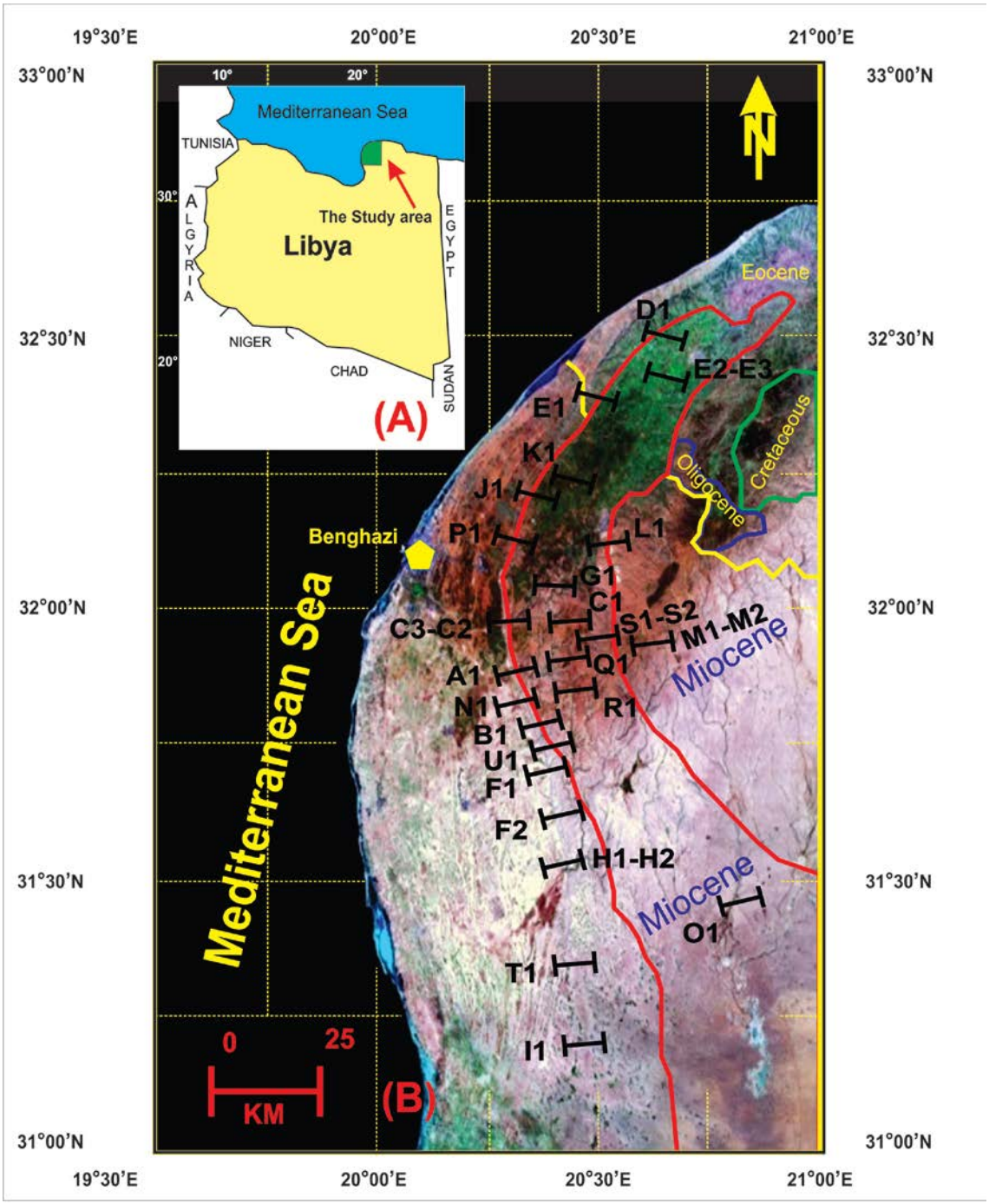

Figure 1. (A) Location map of the study area in northeastern Libya. (B) Landsat image of NE Libya showing the geological boundaries of Cretaceous- Tertiary rocks. The geological boundaries are based on the IRCs sheet-Benghazi (Klen, 1974) and sheet-Soluq (Francis and Issawi, 1977) that were later modified by (El-Hawat et al., 1987).

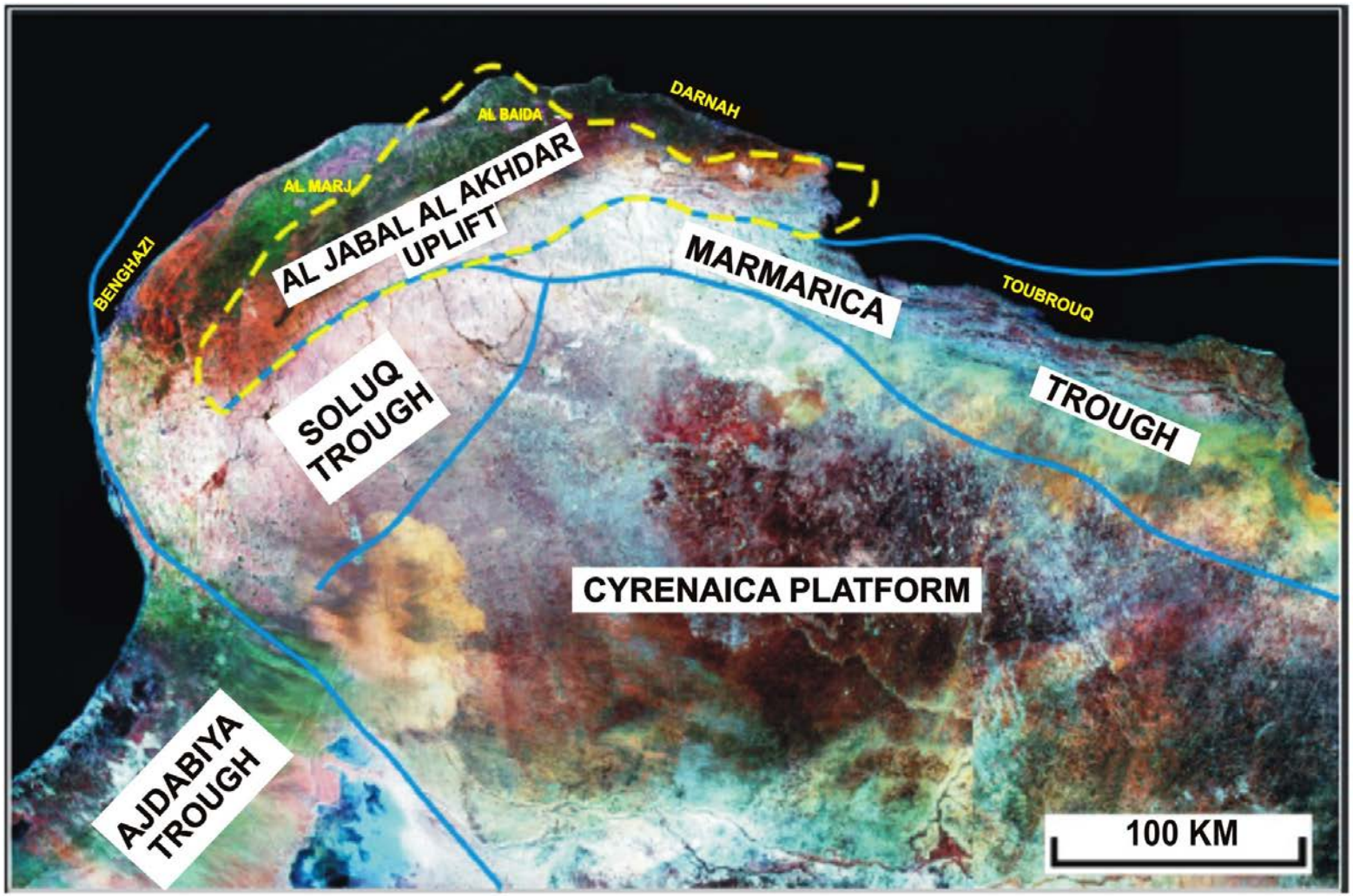

Figure 2. Land-sat false-colored TM© image of the main tectonic provinces of Cyrenaica: Al-Jabal Al-Khdar Uplift; Cyrenaica Platform, Soluq Trough and Marmarica Trough (From El-Hawat, 2007).

Al-Jabal Al-Khdar was tectonically uplifted during the Early Pliocene during the re-opening of the Mediterranean connection to the Atlantic Ocean, and the opening of the Red Sea to the Indian Ocean (El Hawat and Shelmani, 1993). The Al-Jabal Al-Khdar has remained subaerially exposed since the Early Pliocene.

The Middle Miocene Ar-Rajmah Formation (Desio, 1935 a and b) was later sub-divided into the Benghazi and Wadi Al-Qattarah Members (Klen,1974; Rohlich 1974). Subsequently, in the southern part of Cyrenaica the Ar-Rajmah was raised to a group status comprised of the Benghazi, Msus and Sceleidima Formations (Francis and Issawi, 1977; Mazhar and Issawi; 1977; Swedan and Issawi, 1977). Later in the northern part of Cyrenaica, the Benghazi and Wadi Al-Qattarah Members were raised to Formations and the Ar-Rajmah was raised to a group status in Cyrenaica (Figs. 3and 4) based on sedimentological and sequence stratigraphic analysis (El-Hawat and Abdulsamad, 2004).

The Middle Miocene (Langhian-Serravalian) Benghazi Formation is an open marine facies associations of skeletal wackestone and coral boundstone (El-Hawat and Abdulsamad, 2004; El-Hawat and Salem, 1987). The Benghazi Limestone's age was determined (Gregory, 1911; Banerjee, 1980) by marine microfaunal assemblages (e.g. Borelis melo. and other forams).

The Late Miocene (Tortonian-Messinian) Wadi Al-Qattarah Formation was first delineated for the youngest Tertiary deposits in Al-Jabal Al-Khdar (Klen, 1974). The Tortonian unit is cross bedded oolitic and bioclastic grainstone shoals of barrier islands with Messinian back barrier lagoonal mudstone, stromatolites and interbedded evaPorites.

The Wadi Al-Qattarah Formation lateral equivalents are the Al-Sceleidima Formation and Msus Formation (Fig. 4). The Al-Sceleidima Formation is stratigraphically overlain by the Msus Formation and both are shallow marine deposits. The Al-Sceleidema Formation is mixed carbonate and siliciclastic composed of sandstone, calcareous sandstone, claystone, gypsum and limestone. The Msus Formation is mostly bioclastic and oolitic limestone with lesser amounts of gypsum (Francis and Issawi, 1977).

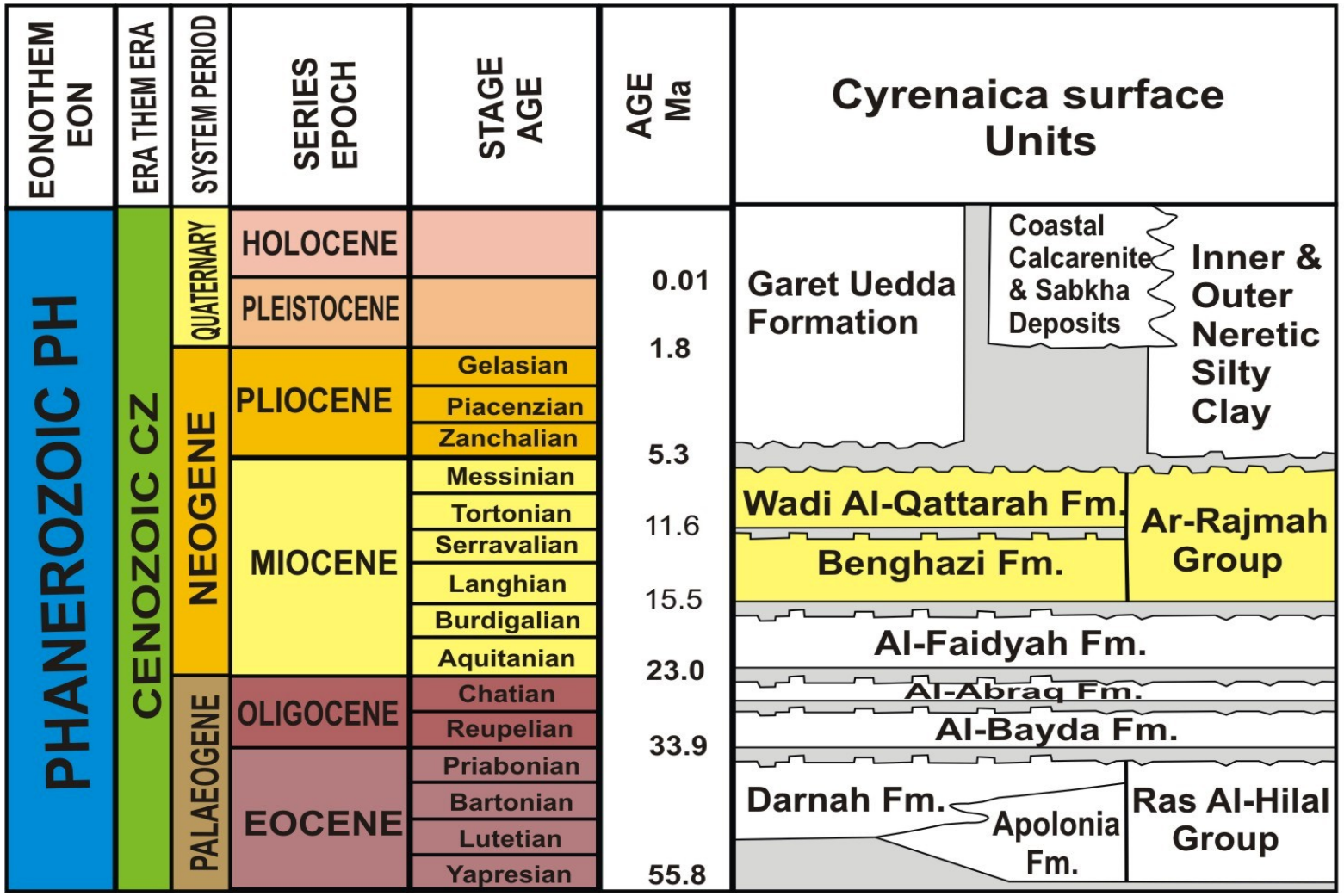

Figure 3. Part of the surface stratigraphy chart of Cyrenaica (El-Hawat and Abdulsamad, 2004). The Miocene units of the proposed study are outlined in yellow.

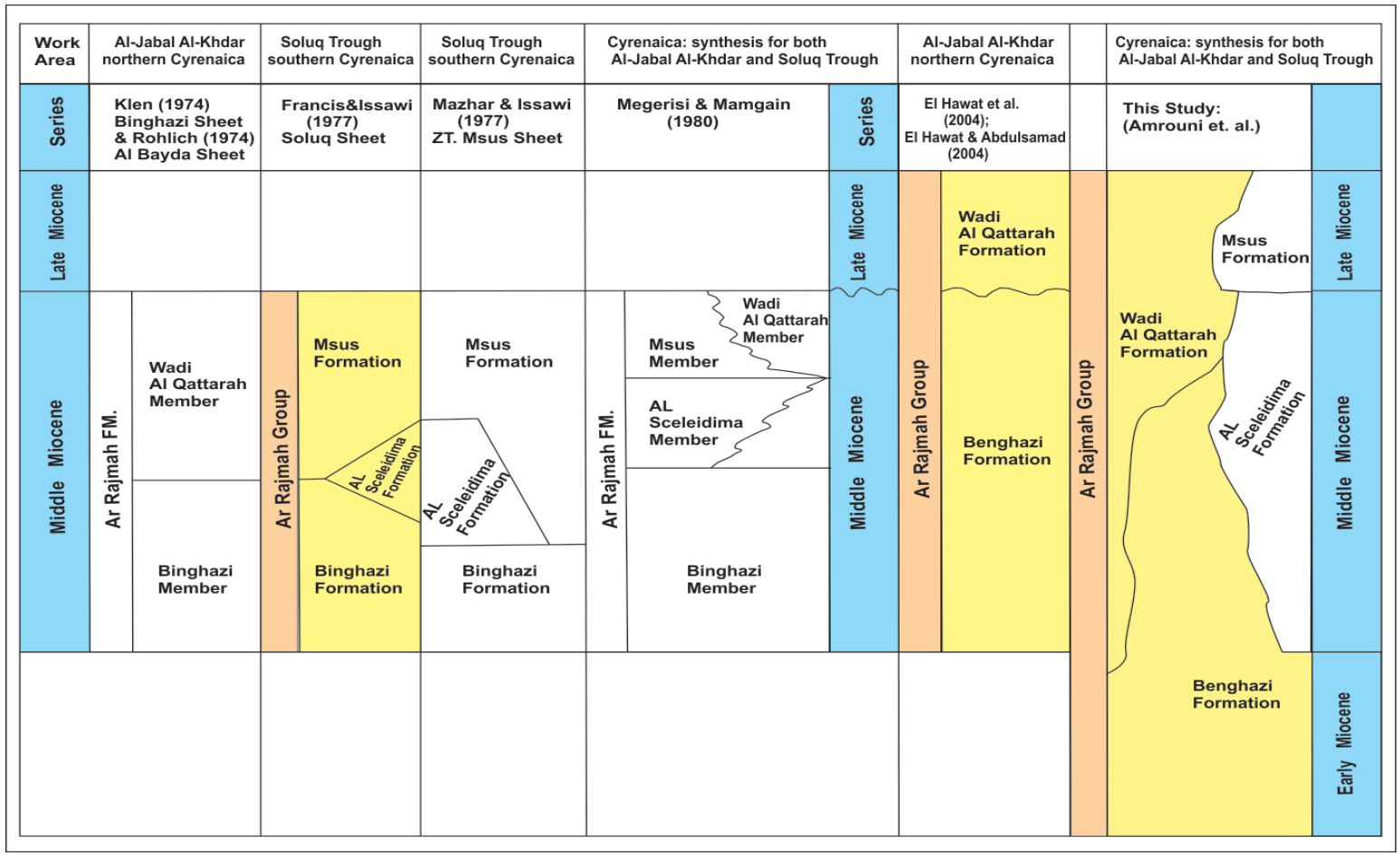

Figure 4. Stratigraphic correlation chart of Cyrenaican Miocene units, a Middle Miocene age was thought for the entire sequence of Ar-Rajmah Group (modified by Amrouni K.S. from El-Hawat and Salem, 1987). Then, it was thought to be Middle and Late Miocene (El-Hawat and Abdulsamad, 2004). Now, Abdulsamad and El Zanati (2013) published a palaeontology based paper supports the presence of the whole Miocene section in the Soluq Trough area in Cyrenaica. This study has chemostratigraphy constrains supports the presence of the whole Miocene in the Cyrenaica in both the Al-Jabal Al-Khdar area and the Soluq Trough area.

However, the recent biostratigraphic analysis of benthic forams in the Miocene rocks of northeast Libya, indicates that the Ar-Rajmah Group preserves the whole Miocene record (Abdulsamad and El-Zanati, 2013).

From a regional perspective, in spite of the difference in the tectonic settings, the Late Miocene exposures of the Al-Jabal Al-Khdar northeast Libya and the Sirt Basin in central Libya are oolitic grainstone shoals and barrier islands with back barrier lagoonal mudstone and evaporite (Amrouni, 2000, 2006). However, the Late Miocene oolitic shoals of the Al-Jabal Al-Khdar have tidal sedimentary structures such as herringbone cross-bedding and reactivation surfaces that do not occur in coeval Sirt Basin units (Amrouni, 2000, 2006).

Methods

The sedimentology and the sequence stratigraphic analysis of the Miocene strata in Cyrenaica involved determining detailed regional facies relationships from field and lab observations. The field work included measuring 29 stratigraphic sections (1150.5 m total thick) bed-by-bed over a distance of 130 km laterally, 14 spectral gamma-ray profiles were constructed using a hand-held gamma-ray scintillometer at 0.5 m intervals, and annotating facies distribution panoramic digital photomosaics. Special attention was given to identifying stratigraphic time surfaces such as sequence boundaries, flooding surfaces and maximum flooding surfaces. The lab work includes petrographic and diagenetic studies of 503 hand samples and their coincident thin sections and stable isotope (δ13C) analyses.

The field measured vertical logs were sampled, and were used in constructing the stratigraphic cross-sections. Vertical measured sections sedimentological data was plotted using a modification of the scheme designed by Selley (1968 a, Fig.2). Bedding terminology follows that of Tucker (1996). The study area divided into (21) segments that each segment has at least one vertical log section, in the North-South stratigraphic cross section. For practical and geological reasons, some segments have more than one

measured vertical log section (C1-C2-C3, E1-E2-E3, F1-F2, H1-H2, M1-M2, and S1-S2).

The depositional environments deduced from the depositional facies associations based on lithology, sedimentary structures, and fauna content (Scholle et al., 1983). The stratigraphic hierarchy and stratigraphic nomenclature of Weber et al. (1995) was used to identify the sequence stratigraphic orders of the Cyrenaican Miocene sequences. 129 paleocurrents were measured (e.g. large- scale planar cross bedding, trough cross bedding, low angle planar cross bedding, herringbone cross bedding, channel long axis, thrombolite long axis, stromatolite long axis, unidirectional clinoforms, and bidirectional clinoforms) to determine the paleocurrent azimuth of these structures.

503 samples were chosen to determine the facies associations and for petrographic analysis and diagenesis of the limestone facies. Blue dye in the epoxy to shows porosity, potassium ferricyanide differentiates ferroan and nonferroan minerals, and Alizarin Red S staining differentiates dolomite and calcite. The limestone rocks were classified using Dunham (1962) with modifications by Embry and Klovan (1971). Cement morphologies were classified following Tucker (1988).

The base of flooding surface is used as the datum for correlating the vertical sections is 14 spectral gamma-ray (U, Th, K) profiles were constructed in the field using a hand-held gamma-ray scintillometer (Radiation Solution Inc., RS-230) at 0.5 m intervals. Further, the vertical profiles of stable carbon isotopes ($\delta^{13}C$) were generated by drilling whole rock samples at 0.5 m intervals from six log sections.

Results

Depositional Facies of the Cyrenaican Miocene Ar-Rajmah Group

The Ar-Rajmah Group depositional facies includes nine carbonate facies and two siliciclastics facies that are grouped into peritidal facies (Table 1 and Figs. 5 and 6), ramp crest facies and subtidal facies (Table 2 and Figs. 7 and 8). The peritidal facies include: 1) evaporite, 2) microbialite (stromatolites, thrombolites, and laminites), 3) pelletal wackestone/packstone, 4) Porites reefs and bioclastic packstone, 5) very fine to fine quartz sandstone, 6) green shale. The ramp crest facies are oolitic grainstone. The subtidal facies include: 1) bioclastic carbonate, 2) reworked bioclastic carbonate, 3) red algae reef, and 4) reworked red algae.

Peritidal facies

Evaporite

Yellow swallow tail gypsum forms lenses up to 15 m thick and tens of meters wide. The evaporite lenses consist of 10 cm to 50 cm thick beds of chevron or lozenge shape gypsum crystals (Figs. 5A and 6A). These evaporite lenses are encased laterally and vertically within either microbialite or siliciclastic units. Dissolution and silica replacement of gypsum are its most prominent diagenetic features. Some gypsum crystals are fragmented and reworked into sand and conglomerate beds.

Table 1. Peritidal Cyrenaican Miocene facies of the Ar-Rajmah Group.

Lithofacies	Characteristics	Interpretation
EvaPorites	Lenses up to 15 m thick and various in widths with sharp top and bottom surfaces; bed thickness ranges 10 cm to 50 cm. Yellow, crystalline swallow tail selentic gypsum in fresh outcrops with Internal chevron or lozenge shape crystals. Some white in color with reworked coarse crystals and rippled. The evaporite lenses usually are encased in microbialite or siliciclastic facies.	Restricted Lagoonal evaporite facies
Microbialites reefs	Microbialites form mounds up to 12 m thick; the beds thicknesses range is from few centimetres up to 3 m with sharp top surfaces that usually have mudcracks. The microbialites are cryptalgal Laminites, stromatolites, and massive domal thrombolites. Internal structure is laminated, massive, or pelletal. Fenestral porosity is common. Have some fossils, ooid, or enriched in quartz grains. Microbialites usually intercalated thin beds of bioclastics or ooids.	Intertidal-supratidal back barrier
Pelletal wackestone /Packstone	Form units of up to 7 m thick, the beds thickness range is 0.5 m up to 2 m. The beds surfaces are sharp or sharp erosional. Laminated, and well bedded mostly associated with microbial or oolitic grainstone facies, however, occasionally associated with reworked red algae and Porites corals facies.	Intertidal back barrier
Bioclastic Porites reefs	Up to 21 m thick units of white massive and branched Porites with very large macro-bivalves, oysters, echinoids, and gastropods and microscopic forams and pellets. Lenticular beds thickness range is 1.5 m to 3 m. Channelled and channels fill is pelletal bioclastics at base that fines up to bioclastic wackestone to mudstone. Reddish brown chert nodules are common in this facies.	Lagoonal bioclastic porite reefal facies
Quartz sandstone	Up to 1 m thick Friable, well rounded, polycrystalline, yellowish to greyish white very fine to fine quarts sandstone with no fossils neither sedimentary structure observed. It reaches 6 m thick as mixed bio-oo-quartz sandstone, cross-bedded, laminated and cross laminated and occasionally bioturbated at the top surface. Fossils are leached bivalves and gastropods.	Estuary mouth
Green Shale	Up to 3.5 m thick, friable, locally laminated green shale with coprolites and fish teeth. Beds thickness range is 0.5 m to 2 m. Contains silt size quartz grains besides gypsum crystals at the base.	Estuary mouth

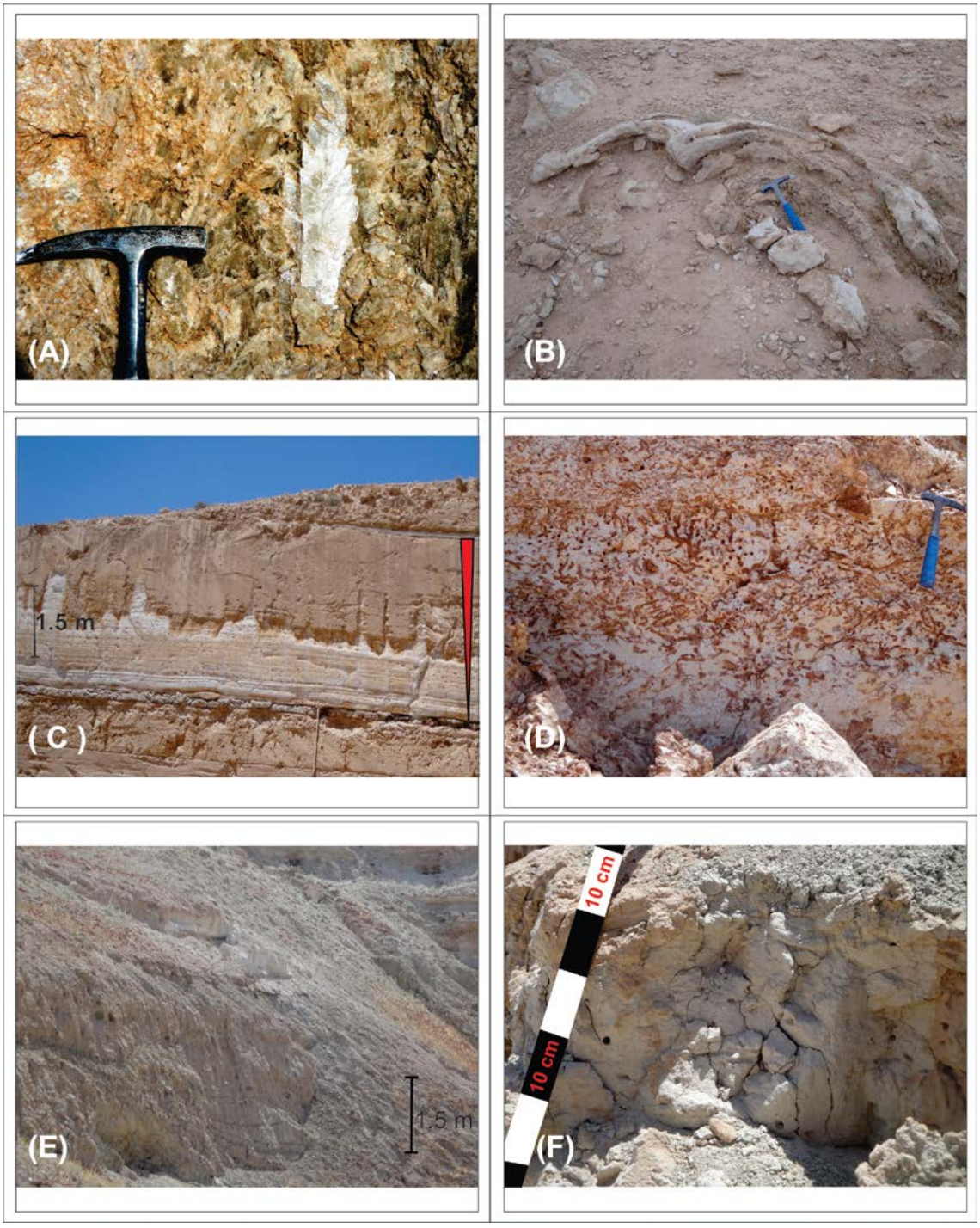

Figure 5. Outcrops of the Peritidal Facies of the Cyrenaican Miocene: (A) Yellow Swallow tail selentic gypsum, (B) Microbial stromatolites, (C) White, very thick Pelletal wackestone to packstone, (D) White branched bioclastic Porites coral reefs, (E) Friable green shale, laminated at base, and (F) Whitish yellow friable fine to very fine quartz sandstone.

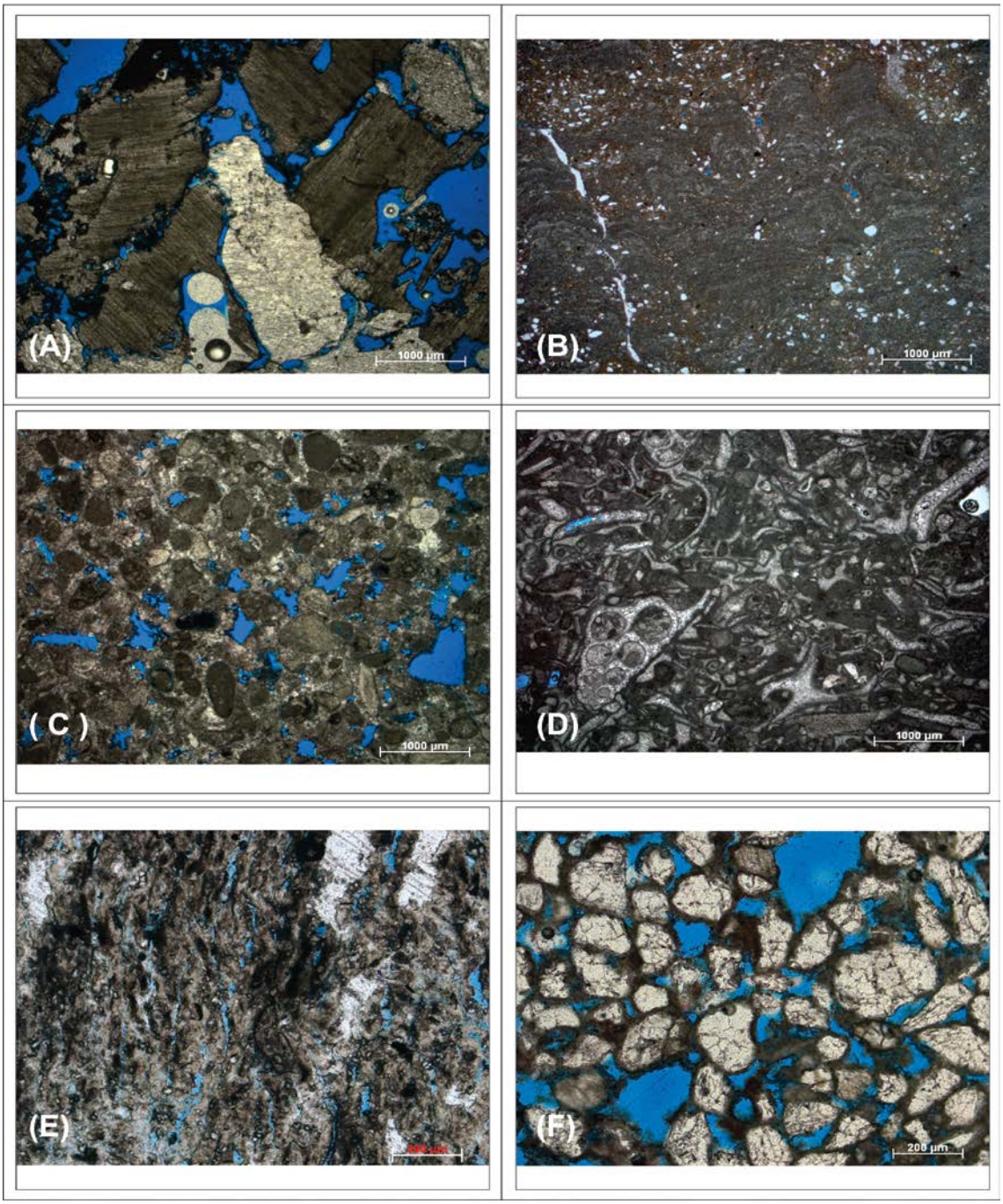

Figure 6. Thin sections of the Peritidal Facies of the Cyrenaican Miocene:(A) Chevron structure of yellow Swallow tail selentic gypsum, (B) Microbial stromatolites of domal and laterally linked lamina, notice the angular silty size quartz grains (C) Pelletal wackestone to packstone, (D) branched bioclastic Porites coral reefs in a pelletal packstone background, (E) Friable green shale with gypsum crystals at base, and (F) friable fine to very fine quartz sandstone, the quartz grains are polycrystalline with some green shale matrix.

Table 2. Ramp crest-subtidal Cyrenaican Miocene facies of the Ar-Rajmah Group.

Lithofacies	Characteristics	Interpretation
Oolitic grainstone facies	Form packages of up to 21 m thick, Channelled, Laminated, x-laminated, well bedded, X-bedded, graded bedding, and 4 m thick unidirectional clinoforms. Beds thickness ranges from 0.5 m to 7 m. Rare fossils that are mostly dwarfed bivalves, gastropods, and forams. Intercalated with microbialites.	Subtidal-intertidal oolitic barrier
Bioclastic mudstone /packstone	Form units of up to 8 m thick, massive, well bedded, cross bedded, laminated, and cross-laminated with bivalves, gastropods, bryozoans, oysters, echinoids, some red algae, and microscopic forams and occasionally corals. Beds thickness range is 0.5 m to 3 m with sharp top and bottom surfaces. Occasionally beds bioturbated at the basal part.	Subtidal open marine facies
Reworked Bioclastic packstone	Piles of up to 8 m thick, well bedded, cross bedded, laminated, cross laminated and channelled with dominantly broken shells of bivalves, gastropods, bryozoans, oysters, echinoids, some red algae, occasional fragmented corals and microscopic forams. Beds thickness range is 0.5 m to 3 m with sharp top and bottom surfaces.	Subtidal open marine facies
Red algal coralline reef	Reefs up to 26 m thick units, with lenticular beds of 1 m to 3 m thick that contain massive bodies contain baseball size heads of coralline red algae with bivalves, gastropods, bryozoans, oysters, echinoids, and microscopic forams with some occasional corals occurrences. The beds basal to top surfaces are sharp. The beds show graded bedding due to changes in fossil sizes. They form bidirectional clinoforms in some localities.	Subtidal open marine facies
Reworked red algal	Form units of up to 11.5 m thick. The beds are of 0.5 m to 3 m thick, well bedded, graded bedding and occasionally massive with sharp base and top surfaces. Most fossils are fragmented red algae with broken shells of bivalves, gastropods, bryozoans, oysters, echinoids, and microscopic forams and occasional coral fragments.	Subtidal open marine facies

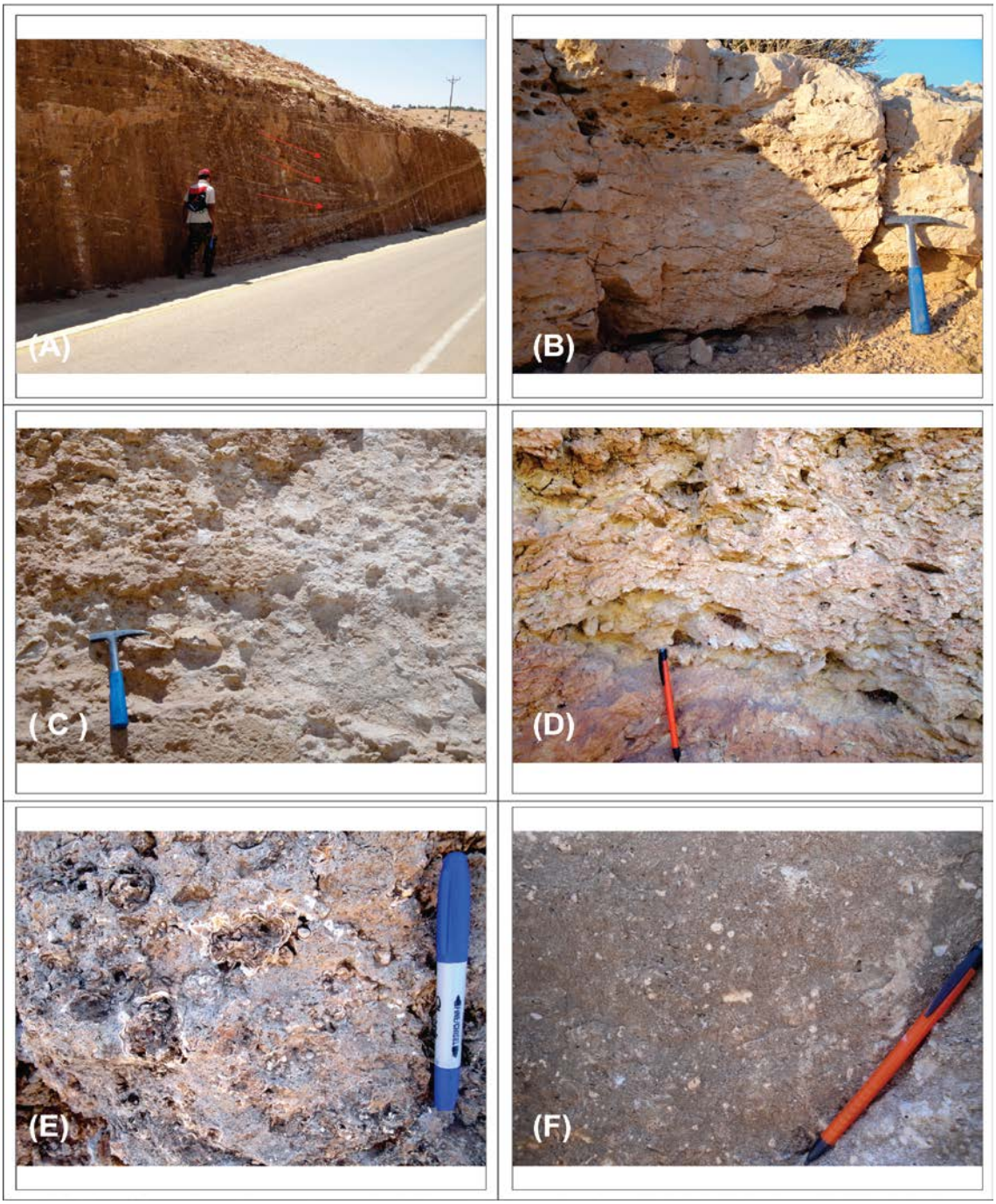

Figure 7. Outcrops of the Ramp Crest-Subtidal Facies of the Cyrenaican Miocene: (A) Oolitic grainstone unidirectional clinoforms, (B) Oolitic grainstone coarsening upwards into fenestral oolitic grapestone, (C) echinoid-rich bioclastic packstone, (D) Reworked marly bioclastic packstone, (E) Red algal packstone, and (F) Reworked red algal packstone.

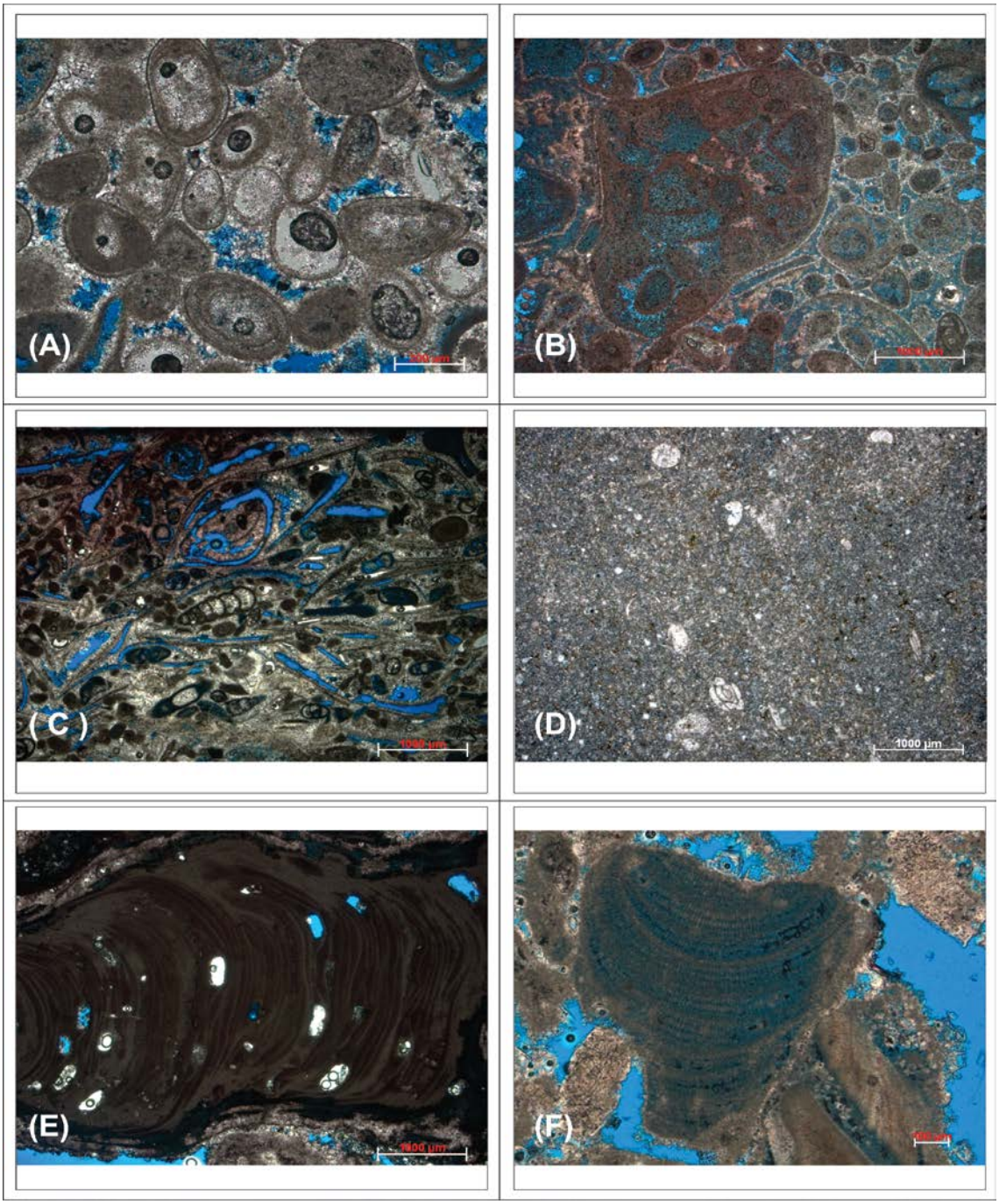

Figure 8. Thin sections of the Ramp Crest-Subtidal Facies of the Cyrenaican Miocene: (A) Partially leached concentric oolitic grainstone, (B) oolitic grainstone mixed with oolitic grapestone, (C) Bioclastic packstone enriched in gastropods, bivalves, and forams, (D) Reworked marly bioclastic wackestone, (E) Red algal packstone, and (F) Reworked red algal packstone.

Microbialite

The microbialite facies (Figs. 5B and 6B) comprises cryptalgal laminite, stromatolite, and thrombolite, and reached a maximum thickness of 12 m. The microbialites bed thickness ranges from a few centimetres up to 3 m, commonly with very sharp upper surface marked by mudcracks. Microbialite facies commonly contain fenestral and vuggy pores. Massive thrombolite domes are the most dominant microbial component. Stromatolite beds commonly elongated laterally linked domal heads. Laminites occur either at the basal part of the stromatolite beds or as separate thinly laminated beds intercalated with yellow gypsum. Some dwarfed bivalves and gastropods occur within the microbial facies.

The microbial facies increase in thickness and frequency towards the Soluq Trough changing from small buildups of 20 cm to 50 cm in diameter in the northern side of the study area into elongated mounds more than 1.5 m in diameter in the south. Laminites dominate the northern part or Al-Jabal Al-Khdar Uplift, whereas stromatolites dominate the central area usually intercalated with oolitic grainstone facies, and thrombolites dominate the Soluq Trough. The microbial facies commonly are intercalated with oolitic grainstone, evaporite, and pelletal wackestone/packstone.

Microbial facies are laminated, massive, or pelletal. The laminated stromatolites form small digits or laterally linked domes. The amount and size of the quartz sand grains in the microbialite facies increases up-section and towards the south. Micritization, recrystallization, and dissolution are the dominant diagenetic features in the microbialite facies. Replacement with gypsum and then silica is common, and diagenetic chert nodules are common in the microbial facies. Dissolution seams are always associated with fracture porosity. The microbialite facies are interpreted to have formed in a restricted setting behind and adjacent to ramp crest ooid shoals.

Pelletal wackestone/packstone

Pelletal wackestone and packstone (Figs. 5C and 6C) units are up to 7 m thick, laminated, cross laminated, well bedded, locally cross bedded, and have normal and reverse graded bedding. Facies associated with the pelletal wackestone/packstone are microbialite, oolitic grainstone, reworked red algae, and Porites coral. Pelletal wackestone/packstone beds range from 0.5 m to 2 m thick. The pelletal facies commonly are mixed with ooids and very fine to fine quartz sand grains in the southern part of the study area. Diagenetic chert nodules occur where pellets are associated with ooid grainstone and microbialite.

The pelletal wackestone/packstone facies commonly are fossil-rich containing small forams, small bivalves, fragmented red algae, Porites, and algae. Many fossils are aligned along a preferred orientation. The pelletal wackestone/packstone facies is interpreted to have formed in a shallow lagoon between the tidal flat facies and ooid grainstone ramp crest facies.

Bioclastic Porites reefs

The bioclastic Porites reefal facies (Figs. 5D and 6D) form white vertical walls reaching up to 21m thick, containing massive and internally branched, thick Porites with white mud matrix between bioclastic grains of very large bivalves, gastropods, oysters, echinoids, forams and pellets. The beds are 1.5-3 m thick, and lenticular in shape. A channelled in this facies is filled with pelletal grainstone and packstone that fines upward into bioclastic wackestone and mudstone. The channels are 1.5-3 m deep and up to 5 m wide. Diagenetic reddish brown chert nodules are common in the bioclastic Porites reefs. Bioclasts are very common in the Porites facies, including Porites, bivalves, gastropods, oysters, echinoids. Forams such as *Borils melo* and *miliolids* are very common in this facies. The bioclastic Porites facies is interpreted to

have formed as irregular patch reefs within a lagoon that developed between the ramp crest and coeval tidal flats.

Quartz sandstone facies

The yellowish to greyish white, friable, massive very fine to fine quartz sandstone (Figs. 5F and 6F) commonly is less than 1 m thick. However, the sandstone reaches up to 6 m thick when interbedded with ooid and bioclastic to form bioclastic-and-ooid rich quartz sandstone. The bioclastic and ooid-rich sandstone facies are laminated, cross laminated, well bedded, cross bedded, and at one occasion bioturbated at the top surface.

Fossils are abundant in the mixed bioclastic-ooid rich quartz sandstone, whereas the pure sandstone is barren of fossils. Fossils are mostly leached small bivalves and gastropods. The quartz sandstone facies is interpreted to have formed in an estuary environment.

Green shale

The green shale (Figs. 5E and 6E) reaches a maximum thickness of 3.5 m, with beds being 0.5 to 2 m thick. The green shale is friable, locally laminated, and contains some silt-grains. Coprolites and fish teeth in the green shale facies were reported by **Francis and Issawi** (1977). The basal part of this green shale usually contains some gypsum. The green shale is interpreted to have formed in an estuary environment.

Ramp crest facies

Oolitic grainstone

The oolitic grainstone (Figs. 7A-7B and 8A-8B) reaches up to 21 m thick and has a variety of sedimentary structures such as channels, lamination, cross-lamination, cross-bedding, and normal and reverse graded bedding. The oolitic grainstone beds range from 0.5 m to 7 m thick and locally form large unidirectional clinoforms up to 4 m thick (Fig. 7A) that are cut by small channels up to 1.5 m deep. The channels fill has soft sediment deformation structures. Occasional diagenetic chert nodules, and bands of chert of up to 20 cm thick, occur in some horizons especially where ooid grainstone is associated with microbialite. At the southern part of the study area, ooid grainstone contains some very fine to fine sand size quartz grains in the matrix.

Forams, small bivalves, and small gastropods are rare in the oolitic grainstone. Ooid grainstone beds are intercalated with microbialite throughout the study area, but the abundance of the microbial and oolitic grapestones increases in the southern part of the study area. Ooid grainstone is interpreted to have formed a continuous high-energy shoal that separated the restricted lagoon from open marine shallow subtidal facies.

Shallow subtidal facies

Bioclastic mudstone /packstone

Bioclastic mudstone and packstone (Figs. 7C and 8C) is up to 8 m thick, with beds ranging from 0.5-3 m thick. Bedding in this facies varies from massive and locally bioturbated to laminated and cross laminated or graded. In addition, some fining upward packstone beds are capped by bioclastic wackestone and coarsening upward bioclastic packstone beds are capped by bioclastic grainstone. Some bioclastic units are dominated

by one large size fossil type such as oysters or echinoids. The oyster beds usually form fining upward channel fill within evaporite beds. Yellow, marly bioclastic wackestone and packstone occur at four different localities. Marly packstone is dominated by large echinoids with less common bivalves and gastropods, whereas the marly wackestone is dominated by bivalves and gastropods. Diagenetic chert nodules occur in this facies where it is associated with corals or microbialites.

Bivalves, gastropods, bryozoans, oysters, echinoids, horn corals, red algae, and forams occur in the bioclastic mudstone/packstone. Fossil sizes vary from very large to dwarf. The bioclastic mudstone/packstone facies was likely deposited in a shallow open marine subtidal setting.

Reworked bioclastic packstone

Reworked bioclastic packstone (Figs. 7D and 8D) is up to 8 m thick, with beds ranging from 0.5 to 3 m thick. Reworked bioclastic grainstone occur in the upper part of many reworked bioclastic packstone beds. The reworked bioclastic packstone facies is locally, cross bedded, graded, and occasionally forms channels. Skeletal fragments of bivalves, gastropods, bryozoans, oysters, echinoids, red algae, local horn corals, and forams are common fossils in the reworked bioclastic packstone. Skeletal fragments are more abundant than intact fossils. Marly reworked bioclastic packstone is dominated by large echinoids with fragmented bivalves and gastropods. *Borils melo* is a very common foram type in this facies. Diagenetic chert nodules occur where this facies contains corals. The reworked bioclastic packstone facies is interpreted to have formed in a shallow subtidal setting.

Coralline red algal reefs

Coralline red algal reefs (Figs. 7E and 8E) reaches up to 26 m thick, and are composed of lenticular shaped beds 1 to 3 m thick. Bidirectional clinoforms occurring in this facies are massive consisting of 10 cm diameter heads of coralline red algae with some large bivalves, gastropods, bryozoans, oysters, echinoids, horn corals, and forams. *Borils melo* forams are very common in this facies. Graded bedding is evident due to rapid changes in fauna sizes even within the same bed. Diagenetic chert nodules are very rare in this facies. The coralline red algal facies formed isolated reefs basinward of the ooid shoal.

Reworked red algae

The reworked coralline red algae (Figs. 7F and 8F) is up to 11.5 m thick, with 0.5 m to 3 m thick beds with sharp top and basal surfaces. The facies is well bedded with graded bedding, but occasionally this facies is massive. Locally, the reworked red algal facies form bidirectional clinoforms of up to 4 m high. The biota in this facies varies from large to dwarfed. The dominant depositional texture is skeletal packstone, but in some beds the very upper part is skeletal grainstone. Diagenetic chert nodules are very rare in this facies.

Fossils are very common in the reworked red algae facies dominantly fragmented red algae with broken shells of bivalves, gastropods, bryozoans, oysters, echinoids, and forams such as *Borils Melo*. The reworked coralline red algal facies is interpreted to have formed in a shallow subtidal setting.

Sequence Stratigraphy of the Cyrenaican Miocene Ar-Rajmah Group

The Miocene succession of Cyrenaica (Figs. 9-13) is composed of cyclic rocks successions whose facies stacking patterns defined two 2nd-order supersequences (SS1 and SS2). The basal succession (SS1) is composed of Aquitanian-Burdigalian rocks (Figs. 9-13), whereas the upper succession (SS2) contains Langhian-Messinian rocks. The base of SS1 is not recorded within the study area so SS1 records a long-term sea level fall, but SS2 is complete and records a long-term transgression-regression. SS1 is comprised of two 3rd-order sequences (S1 and S2), whereas SS2 is comprised of four 3rd-order sequences (S3-S6). These 3rd-order sequences are correlative throughout the area. Each 3rd-order sequence is composed of meter-scale shallowing upward parasequences that are locally, but not regionally, correlative. Table 3 outlines the detailed description of supersequences SS1 and SS2, sequences S1-S6, and the description of the 20 parasequences (PS1-PS20). A brief discussion of the sequences and parasequences is outlined here.

Measured section F1 (Fig. 9) is the best vertical profile that comprises all vertical facies changes through the Miocene. F1 is 73 m thick and includes the entire Cyrenaican Miocene assemblages. The Early Miocene is comprised of S1 and S2, the Middle Miocene is S3, and the Late Miocene is S4, S5, and S6. The S1 3rd-order sequence is 15 m in thickness and the lower 10.5 m is Aquitania of the Early Miocene overlain by 4.5 m covers the lower part of the Burdigalian. The S2 3rd-order sequence is 15 m thick and was deposited during the Burdigalian age of the Early Miocene. The S3 3rd-order sequence is 22.5 m thick and was deposited during the Middle Miocene Langhian and Serravallian. The 11.5m thick S4 3rd-order sequence and the 5.5 m thick S5 3rd-order sequence were deposited during the Late Miocene Tortonian. The S6 3rd-order sequence is 3.5 m thick was deposited during the Late Miocene Messinian.

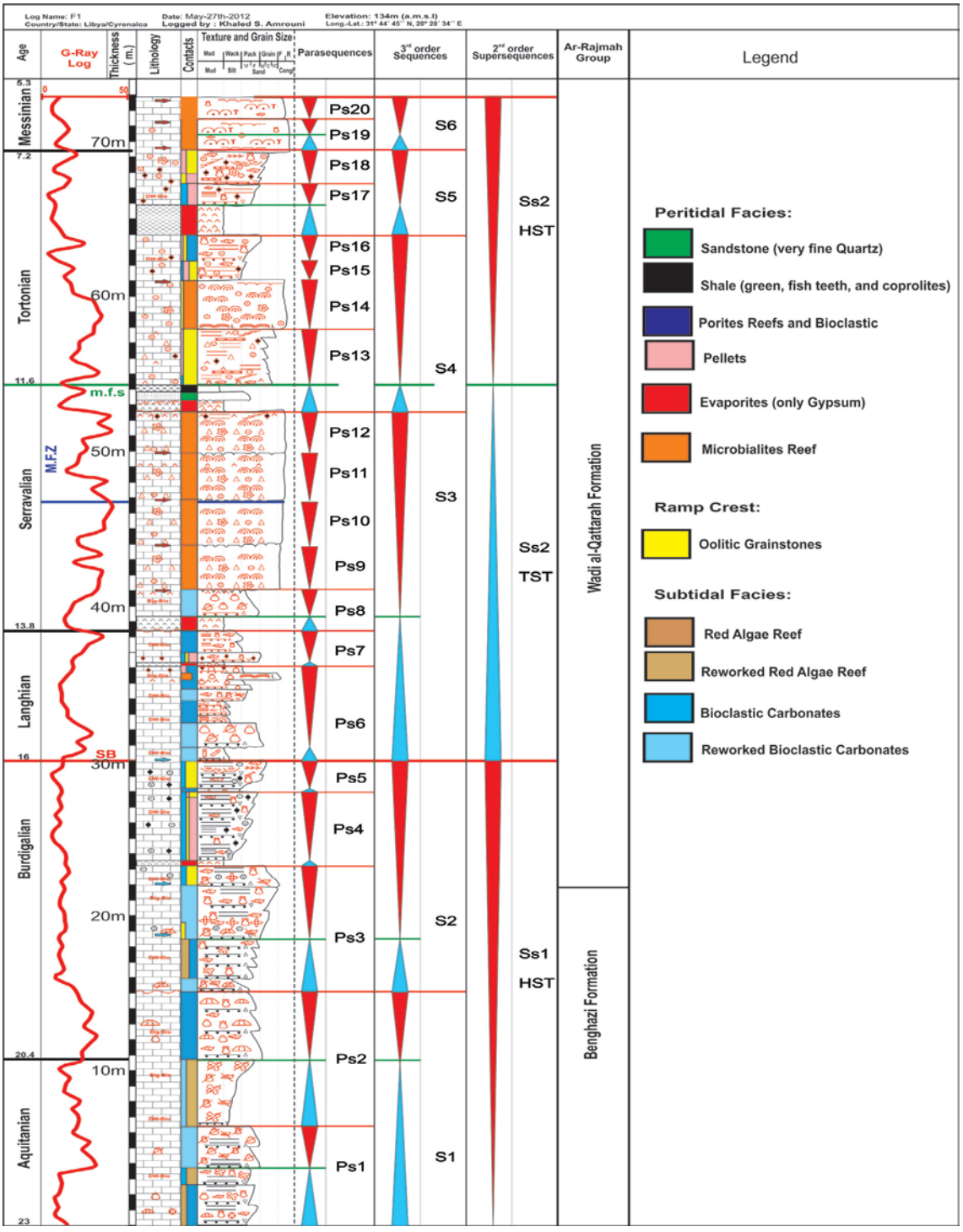

Figure 9. Ideal type section in the sequence stratigraphic context of the Cyrenaican Miocene carbonate platform, Ar-Rajmah Group: Stratigraphic log section F1, G-Ray profile, formations and sequence stratigraphic annotations.

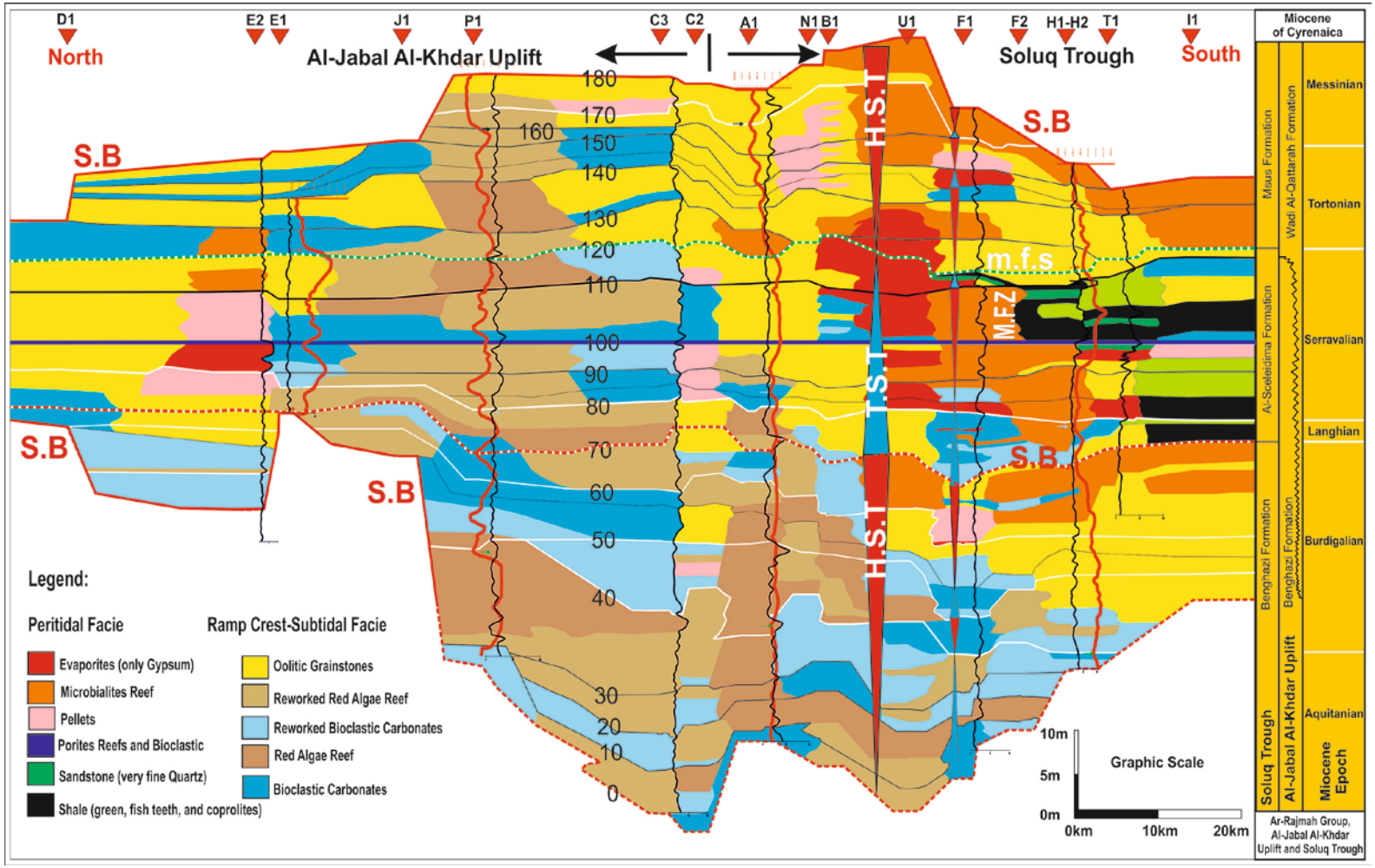

Figure 10. Sequence stratigraphic framework of the Cyrenaican Miocene carbonate platform, Ar-Rajmah Group: inverted red triangles refer to the locations of the stratigraphic log section, G-Ray profile are thin black curves, Carbon stable isotope profiles are thick red curves, formations names, and sequence stratigraphic annotations. (modified from Amrouni et. al., 2013).

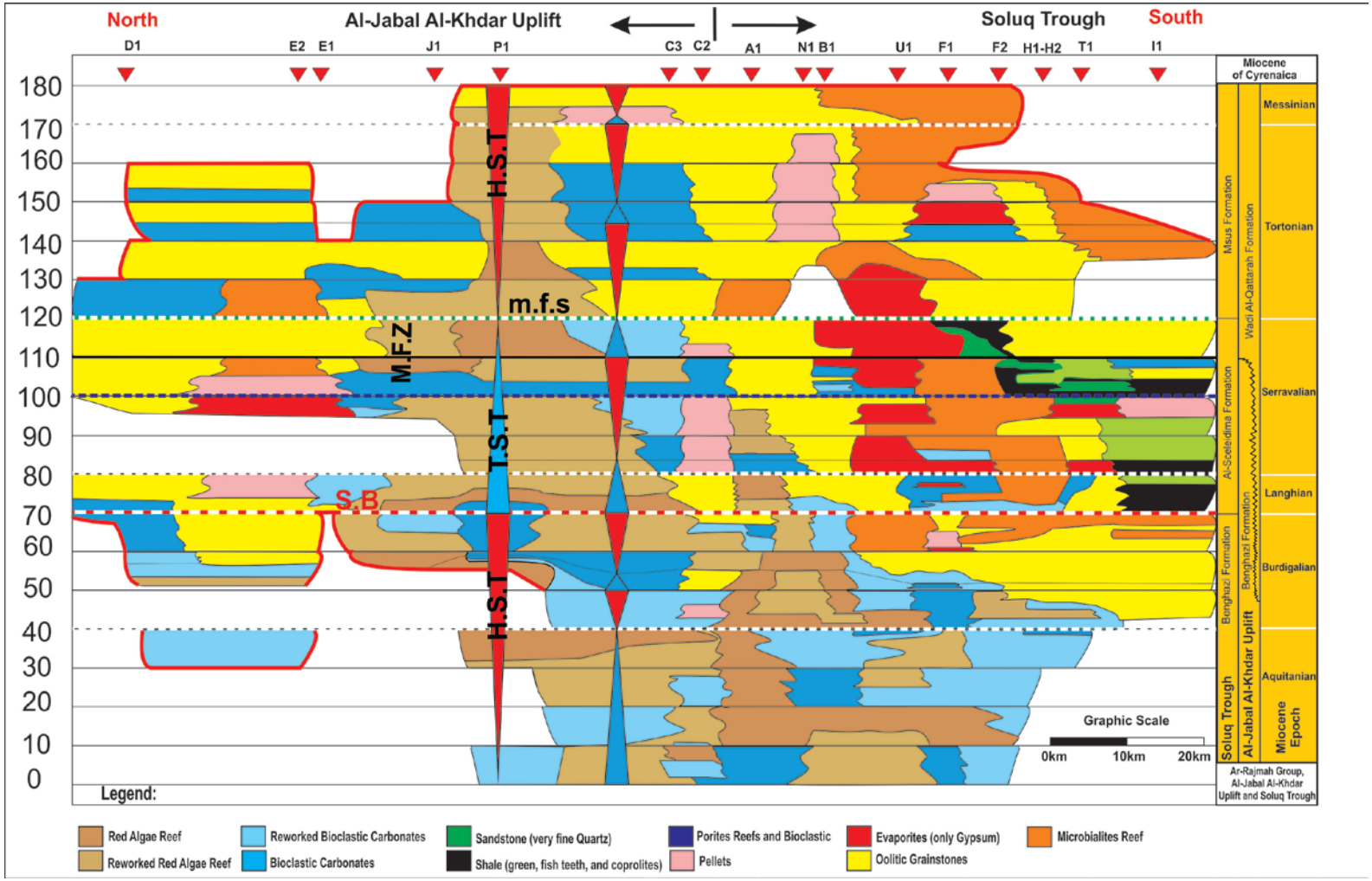

Figure 11. Wheeler chronostratigraphic diagram of the Cyrenaican Miocene carbonate platform, Ar-Rajmah Group.

Figure 12. Annotated field photographs for the Cyrenaican Miocene Carbonate Platform surfaces: (A) Maximum flooding surface (mfs), (B and C) The unconformity surface between the older 2nd -order supersequence (Early Miocene) and the younger 2nd-order supersequence (Middle and Late Miocene), (D and E) the unconformity surface of around 35Ma duration between the Eocene and the Miocene.

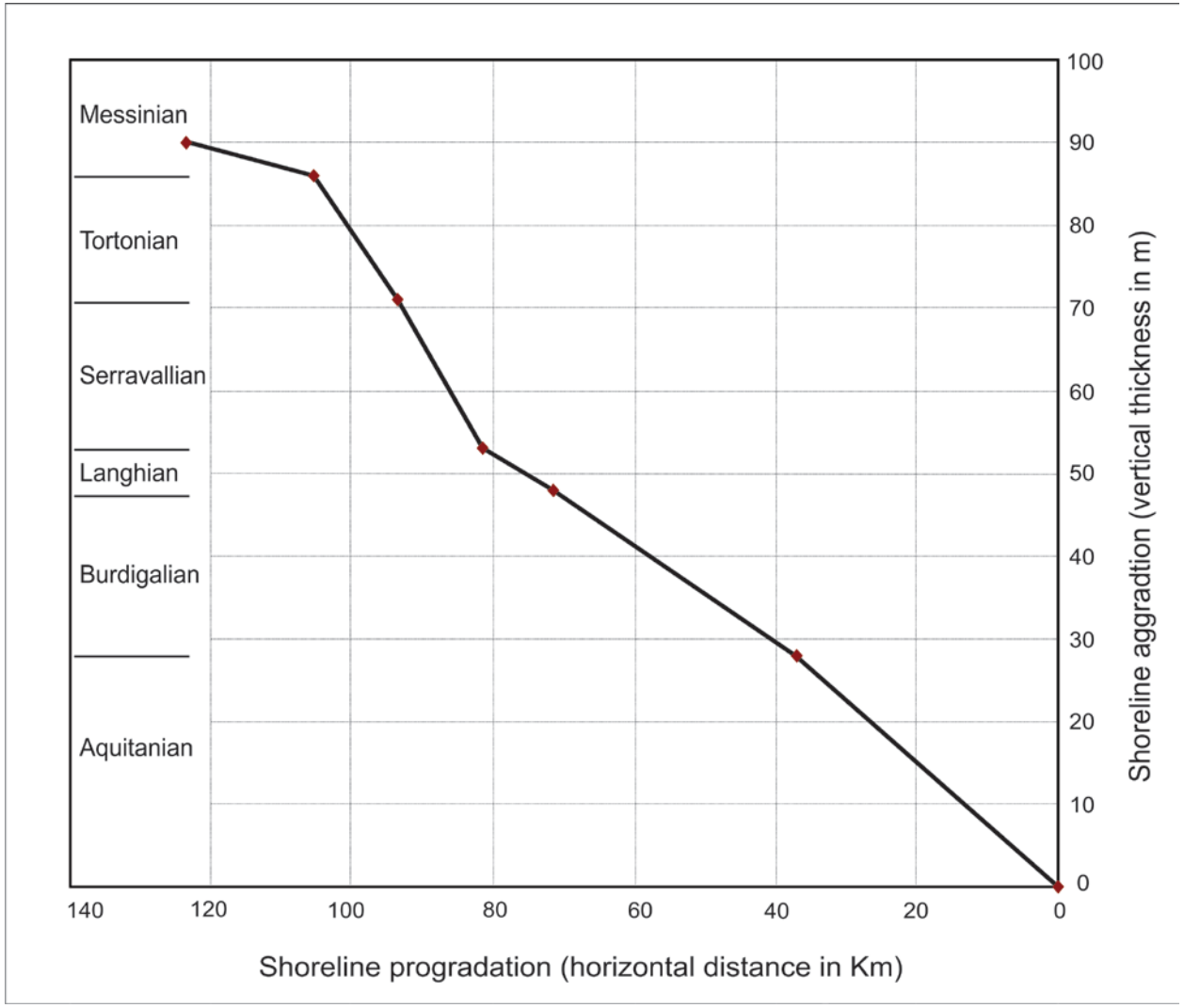

Figure 13. The Cyrenaican sequences shoreline aggradation /progradation curve throughout the Miocene time.

Table 3. Summary of sequence stratigraphy of the Cyrenaican Miocene, Ar-Rajmah Group.

2nd Order Sequence	2nd Order systems Tracts	3rd Order Sequences	Para-sequences	Occurrence	Thickness	SB	TST	MFS	HST
SS2	HST 25 m	S6	PS20 - PS19	Covers the Messinian age	2 to 5 m thick (not fully preserved because the top surface is the present day exposure surface)	Sharp surface at the top of microbialites, oolitic grainstone, bioclastic packstone, and red algal packstone facies	1 to 2 m thick deepening upward unit of reworked red algal packstone, oolitic grainstone, and pelletal packstone facies	Placed at the top of the oolitic grainstone facies, within microbialites facies, pelletal packstone facies, oolitic grainstone facie, and reworked red algae packstone facies	2.5 to 4 m thick shallowing upward unit of microbialites facies, pelletal packstone facies, oolitic grainstone facies, and reworked red algal packstone facies
		S5	PS18 - PS17	Covers the Tortonian age	5 to 11 m thick	Sharp surface at the top of microbialites, oolitic grainstone, bioclastic packstone, and red algal packstone facies	1 to 2 m thick deepening upward unit of reworked red algal packstone, bioclastics packstone, oolitic grainstone, pelletal packstone, ,and evaporite facies	Placed at the top of the evaporite facies, within pelletal packstone facies, oolitic grainstone facie, and reworked red algae packstone facies	2 to 10 m thick shallowing upward unit of microbialites facies, pelletal packstone facies, oolitic grainstone facies, bioclastic packstone facies, and reworked red algal packstone facies
		S4	PS16 - PS13		5 to 13 m thick	Sharp surface at the top of microbialites, oolitic grainstone, bioclastic packstone, and red algal packstone facies	1 to 6 m thick deepening upward unit of reworked red algal packstone, reworked bioclastics packstone, oolitic grainstone, pelletal packstone, green shale facies, sandstone facies, and reworked evaporite facies	Placed at the top of the evaporite facies, the green shale facies, bioclastic packstone facies, red algal packstone facies within evaporite facies, oolitic grainstone facie, and reworked red algae packstone facies	6 to 11 m thick shallowing upward unit of evaPorites facies, microbialites facies, pelletal packstone facies, oolitic grainstone facies, bioclastic packstone facies, and reworked red algal packstone facies
	TST 26 m	S3	PS12 – PS6	Covers the Middle Miocene, Langhian and Serravallian ages	13 to 22 m thick	Sharp surface at the top of microbialites, oolitic grainstone, bioclastic packstone, and reworked red algal packstone facies, and bioclastic packstone coral Porites facies	2 to 8 m thick deepening upward unit of red algal packstone, bioclastics, oolitic grainstone, pelletal packstone, and microbialites facies.	Placed at the top of the evaporite facies, the green shale facies, within microbialites facies, pelletal packstone, bioclastic packstone, and reworked red algae facies	13 to 16 m thick shallowing upward unit of evaPorites facies, microbialites facies, pelletal packstone facies, sandstone facies, green shale facies, oolitic grainstone facies, bioclastic packstone facies, and reworked red algal packstone facies
SS1	HST 46 m	S2	PS5 - PS3	Covers the Burdigalian age	5 to 15 m thick ,	Sharp erosional surface at the top of echinoid dominated bioclastic packstone facies	1 to 4 m thick deepening upward unit of red algal packstone, bioclastic packstone, oolitic grainstone and bioclastic packstone coral Porites facies	Placed at the top of and within red algal packstone facies bioclastic packstones facies, and oolitic grainstone facies	5 to 12.5 m thick shallowing upward unit of microbialites facies, pelletal packstone facies, oolitic grainstone, reworked (bioclastic packstone, red algal packstone), and bioclastic packstone coral Porites facies
		S1	PS2 - PS1	Covers the Aquitania age and lower part of the Burdigalian age	3 to 30.5 m thick	Sharp surface at the top of Eocene Numulitic Packstone	2 to 28 m thick deepening upward unit of bioclastic packstone and red algal packstone , and bioclastic packstone coral Porites facies	Placed at the top and within the deep facies red algal packstone, beneath echinoid dominated bioclastic packstone facies	3 to 10 m thick shallowing upward unit of echinoid dominated bioclastic packstone facies), red algae packstone, oolitic grainstone, and bioclastic packstone coral Porites facies

3rd-order sequence S1

From the base, the S1 is a 10.5 m thick deepening upward unit capped by 4.5 m thick a shallowing upward unit. Fossil size decreases upward in the deepening upward portion, whereas increases upward in the shallowing upward. It comprises two shallowing upward parasequences, PS1 6.5m thick andPS2 8.5 m thick.

The (PS1) is 6.5 m thick, and made up of 4 m thick deepening upward bioclastic packstone facies that deepens upward into coralline red algae, and a 2.5 m thick shallowing upward unit of reworked bioclastic packstone. The bioclastic packstone facies is whitish grey, and contains large bivalves, gastropods, echinoids, and oysters. The coralline red algae packstone facies is whitish grey, and contains small size red algae, bivalves and gastropods. The reworked bioclastic packstone facies is white in color, and contains fragmented bivalves, gastropods, and oysters.

The 8.5 m thick (PS2) is made of a deepening upward of 4.5 m thick reworked red algal packstone overlain by a shallowing upward unit of 4 m thick of bioclastic packstone facies dominated by large echinoids. The reworked red algal packstone is white in color, massive, with reverse graded bedding, and made up of fragments of red algae, bivalves, and gastropods. The echinoid dominated bioclastic packstone is white in color, with normal graded bedding, dominated by large echinoids with oysters, bivalves, and gastropods.

3rd-order sequence S2

The S2 comprises three main parasequences (PS3-PS5). The (PS3) is 8.5 m thick, the (PS4) is 4.5 m thick, and the (PS5) is 2m thick.

The 8.5 m thick PS3 is made up of two units. The basal 3.5 m deepening upward unit is reworked bioclastic packstone overlain by bioclastic packstone. The upper 5 m coarsening upward unit is reworked bioclastic facies capped by oolitic grainstone. The 1m thick reworked bioclastic packstone is the basal part of the 3.5 m thick deepening

upward unit, and includes fragmented echinoids, bivalves, and gastropods. The upper 2.5m thick bioclastic packstone of the deepening upward unit is dominated by bivalves, gastropods, and less amount of intact red algae. It is white in color with cyclic normal graded bedding. Fossils decrease upward in size and amount in the above 5 m thick shallowing upward unit. The 3.5 m thick reworked bioclastic facies is intensively bioturbated at the base, well bedded at top, with reverse graded bedding, and contains fragmented and intact large size echinoids, bivalves, and gastropods. The 1.5 m thick oolitic grainstone facies is moderately bioturbated, well bedded, with normal graded bedding, and contains fragmented and intact small size bivalves and gastropods.

The 4.5 m thick (PS4) is made of 0.2 m thick deepening upward of yellow swallow tail selentic gypsum evaporite facies with no fossils preserved, and 4.3 m thick shallowing upward unit of pelletal packstone facies that includes some ooids, intact small size bivalves and gastropods. The pelletal facies are white in color, laminated, well bedded, and shows multiple reverse graded bedding sedimentary structure.

The 2 m thick (PS5) is made of 0.2 m thick deepening upward unit of bioclastic wackestone facies that contains intact dwarfed bivalves, and gastropods, and 1.8 m thick shallowing upward unit of cross bedded oolitic grainstone facies that is white in color, laminated, trough cross bedded, herring-bone cross bedded, with multiple reverse graded bedding. It contains some pellets, and very rare intact small size bivalves and gastropods.

3rd-order sequence S3

The S3 is 22.5 m thick and covers the Middle Miocene Langhian and Serravallian ages and made up of 9.5 m thick deepening upward unit capped by 13 m thick shallowing upward unit. In these two units the fossils size always increases upward. The 9.5 m deepening upward unit includes two parasequences of 6 m thick (PS6), and 2.5 m thick (PS7) that both cover the Langhian age, and the 13 m shallowing

upward unit includes five parasequences 2.5 m thick (PS8) and 11.5 m thick (PS9-PS12) that cover the Serravallian age.

The 6 m thick (PS6) is made of 1 m thick deepening upward intensively bioturbated reworked bioclastic wackestone facies that is white in color, with normal graded bedding, and has no fossils, and 5 m thick shallowing upward unit of interbedded reworked bioclastic packstone facies and bioclastic wackestone facies that capped by thin layer of laterally laminated microbialites facies. The reworked bioclastic packstone facies are dominated by intact and fragmented large oysters at the base with normal graded bedding, where in the upper part is dominated by intact and broken bivalves and gastropods with reverse graded bedding. The bioclastic wackestone facies is dominated by bivalves and gastropods in the lower part with normal graded bedding and lamination, and by large intact oysters in the upper part with normal graded bedding. The laterally linked laminated microbialites facies that associated with some pellets marks the top of this shallowing upward unit.

The 2.5 m thick (SP7) is made of 0.2 m thick deepening upward unit of evaporite facies of yellow color sallow tail selenitic gypsum, and has no fossils preserved, and 2.3 m thick shallowing upward unit of pelletal packstone facies that overlain by bioclastic wackestone facies. The pelletal packstone facies is dominated by intact small bivalves and gastropods with reverse graded bedding, where the bioclastic wackestone facies is dominated by small bivalves and gastropods with normal graded bedding and lamination.

The 2.5 m thick (PS8) is made of 1 m thick deepening upward unit entirely of evaporite facies of yellow color sallow tail selenitic gypsum, and has no fossils preserved, and 1.5 m thick shallowing upward oyster dominated reworked bioclastic packstone. It contains fragmented and intact large oysters and shows normal graded bedding with mudcracks at the top surface.

The 11.5 m thick shallowing upward unit forms 4 shallowing upward parasequences of microbialites of 3 m thick (PS9), 3 m thick (PS10), 3 m thick (PS11), and 2.5 m thick (PS12). They are made of stromatolites that increase in size upwards and

always associated with ooids, oncoids, and pisoids, and have greyish white chert nodules. The 4 stromatolites parasequences are separated from each other by mudcracks at top surfaces. The upper two microbialites shallowing upward units have some gypsum. At the very top part of the very upper microbialites shallowing upward unit there is pellets association, well bedding and very low angle cross bedding sedimentary structures.

3rd-order sequence S4

The S4 is 11.5 m thick and covers the lower part of the Late Miocene Tortonian age. This 11.5 m thick 3rd order sequence is made up of 2 m thick deepening upward unit capped by 9.5 m thick shallowing upward unit. The S3 contains least 4 parasequences of 5.5 m thick (PS13), 3 m thick (PS14), 1 m thick (PS15), and 2 m thick (PS16).

The 5.5 m thick (PS13) is made up of 2 m thick deepening upward unit of reworked and rippled white evaporite bed with conglomeratic size evaPorites facies of yellow sallow tail selentic gypsum followed by friable fine to very fine quartz sandstone facies and green shale facies, and The 3.5m shallowing upward unit of cross bedded oolitic grainstone facies with some pellets, and evaPorites. The evaPorites facies is white in color, rippled, with reworked conglomeratic size yellow gypsum crystals, and microbial-like internal structures in it. The oolitic grainstone facies is very well bedded; planar cross bedded, laminated, with fenestral structures, and contains some intact bivalves and gastropods at the basal part.

The 3 m thick (PS 14) shallowing upward unit is made up of microbialites facies of stromatolites with basal laterally linked stromatolites, and association of ooids, oncoids, and pisoids. The top surface of this shallowing upward unit has mudcracks.

The 1 m thick (PS 15) shallowing upward unit is oolitic packstone associated with pellets and contains intact bivalves and gastropods fossils. It is well bedded with reverse graded bedding.

The 2 m thick (PS 16) shallowing upward unit is bioclastic packstone facies dominated by intact dwarfed bivalves and gastropods. It has some pellets, and ooids. It is well bedded with reverse graded bedding.

3rd-order sequence S5

The S5 is 5.5 m thick and covers the upper part of the Late Miocene Tortonian age. It is made up of 2 m thick deepening upward unit capped by two shallowing upward units of 1.5 m and 2 m thick. The S5 comprises two parasequences (PS 17) and (PS 18).

The 3.5 m thick (PS 17) is made up of 2 m thick deepening upward unit of entirely evaPorites facies of yellow sallow tail selentic gypsum, and 1.5m shallowing upward unit made up of pelletal packstone facies that is very well bedded with reverse graded bedding, and conations intact dwarfed bivalves and gastropods.

The 2 m thick (PS18) shallowing upward unit is cross bedded oolitic grainstone facies with some pellets, oncoids, and pisoids. It is very well bedded; trough cross bedded, planar cross bedded, small scale herring-bone cross bedded, with fenestral structures, and contains some intact bivalves and gastropods.

3rd-order sequence S6

The S6 is 3.5 m thick and covers the Late Miocene Messinian age. The S6 3.5 m thick is made up of 1 m thick deepening upward unit capped by two shallowing upward units of 1 m thick, and 1.5 m thick . The S6 is made up entirely of microbialites facies of structureless thrombolites heads. The S6 consists of two parasequences of 2.5 m thick (PS19) and 1 m thick (PS20).

The (PS19) is made up of 1 m thick deepening upward unit of structureless thrombolite heads that intercalates upwards with ooids and some intact dwarfed bivalves and gastropods, with mudcracked basal contact, and 1 m thick shallowing upward unit of

structureless thrombolites heads, intercalates with ooids, and conations intact dwarfed bivalves and gastropods with transitional basal surface and sharp mudcracked top surface. The (PS20) 1.5 m shallowing upward unit is structureless thrombolites heads, and contains intact dwarfed bivalves and gastropods. The basal surface is sharp and the upper surface has mudcracks.

In this study , the Cyrenaican Miocene carbonate platform, the changes in the gamma-ray profiles patterns, and the changes in the $\delta\ ^{13}C$ stable isotope curves patterns are in excellent agreement with the sedimentological analysis, and the field observed stratigraphic time surface and the correlated stratigraphic time sections. All data from these geological, geophysical, and geochemical methods support each other and helped to detect the precise time surfaces, parasequences, and sequences.

Palaeocurrents Data Analysis of the Cyrenaican Miocene Ar-Rajmah Group

The total number of the measured palaeocurrent data sets from the studied Cyrenaican Miocene carbonate platform is 129 readings (Fig. 14, & Tables 4 and 5). A data set of 87 readings measured from the unidirectional large scale planar and trough cross bedding of the oolitic grainstone facies. A data set of 2 readings measured from the unidirectional low angle planar cross bedding of the oolitic grainstone facies. A data set of 8 readings measured from the bidirectional herring bone cross bedding of the oolitic grainstone facies. A data set of 6 readings measured from the unidirectional clinoforms of the oolitic grainstone facies. A data set of 20 readings measured from the bidirectional long axis of microbialites facies. A data set of 2 readings measured from the bidirectional long axis of the tidal channel in the bioclastic Porites facies, the channel filled by pelletal packstone facies that fines up into bioclastic wackestone facies. A data

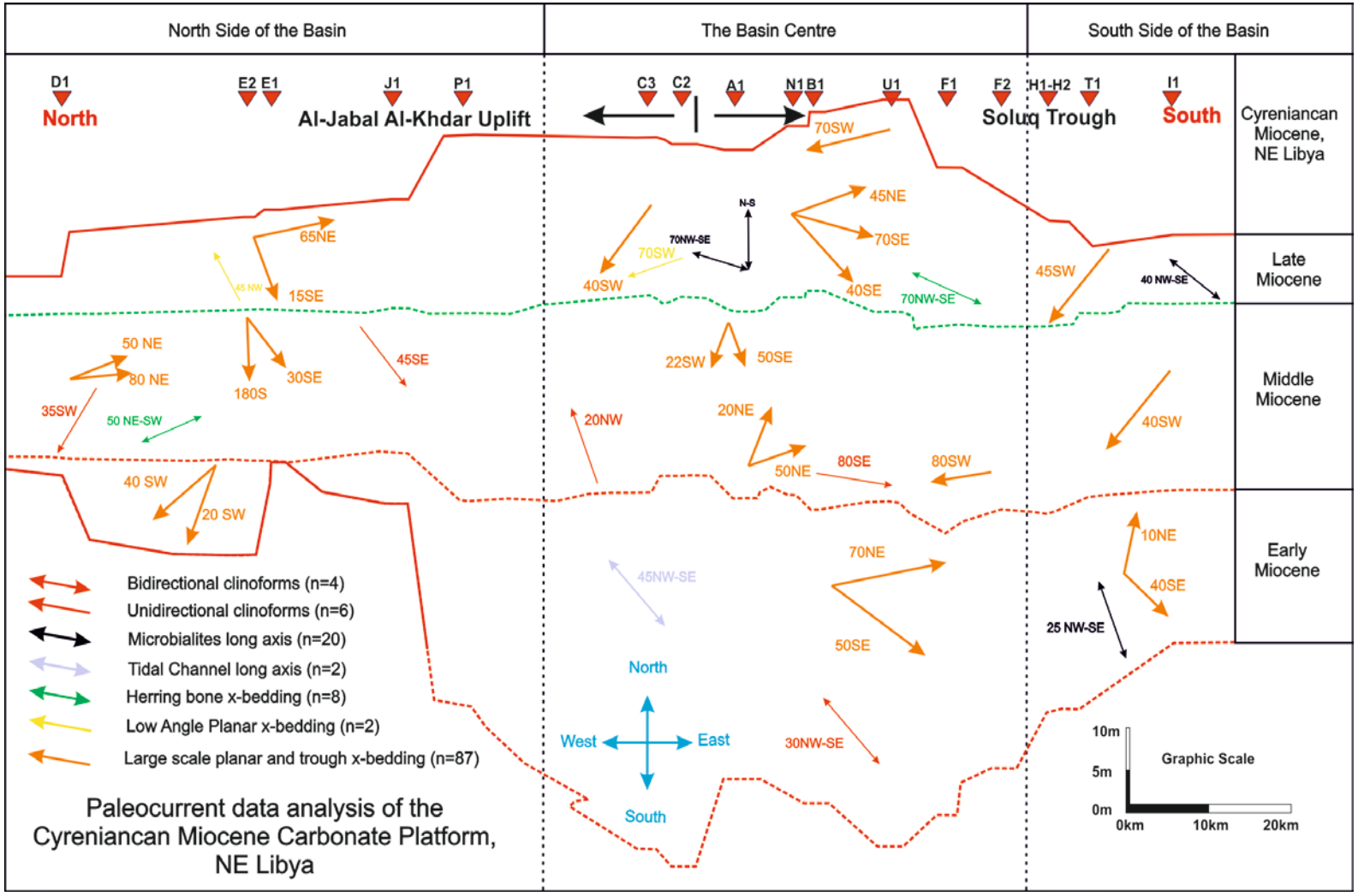

Figure 14. Palaeocurrents data analysis of the Cyrenaican Miocene carbonate platform, Ar-Rajmah Group.

Table 4. Palaeocurrent data of the Cyrenaican Miocene Ar-Rajmah Group.

Log Name	Elevation (m)	360 Direction in Degrees	Number of Readings	Facies
Bidirectional clinoforms				
B1	4.5-8.5	150	1	Reworked Bioclastic Packstone
B1	4.5-8.5	330	1	Reworked Bioclastic Packstone
U1	0-9m	340	1	Red algal-Reworked Red algal facies
U1	0-9m	160	1	Red algal-Reworked Red algal facies
Unidirectional Clinoforms				
B1	27.5-30	90	1	Oolitic grainstone
B1	27.5-30	105	2	Oolitic grainstone
C1	23.5-26.5	340	1	Oolitic grainstone
D1	1.5-6m	215	1	Oolitic grainstone
E1	10-13.5m	135	1	Oolitic grainstone
Microbialites Long axis				
F1	71.5-73	0	1	Thrombolites Microbialites
F1	71.5-73	180	1	Thrombolites Microbialites
F1	58-61	295	1	Stromatolites Microbialites
F1	58-61	115	1	Stromatolites Microbialites
F1	58-61	280	1	Stromatolites Microbialites
F1	58-61	100	1	Stromatolites Microbialites
I1	16-18m	300	1	Thrombolites
I1	16-18m	120	1	Thrombolites
I1	16-18m	340	1	Thrombolites
I1	16-18m	160	1	Thrombolites
I1	16-18m	15	1	Thrombolites
I1	16-18m	195	1	Thrombolites
I1	12-15m	300	1	Thrombolites
I1	12-15m	120	1	Thrombolites
T1	34-37m	325	1	Thrombolites Microbial Facies
T1	34-37m	145	1	Thrombolites Microbial Facies
T1	34-37m	320	1	Thrombolites Microbial Facies
T1	34-37m	140	1	Thrombolites Microbial Facies
T1	3-7.5m	335	1	Thrombolites Microbial Facies
T1	3-7.5m	155	1	Thrombolites Microbial Facies
Tidal Channel Long Axis				
S2	2.5-7m	315	1	Bioclastic Porites Facies
S2	2.5-7m	135	1	Bioclastic Porites Facies
Herring-Bone Cross Bedding				
F1	67.5-8.5	285	1	Fenestral Oolitic grainstone
F1	67.5-8.5	100	1	Fenestral Oolitic grainstone
Q1	20	320	1	Oolitic grainstone
Q1	20	160	1	Oolitic grainstone
D1	12.5	50	1	Oolitic grainstone
D1	12.5	230	1	Oolitic grainstone
D1	5	50	1	Oolitic grainstone
D1	5	235	1	Oolitic grainstone
Low Angle Planar Cross Bedding				
E1	17.5	315	1	Oolitic grainstone
C3	73	250	1	Oolitic grainstone

Table 5. Palaeocurrent data of Planar and trough cross bedding of the Cyrenaican Miocene Ar-Rajmah Group.

Log Name	Elevation (m)	360 Direction in Degrees	Number of Readings	Facies
Large Scale Planar and Trough Cross Bedding				
A1	51-53	200	2	Oolitic grainstone
A1	51-53	204	3	Oolitic grainstone
A1	47-49m	130	2	Oolitic grainstone
A1	45m	30	3	Oolitic grainstone
B1	28.5-29.5	55	2	Oolitic grainstone
C1	47.5	215	1	Oolitic grainstone
C1	46.5	210	2	Oolitic grainstone
C1	20	220	1	Oolitic grainstone
D1	10.5	80	2	Oolitic grainstone
D1	10.5	130	1	Oolitic grainstone
D1	9.5	80	2	Oolitic grainstone
D1	4m	145	1	Oolitic grainstone
E1	17	65	1	Oolitic grainstone
E1	16.5	165	2	Oolitic grainstone
E1	16	60	1	Oolitic grainstone
E1	14	180	1	Oolitic grainstone
E1	14	150	2	Oolitic grainstone
E2	9-13m	200	2	Oolitic grainstone
E2	4-7m	220	3	Bioclastic Grainstone
F1	67.5-69.5	45	2	Fenestral Oolitic grainstone
F1	67.5-69.5	50	2	Fenestral Oolitic grainstone
F1	67.5-69.5	140	2	Fenestral Oolitic grainstone
F1	67.5-69.5	120	1	Fenestral Oolitic grainstone
F1	67.5-69.5	110	1	Fenestral Oolitic grainstone
F1	30	70	5	Oolitic grainstone
F2	18-21m	130	3	Bioclastic grainstone
H1	14m	0	1	Bio-Oolitic grainstone
H1	14m	10	1	Bio-Oolitic grainstone
H1	10m	140	5	Bio-Oolitic grainstone
C3	72	245	3	Oolitic grainstone
N1	26m	20	5	Oolitic grainstone
N1	23m	50	3	Oolitic grainstone
Q1	20.5	220	2	Oolitic grainstone
Q1	14	120	3	Oolitic grainstone
U1	83.5	250	2	Bio-Microbial-Oolitic grainstone
U1	73	125	3	Oolitic grainstone
U1	40.5-44.5m	260	2	Oolitic grainstone
I1	38m	220	3	Bioclastic Packstone
I1	28	220	1	pelletal packstone
T1	27-33m	220	3	Fenestral Oolitic grainstone

set of 4 readings measured from the bidirectional clinoforms of the red algal reef facies, reworked red algal facies, and reworked bioclastic packstone facies.

In the southern part and the central part of the Cyrenaican Miocene basin, there is a NW-SE trend constantly taken by the bidirectional clinoforms, the bidirectional channels long axis, the bidirectional microbialites long axis, and the bidirectional herring bone cross bedding. In the northern part of the basin the bidirectional herring bone cross bedding has completely the opposite trend which was NE-SW.

The unidirectional clinoforms of the oolitic grainstone facies are restricted mainly to the Middle Miocene, and always have sharp basal surface and underlained by reworked bioclastic packstone facies or bioclastic packstone/wackestone facie. Bear in mind that the oolitic grainstone facies progradation was from the southern end and northern end of the basin towards the basin centre. During the Middle Miocene the unidirectional clinoforms move to the SW and SE directions in the northern part of the basin, where they move to the NW and SE directions in the central part of the basin. These clinoforms are lobes carried from the relatively deeper parts of the basin and spilled over the shallower parts of oolitic shoals.

The unidirectional large scale planar and trough cross bedding of the oolitic grainstone facies have different patterns in time and space within this Miocene basin. For instance, through the Miocene the palaeocurrents azimuth in the northern side of the basin always have the opposite direction for the palaeocurrents azimuth in the southern part of the basin, where the palaeocurrents azimuth in the basin centre always trying to maintain the same direction. During the Early Miocene the palaeocurrent azimuth in the northern side of the basin was in the SW direction, where in the southern and central parts were in the NE to SE directions. During the Middle and Late Miocene the palaeocurrents azimuths inverted, where the palaeocurrents azimuth of the northern side of the basin became NE to SE, the palaeocurrents azimuth of the southern part became SW, and the palaeocurrents azimuth in the central part stayed the same NE to SE most of the time. The inversion in the palaeocurrent azimuth most probably happened due to the

change between inlets that dominated during Early Miocene and outlets dominated the Middle and Late Miocene after the establishment of the oolitic grainstone shoals.

Discussion

Stratigraphic Chart and Chemostratigraphic Constrains on the Cyrenaican Miocene

Through time, geologists have been working on the Cyrenaican geological province to understand its sedimentological nature and to build its stratigraphy (Fig., 3&4). This integrated sedimentology-sequence stratigraphy-chemostratigraphy-diagenesis study reveals that the Cyrenaican carbonate platform preserves the whole Miocene section.

Geological investigations in Al-Jabal Al-Khdar were pioneered by Gregory (1911), who was the first to lay the foundation for the stratigraphic nomenclature of most the stratigraphic units. Al-Jabal Al-Khdar geomorphology, stratigraphy and hydrogeology were studied by Desio (1935 a and b, 1939). Floridia (1935); Marchetti (1934a, 1934b, 1938); Marinelli (1920); Silvestri (1928, 1929) and Stefanini (1923a, 1923b, 1935). Most of the Italian geological studies in Al-Jabal Al-Khdar were later reviewed by Desio (1968). The first comprehensive geological map of Libya, at a scale 1:20,000 was published by the USGS (Conant and Goudarzi, 1964, 1967). The first noteworthy publication on the geology of Al-Jabal Al-Khdar was edited by F.T. Barr of OASIS and published in the 1968. Pieterz (1968), Kleinsmied and Vander Berg (1968), and then later Barr and Weeger (1972) had studied Al-Jabal Al-Khdar surface geology. The Industrial Research Centre decision to re-map the country on a scale 1:250,000 resulted in the publication of a series of maps and explanatory booklets on Al-Jabal Al-Khdar these include sheets of Benghazi (Klen, 1974); Al Bayda (Rohlich, 1974); Dernah (Zert, 1974); Solug (Francis and Issawi, 1977); Zt. Masus (Mazhar and Issawi, 1977); Bir Hacheim (Swedan and Issawi, 1977) and Al Bardia (El Deftar and Issawi, 1977);

Ajdabya (Giglia, 1984); Wadi al Hamin (Carmignani, 1984); Wadi al Khali (Giammarino, 1984) and Al Mufawwaz (Manetti, 1984). ElKhodary (1980) studied the planktonic forams from the Middle Eocene escarpment of Al-Jabal Al-Khdar. Rohlich (1980) studied the tectonic development of Al-Jabal Al-Khdar. El-Hawat and Salem 1985, 1987, Megerisi and Mamgain, 1980 tried to rectify the stratigraphic subdivision, simplify nomenclature and rematch the geological boundaries of Al-Jabal Al-Khdar. El Arnauti and Shelmani (1985) studied the stratigraphic and structural setting of north-eastern Libya. El Hawat and Salem (1987), studied the Sedimentology of the Miocene sequence of Al-Jabal Al-Khdar. Rholich (1978, 1980) published Geologic development of Al-Jabal Al-Khdar and Tectonic development of Al Jabal al Akhdar respectively. El Hawat and Shelmani (1993) published booklet of short notes and guidebook of geology of Al-Jabal Al-Khdar. El Hawat and Abdulsamad (2004) published a field guide to the geology and archaeology of Cyrenaica. Abdulsamad and El-Zanati (2013) published Miocene benthic foraminifera from the Soluq area, NE Libya: biostratigraphy and environmental significance; this palaeontology based paper indicates the presence of the whole Miocene section in the Soluq Trough area in Cyrenaica.

The Miocene succession NE Libya exposed at the north-western part of the Al-Jabal Al-Khdar and extends southward to Soluq trough. It was studied by El-Hawat (1980b) El Hawat and Salem (1987), the I.R.C. mapping (Klen, 1974) Benghazi sheet NI 34-14, and (Francis and Issawi, 1977) Soluq sheet NH 34-2. So far, no sequence stratigraphic research has been conducted on Miocene section exposed in the NE part of Libya. The aim of this study is to document the detailed sedimentological nature of the Miocene sequence, Ar-Rajmah Group in Al-Jabal Al-Khdar and its equivalent in Soluq trough towards the south, and applying the sequence stratigraphic concepts on this mixed carbonate-siliciclastic succession.

The sedimentological study to identify the depositional facies and environments leads to the reconstruction of the palaeogeography and together with palaeocurrent directional data have to be used as a tool in the palaeotopographic construction and the depositional environments distribution. The sequence stratigraphic study has been based

on the determination of time surfaces such as sequence boundary s.b, transgressive surface t.s. and maximum flooding surface m.f.s. and facies geometries, architecture and vertical stacking pattern. By that, the depositional systems and their depositional systems tracts (transgressive systems tract T.S.T, highstand systems tract H.S.T and lowstand systems tract L.S.T) can be deduced and delineated.

Depositional Model and Shoreline Progradation of the Cyrenaican Miocene Ar-Rajmah Group

The evolutionary depositional model of this current study revealed the dominant depositional theme on the Cyrenaican-ramp system. It highlighted the dominant and laterally continuous bodies of oolitic grainstones, microbial carbonates, and red algae that are important targets as subsurface oil reservoirs.

The Cyrenaican Miocene carbonate platform is a ramp system. Through the Miocene the peritidal and ramp crest facies were constantly prograding over the subtidal facies (Fig. 15&16). The peritidal facies are evaPorites, microbialites, pelletal packstone, bioclastic Porites, sandstone, and green shale. The ramp crest is oolitic grainstone, and subtidal facies are reworked bioclastic packstone, reworked red algal facies, bioclastic packstone, and coralline red algal packstone. The coralline red algal packstone facies and bioclastic packstone facies dominated the lower part of the Cyrenaican platform and formed its rhodalgal dominated ramp during the Early Miocene. The rhodalgal dominated ramp facies had been progressively replaced by the ramp crest oolitic grainstone facies and the microbialites dominated peritidal facies in the middle and upper parts of the platform and formed the microbialites-ooids dominated ramps during the Middle and Late Miocene. In addition, throughout the Miocene the shoreline vertical aggradation became progressively higher than the shoreline horizontal progradation (Fig.13). For instance, during the Early and Middle Miocene; the Aquitanian, Burdigalian and Langhian ages, the shoreline horizontal progradation was higher than the shoreline vertical aggradation, where in the Middle and Late Miocene,

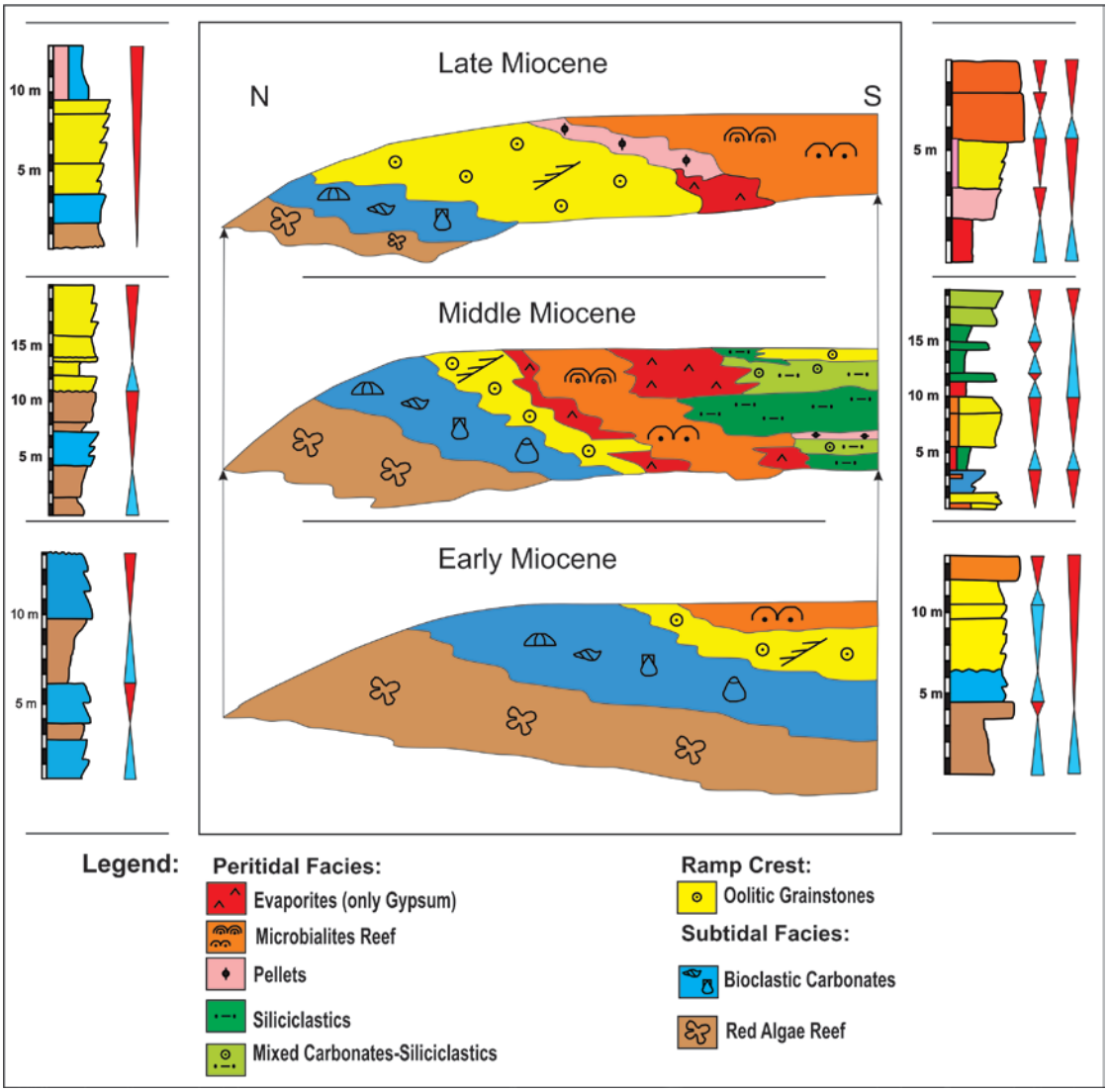

Figure 15. Evolutionary depositional model of the Cyrenaican Miocene carbonate platform, Ar-Rajmah Group.

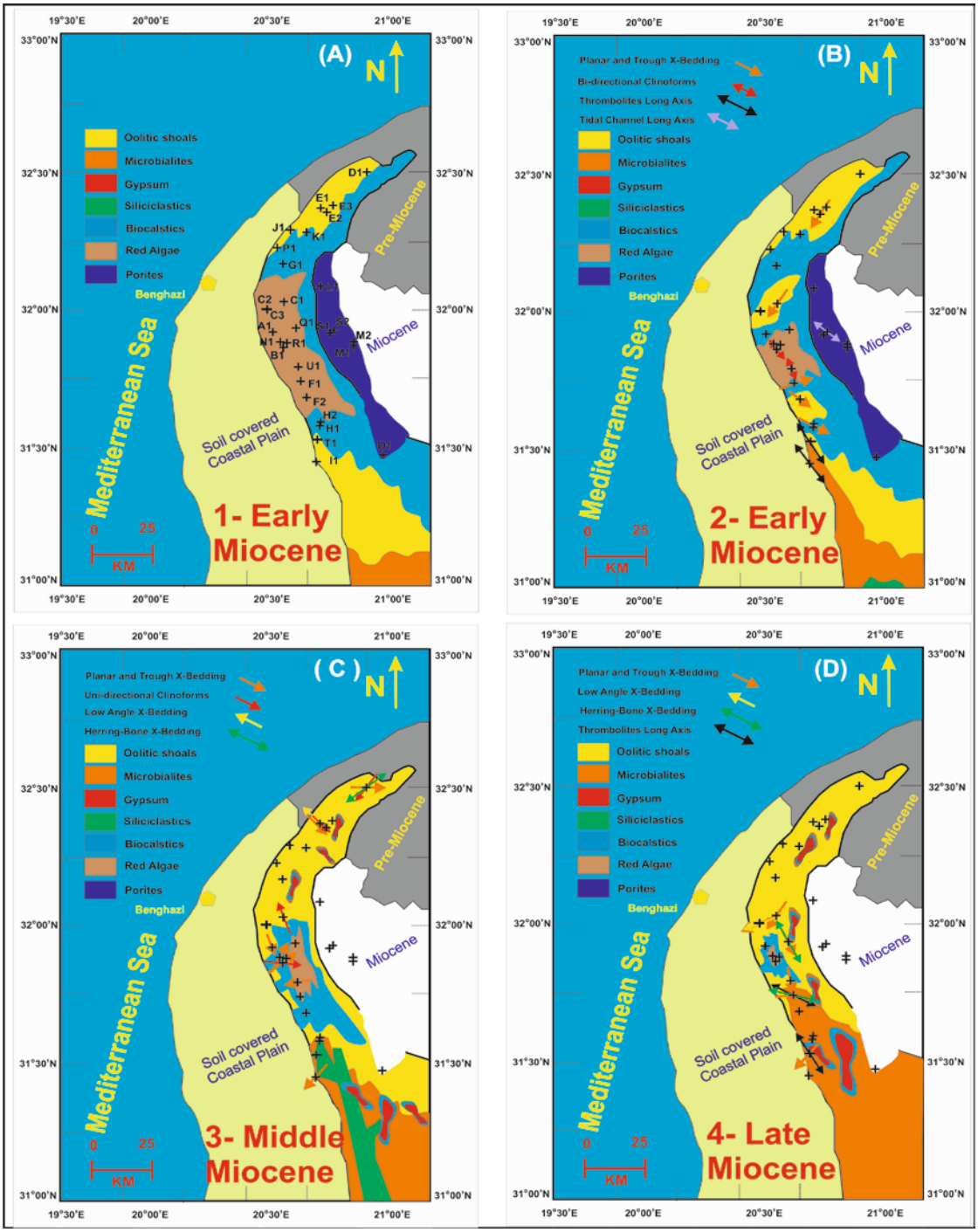

Figure 16. Depositional facies paleogeography and palaeocurrents of the Cyrenaican Miocene carbonate ramp, Ar-Rajmah Group.

the Serravallian and Tortonian ages, the shoreline vertical aggradation was higher than the shoreline horizontal progradation.

The Depositional Models of the Mediterranean Region

The Miocene of the Mediterranean region has four types of reef builders (Table 6), can be comprised in two facies models (Franseen et.al. 1996). The Miocene four types of reef builders are: (1) Dominant Hermatypic coral reefs (associated with red algae, bryozoans, and benthic forams), (2) Dominant ahermatypic coral mounds and thickets, (3) Rhodalgal mounds and biostromes, and (4) Stromatolite mounds and blankets (interbedded with oolitic and bioclastic grainstones). The Miocene has two Facies Models: (1) fringing coral reef with poorly developed or absent lagoons, (2) ramp of dominant sigmoidal rhodalgal facies with large benthic forams.

Rhodalgal thrives in all ages of the Miocene, however, coral reefs thrive and diverse during warm ages. Also, terrigenous supply and upwelling of cold nutrients waters will reduce coral diversity or replace it into rhodalgal. Stromatolites developed in marine environment unfavourable for coral reefs and rhodalgal carbonates (Franseen et.al. 1996).

Miocene Sequence Stratigraphic Framework of the Mediterranean Region, 2nd-Order Sequences

The Miocene of the Mediterranean (Table 7) consists of three 2nd-order sequences (Haq et.al, 1987). TB1 is the lower 2nd order sequence (21-30 my) includes Chattian of the Oligocene up to most of the Aquitanian Miocene. TB2 is the middle 2nd-order sequence (21-10.5 my) comprises uppermost Aquitanian, Burdigalian, Langhian, and Serravallian. TB3 is the upper 2nd-order sequence (10.5-0 my) includes Tortonian, Messinian, and up to Holocene (Esteban, 1996).

Table 6. Comparison between the Miocene reef builders types and platforms style in the Mediterranean region and the Cyrenaica, NE Libya.

Mediterranean Miocene Reef Builders (Franseen et.al. 1996)	**Mediterranean Miocene Platform Style (Franseen et.al. 1996)**	**Cyrenaican Miocene Reef Builders (this study)**	**Cyrenaican Miocene Platform Style (this study)**
Dominant Hermatypic coral reefs (associated with red algae, bryozoans, and benthic forams). Dominated the Aquitanian, Langhian, and Tortonian warmer Miocene ages	The hermatypic coral reefs developed as fringing reefs, patch reefs, and sometimes as extensive barrier reefs.		
Dominant ahermatypic coral mounds and thickets			
Rhodalgal mounds and biostromes. Dominated the Burdigalian, and Serravallian colder Miocene ages.	Rhodalgal mounds and biostromes form well-developed ramps. Rhodalgal repeatedly alternated with hermatypic coral reefs	Red algal mounds and biostromes. Dominated the Early Cyrenaican Miocene.	Red algal mounds and biostromes form well-developed ramp. Occasionally intercalated with hermatypic patch coral reef, and laterally changed into Porites in the Early Miocene only.
Stromatolite mounds and blankets (interbedded with oolitic and bioclastic grainstones). Dominated the Serravallian and Messinian Miocene ages of crises.	Stromatolites developed on shelf margins, slopes, shelf interiors, and basin floors	Microbialites mounds and patches (interbedded with oolitic grainstone, bioclastic packstone, and evaPorites). Dominated the Middle and Late Cyrenaican Miocene.	Microbialites developed on shelf interior and progrades on the oolitic grainstone facies.

Table 7. Synthesis of the Mediterranean Miocene three 2nd-order supersequences and the associated global events.

2nd Order sequences	Tectonic Event	Time		Sea Level and climate	Dominant Lithology
The Upper TB3 (10.5-0 Ma)	Repeated Alpine tectonic uplifts, the Mediterranean seaways in the west gradually isolated from the Atlantic Ocean, land-locked Mediterranean ocean	Late Miocene	Messinian	Prolonged sea level fall	Sediment accumulation of thick extensive evaporite deposits "Messinian Crisis" interbedded with marine, restricted marine, brackish, and hypersaline sediments.
			Tortonian		Coral reefs developed, but were smaller in the Early Tortonian.
	The collided Arabian-Turkish plates uplifted: semi-closed Mediterranean Ocean, complete disconnection in the east to the (Indo-Pacific), and narrow shallow seaways in the west to the (Atlantic Ocean)	Middle Miocene	Latest Serravallian	Major global sea level fall	Read beds and evaPorites dominated the eastern Mediterranean, where open marine coral reefs during global highstands dominated the central and western Mediterranean.
The Middle TB2 (21-10.5 Ma)			Serravallian	Subtropical to temperate, colder climate dominated	Poor fauna, thick evaPorites deposits "Serravallian Crisis". Rare rhodalgal and coral occurrence observed only in the Gulf of Suez.
			Langhian- Late Burdigalian	Warmer climate dominated	Climate allowed moderately diverse coral "Porites" to develop extensive carbonate platforms, and an unconformity surface separates the two coral reef units of the upper most Burdigalian and Langhian.
	The Arabian-Turkish plates collision interrupted marine connection with the Indo-Pacific region in the east	Early Miocene	Early Burdigalian	Sea level fall, Cool climate	Temperate water rhodalgal and foramol carbonate facies dominated, the organic rich marls and diatomaceous sediments deposited in the basin.
The Lower TB1 (30-21 Ma)			Aquitanian	Sea level fall, Tropical to subtropical	Extensive rhodalgal, highly diverse coral reefs, and evaporite deposits in shallower areas.
			Sea level fall, global cooling due to increased Antarctic glaciation		Extensive evaporite deposits in straits, and brackish marine conditions dominated in the eastern Paratethys.
	Ural rise due to the plate movement in the pacific region	Oligocene	Chattian	Sea level fall global climatic minimum	

Synthesis of the Mediterranean Miocene three 2nd order sequences based on (Evan K. Franseen et.al. 1996; Esteban, 1996; Haq et.al, 1987; Hallam, 1981; Barron and Keller, 1982; Sensu Lees and Buller, 1972; Carannante et.al. 1988; Purser et al, 1996; Buchbinder et al 1993, and 1996 edited by Franseen et.al. 1996; Permanyer and Esteban, 1973; Orszag-Sperber and Piolt, 1976; Lietz and Schwarzbach, 1970; Chevalier, 1961; Wijsman-Best and Boekschoten, 1982; Esteban, 1996; Rogl et al, 1978; Demarcq, 1984, 1985; Rouchy, 1982a, b; Scott and McGovean, 1985)

The Mediterranean Miocene 2nd and 3rd-order cycles have a very distinctive faunal dominance. The T.S.T is dominated by rhodalgal; H.S.T is dominated by coral reef, while late T.S.T and early H.S.T is dominated by siliciclastic and stromatolites (Franseen et.al. 1996). In cases when the coral reefs are absent in the 2nd and 3rd-order sequences, all the systems tracts will be dominated by rhodalgal facies and significant lithological variations such as large scale sigmoidal clinoforms of rhodolithic facies, mollusc, forams, or echinoid beds. The rhodalgal facies form extensive Miocene ramps (Franseen et.al. 1996).

Miocene Sequence Stratigraphic Framework of the Cyrenaican Ar-Rajmah Group, Regionally Correlative 2nd -and 3rd-Order Sequences

For the 2nd order supersequences in the Cyrenaican Miocene carbonate platform the HST of SS1, Early Miocene, is dominated by rhodalgal that associated with echinoid-rich beds, large oyster-rich beds, small patches of horn corals, massive and branched thick *Porites* corals restricted only to the eastern part, and large scale microbialites and oolitic shoals restricted only to the south. The TST of SS2, Middle Miocene, is dominated by microbialites, evaporates facies, oolitic shoals in association with reworked rhodalgal facies in the northern part, and siliciclastic facies in the southern part. The HST of the SS2, Late Miocene, is dominated by oolitic shoals microbialites in association with reworked rhodalgal facies, and evaPorites facies dominant in the southern part.

For the SS1 of the Cyrenaican Miocene, the early HST of is dominated by rhodalgal and bioclastic packstone open marine facies. For the SS2 of the Cyrenaican Miocene, the late T.S.T is dominated by microbialites, evaporates in association with siliciclastic and the early H.S.T oolitic shoals in association with microbialites and evaporates facies.

The Ar-Rajmah Group Miocene carbonate rocks record two 2nd-order supersequences (97 m maximum thickness); contain six 3rd order sequences, and at least 10 higher frequency 3rd order sequences. The older 2nd order sequence is not complete and only the shallowing upward unit (HST) preserved, where the younger 2nd-order sequence is complete and both the deepening upward unit (TST), and the shallowing upward unit (HST) are preserved. The TST of the younger 2nd-order sequence is separated by a sharp disconformity surface from the preserved HST of the older 2nd order sequence, and by maximum flooding zone from the HST of the younger 2nd order sequence (Figs. 11). The HST of the older 2nd-sequence is the Early Miocene Benghazi Formation (46 m maximum thickness), the TST and HST of the younger 2nd order sequence occur in the Middle and Late Miocene Wadi Al-Qattarah Formation (26 m and 25m maximum thicknesses respectively). The HST of the older 2nd order sequence includes two 3rd order sequences, S1 and S2. It is composed mainly of coral reefs, Porites, red algae (rhodoliths), and open marine skeletal packstone containing large bivalves, gastropods, oysters, and echinoids. The TST of the younger 2nd order sequence includes only one 3rd-sequences named S3. It has reworked red algae fragments at its base, shallowing upward into bioclastic grainstone, capped by cross-bedded oolitic grainstone. Microbialites (stromatolites, thrombolites, and laminites), and evaPorites associated with pelletal mudstone, pelletal packstone, interbedded with fine to very fine quartz sandstone and green shale mark the upper part of this 3rd-order sequence. The siliciclastics appear only in the southern part of the field area. The HST of the younger 2nd order sequence includes three 3rd-order sequences S4, S5, and S6. It is dominated by continuous bodies of oolitic grainstone and microbialites associated with some bioclastic carbonates, red algae, and pellets. The shallowing upward parasequences range in thickness from 2 m to more than 8.5 m. In the study area, the peritidal facies are thicker in the south, where the ramp crest-subtidal facies thicker in the north. Also, the peritidal facies are dominant in the younger sequences, while the ramp crest-subtidal facies dominant in the older sequences.

On a regional scale, the Miocene carbonate rocks of the Cyrenaica have different facies and sequences patterns than the Mediterranean region. The Cyrenaican Early Miocene is dominated by red algae, while the Middle and Late Miocene are dominated by oolitic grainstone and microbialites. On the Mediterranean region, the Early Middle Miocene rocks are coral reefs that change vertically into red algae, while the Late Miocene is evaPorites and coral reefs (e.g. Franseen, 1996).

In the study area, the peritidal facies are thicker in the south, where the ramp crest-subtidal facies thicker in the north. Also, the peritidal facies are dominant in the younger sequences, while the ramp crest-subtidal facies dominant in the older sequences. There are notable differences between these six 3rd-order sequences of the Cyrenaican Miocene. Thicknesses of the bioclastic facies and the red algal facies decrease upwards through time, whereas the thicknesses of the oolitic grainstone facies and the microbial facies increase upwards through time. Generally, the rate of shoreline aggradation increases and becomes higher than the rate of progradation through the Cyrenaican Miocene time (Fig.13). In addition, the thick evaporite facies only dominates the 3rd-order sequences of the Serravallian and the Tortonian. The peritidal siliciclastic facies influence is only restricted to the 3rd-order sequences of the Langhian and Serravallian of the Middle Miocene. The peritidal and ramp crest facies progrades from both south and north sides of the basin towards the subtidal facies in the basin centre. The maximum flooding zone (MFZ) is the high G-Ray zone with relative enrichment in the $\delta\ ^{13}C$ carbon stable isotopes signature, and has very thick beds of evaPorites facies, oolitic grainstone facies, microbialites facies, green shale facies, pelletal packstone facies, reworked red algal facies, and bioclastic packstone facies.

Paleogeographic maps with palaeocurrents analysis of the Cyrenaican Miocene Ar-Rajmah Group

The reconstruction of the palaeogeographic maps for the study area proved that the Cyrenaican Miocene carbonate platform deposited within a structurally controlled elongated water body that extends roughly north-south parallel to two major fault lines that form the present day lower and upper escarpments (Fig. 16). This elongated water body was shallow at both northern and southern ends and deep in the middle. The ramp crest oolitic grainstone facies and the peritidal facies started since the Early Miocene to prograde from the northern and southern ends of the elongated basin towards the ramp subtidal facies in centre of the elongated basin. During the Middle and Late Miocene the ramp crest oolitic grainstone facies kept prograding towards the basin centre filling up the space on the expenses of the ramp subtidal bioclastic packstone and red algal packstone facies.

The Miocene palaeography of the Mediterranean region

The Miocene palaeography of the Mediterranean region was largely affected by different tectonic events. The first tectonic event was in the north, the rise of the Ural Mountains, due to the late Oligocene plate movement in the Pacific region. The second was in the east, the Arabian and Turkish plates collision during Early Miocene, interrupted the marine connection with the Indo-Pacific region. The third event was during the latest Serravallian, the collided Arabian and Turkish plates uplifted along with a major global sea level fall. The Mediterranean ocean became semi-closed, disconnected completely from the Indo-Pacific in the east, but still connected with narrow shallow seaways with the Atlantic Ocean in the west. The fourth event was in the west during the Messinian; the Mediterranean gradually isolated from the Atlantic Ocean and became a completely land-locked ocean due to the repeated Alpine tectonic uplifts (Esteban, 1996).

Due to paleogeographic differences in the Mediterranean region during the Miocene, the depositional sedimentary packages affected and varied. The Miocene of the tectonically active eastern Mediterranean region suffered from early isolation and alternation of evaPorites and rhodalgal carbonate ramps. The Miocene of the stable central Mediterranean region shows dominant open marine conditions that change gradually upward into restricted marine environments. The Miocene of western Mediterranean region suffered from the siliciclastic influx and continental-lacustrine deposits due to repeated tectonism.

Paleoclimate of the Cyrenaican Miocene Ar-Rajmah Group

The paleoclimate of the Cyrenaican Miocene platform can be deduced from the carbonate rocks components and depositional facies (Table 6). The Early Miocene is dominated by the open marine coralline red algal facies, and bioclastic packstone facies, besides the lagoonal bioclastic Porites coralline facies. On the other hand, the Middle and Late Miocene are dominated by the oolitic grainstone facies, microbialites facies, and evaporite facies that through time replaced gradually and completely the open marine facies. These changes in the carbonate facies through time indicate that the climate during the Early Miocene was warm and humid to allow the coralline facies to dominate. However, during the Middle and Late Miocene the climate became colder, and semiarid that led to the gradual displacement of the coralline facies by the microbialites facies and the evaPorites facies.

The Miocene Paleoclimate of the Mediterranean Region

The Miocene coral reefs reflect a global cooling trend associated with a decrease in coral diversity. The environmental conditions change from open marine, humid tropical to land-locked semiarid and marginally subtropical (Esteban, 1996).

During the Aquitanian the Mediterranean climate became tropical to subtropical with sea level fall and global climatic minimum (Hallam, 1981). It was an open ocean with extensive rhodalgal and highly diverse coral reefs. EvaPorites deposited in the shallower areas (Esteban, 1996).

Sea level fall and Antarctic glaciation led to global cooling that coincide with Early Miocene collision (Barron and Keller, 1982). The Early Burdigalian cool climate allowed only the temperate water rhodalgal and foramol carbonate facies to dominate (Sensu Lees and Buller, 1972; Carannante et.al. 1988). The organic-rich marls and diatomaceous sediments deposited in the basin (Esteban, 1996).

The Late Burdigalian and Langhian were dominated by a warmer climate that allowed moderately diverse corals to develop extensive carbonate platforms in the Mediterranean region (Purser et al, 1996; Buchbinder et al 1993, and 1996; Permanyer and Esteban, 1973; Orszag-Sperber and Piolt, 1976; Lietz and Schwarzbach, 1970; Chevalier, 1961; Wijsman-Best and Boekschoten, 1982; Esteban, 1996). An unconformity surface separates the two coral reef units of the upper most Burdigalian and Langhian. *Stylophora*, *Porites*, and *Tarbellastraea* are the dominant Langhian coral reefs constituents (Esteban, 1996).

The Serravallian is dominated by a colder climate and poor subtropical to temperate fauna associated with thick evaPorites deposits in the Mediterranean (Esteban, 1996). This event is called “Serravallian crisis” by (Rogl et al, 1978; Demarcq, 1984, 1985), where its depositional facies relationships and patterns are similar to the Messinian evaPorites facies (Rouchy, 1982a, b). However; a rare Serravallian rhodalgal with coral reef observed in the Gulf of Suez (Scott and McGovean, 1985).

During the latest Serravallian the collided Arabian and Turkish plates uplifted along with a major global sea level fall. The Mediterranean ocean became semi-closed, disconnected completely from the Indo-Pacific in the east, but still connected with narrow shallow seaways with the Atlantic Ocean in the west. The eastern part was dominated by red beds and evaPorites, while the central and western parts became dominated by open marine coral reefs during global high stands (Esteban, 1996).

During the Tortonian and Messinian coral reefs developed; however, they were smaller in the Early Tortonian. During Messinian, the Mediterranean gradually isolated from the Atlantic Ocean, thick and extensive evaPorites precipitated, due to the repeated tectonic uplifts, sea level falling and sediments accumulation. The evaPorites inter-bedded with marine, restricted marine, brackish, and hypersaline sediments (Esteban, 1996).

Conclusions

The Ar-Rajmah Group of the Cyrenaica Platform is a ramp system with irregular palaeotopography. The platform has two 2nd-order supersequences that include six 3rd order sequences. The oldest 2nd-order supersequences made of HST, where the youngest 2nd order supersequence made of TST, and HST. The TST is separated by a sharp unconformity surface from the older HST, and by a maximum flooding zone from the younger HST. The HST of the older 2nd-order supersequence represents the Benghazi Formation of the Early Miocene. The TST and HST of the younger 2nd-order supersequence represent the Wadi Al-Qattarah Formation and its lateral equivalents Al-Sceleidima Formation and Msus Formation. The shallowing upward 3rd-order sequences range in thickness from 3.5 m to more than 22.5 m.

The Early Miocene ramp system is dominated by red algal and bioclastic facies, the Middle and Late Miocene ramp system is dominated by microbial-oolitic grainstone facies in association with evaPorites. The Porites corals are only present in the Early Miocene, whereas the siliciclastic facies are only present in the Middle Miocene. This outcrop study of the Ar-Rajmah Group extends for more than 130 km along a dip profile and its excellent 3-D exposure makes it an analogue for ooid grainstone, microbial carbonate, and red algae reservoirs in the subsurface within the Mediterranean region and globally.

CHAPTER III

STABLE ISOTOPE CHEMOSTRATIGRAPHY OF THE CYRENAICAN MIOCENE AR-RAJMAH GROUP, AL-JABAL AL-KHDAR UPLIFT AND SOLUQ TROUGH, NE LIBYA

Overview

Four measured sections (each 25-75 m thick) of the Miocene Ar-Rajmah Group carbonate rocks in Cyrenaica, northeast Libya (Fig. 17), were sampled every 0.5 m for whole rock stable isotope ($\delta^{18}O$, $\delta^{13}C$) chemostratigraphy. The Ar-Rajmah Group chemostratigraphic data indicates this unit preserves a record of almost the entire Miocene. The Early Miocene stable isotope record is generally enriched in both $\delta^{18}O$ and $\delta^{13}C$, the Middle Miocene is enriched in $\delta^{13}C$ but depleted in $\delta^{18}O$, and the Late Miocene is depleted in both $\delta^{18}O$ and $\delta^{13}C$. The $\delta^{18}O$ data ranges from -9.2 to 3.7 ‰ VPDB, and the $\delta^{13}C$ data ranges from -6.7 to 3.0 ‰ VPDB.

The shallowing upward Cyrenaican Miocene carbonate rocks are made up of two shallowing upward 2nd-order supersequences (SS1-SS2) that contain six 3rd-order sequences (S1-S6). Two important chemostratigraphic events are recorded in the 3rd-order sequences in the Cyrenaican Miocene. The Cyrenaican Middle Miocene 3rd-order sequence 3, Langhian-Serravallian, has the highest enrichment of both oxygen and carbon isotopes, which coincides with the Monterey carbon maximum event, a high gamma ray zone of the maximum flooding zone, and siliciclastic influx. The increased $\delta^{13}C$ upward enrichment in 3rd-order sequence 3 was produced by increased carbonate productivity and river runoff. The Tortonian 3rd order sequence 4 has the most depleted $\delta^{13}C$ and $\delta^{18}O$ records and both are depleted progressively up section due to the emergence of the progressively shallowing restricted shallow-water carbonate platform.

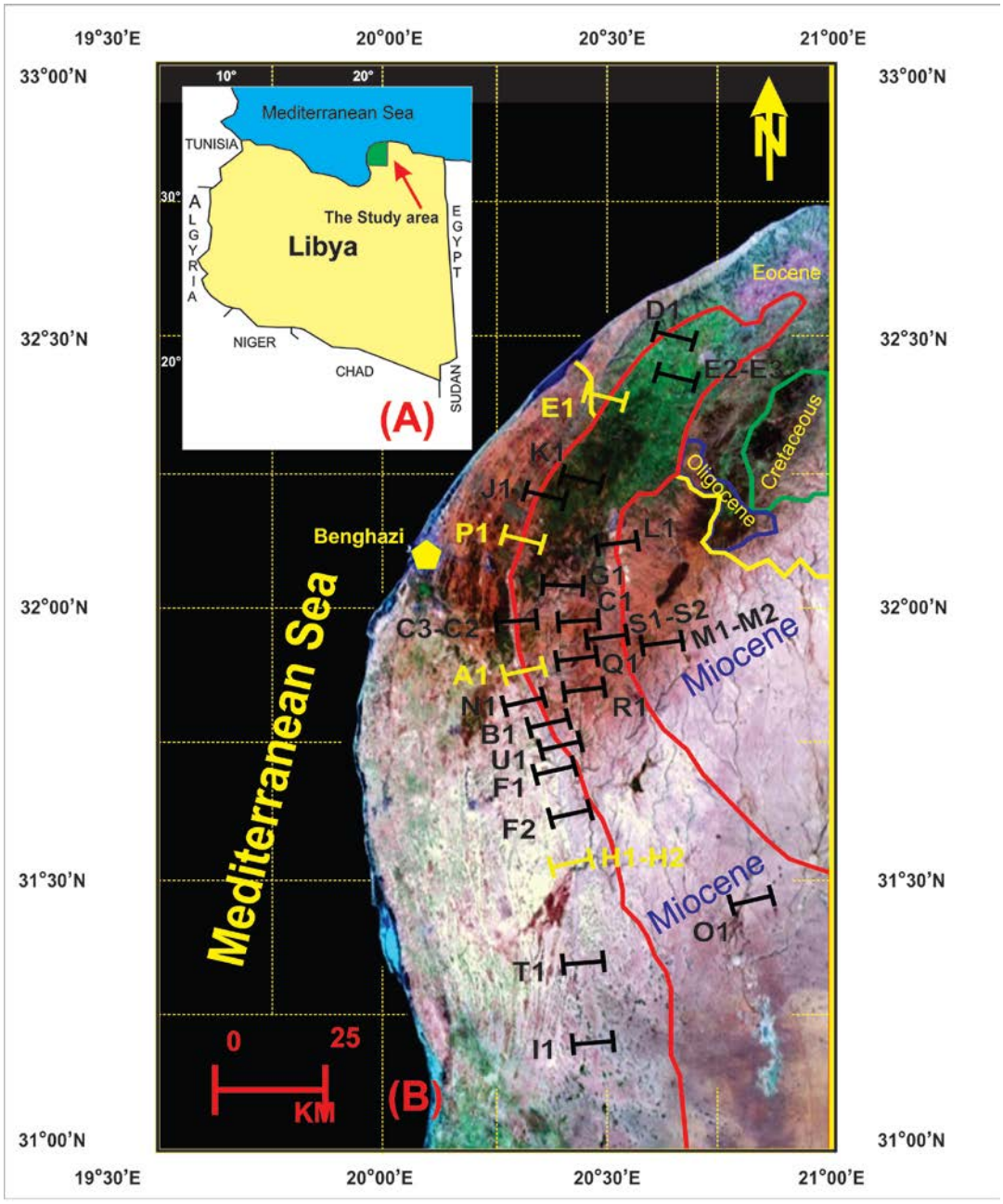

Figure 17. (A) Location map of the study area in northeastern Libya. (B) Landsat image of NE Libya showing the geological boundaries of Cretaceous- Tertiary rocks. The geological boundaries are based on the IRCs sheet-Benghazi (Klen, 1974) and sheet-Soluq (Francis and Issawi, 1977) that were later modified by (El-Hawat et al., 1987). Measured sections are shown by colored bars, the yellow colored bars represent sections sampled for chemostratigraphy.

Introduction

Carbon and oxygen isotopes variations occur due to the changes in the chemical composition and temperature of the oceans. Thus, a common procedure to decipher the geologic record of an area, is to analyze the carbon and oxygen isotopes of the carbonate rocks to trace the chemical composition and temperature of paleooceans, paleoclimate changes due to glacial and non-glacial periods, and diagenetic waters (Shackleton and Opdyke,1973; Weissert and Lini, 1991; Marshall, 1992; Jenkyns, 1995; Emiliani,1955; Weissert et al., 1998; Veizer et al., 1999; Stoll and Schrag, 2000; Erbacher et al,. 2002; Brand,2004; Grossman et al., 2008; and Grossman, 2012a). In addition, carbon isotopes of carbonate rocks can be utilized as a geochronological tool for isotope stratigraphy (Veizer et al., 1999; Halverson et al., 2005), and as a proxy for sea level changes (Föllmi et al., 1994, 2006; Weissert et al., 1998, and Fanton and Holmden, 2007). On the other hand, carbon and oxygen variations in the shallow carbonate rocks may record overprinted local diagenetic signatures rather than secular global ocean signatures (Allan and Matthews, 1982; Patterson and Walter, 1994; Xiong and Heckel, 1996; and Immenhauser et al., 2003).

Paleoclimate and ocean chemistry of the Miocene carbonate rocks of the Mediterranean region were studied through bioclast and bulk stable isotopes by many workers (Jacobs et al., 1996; John et al., 2003; Kocsis et al., 2008; Mutti et al., 1997,1999, and 2006; Brandano et al., 2010; Reuter et al., 2003; Sanchez-Almazo et al., 2001; Arenas et al., 1997; Janson et al., 2010; Harzhauser and Piller, 2007; and Piller et al., 2007). The global Miocene oxygen and carbon curves were synthesized using deep-sea benthic forams (Zachos et al., 2001). Global events in carbon and oxygen stable isotopes are the Mid-Miocene climatic optimum (Zachos et al., 2001), Mid-Miocene increasing continental weathering (John et al., 2003), coralline red algal dominance and global coral extinctions in the Miocene (Halfer and Mutti, 2005), Middle Miocene Monterey carbon maximum (Vincent and Berger, 1985), and Miocene glacial eustatic events explained by oxygen isotopic variations (Abreu and Anderson, 1998).

The Miocene Ar-Rajmah Group is composed of open marine coralline red algal, bioclastic packstone/wackestone, lagoonal bioclastic Porites coral, ramp crest oolitic grainstone, tidal microbialite, evaporite, and some estuarine green shale and quartz sandstone (Amrouni et al, 2013; El-Hawat and Abdulsamad, 2004; Francis and Issawi, 1977; Klen,1974; Rohlich 1974).

This paper presents bulk-rock $\delta^{18}O$ and $\delta^{13}C$ stable isotope curves for Miocene carbonate rocks of Cyrenaica, NE Libya (Figs. 18 and 19). In addition, this study ties the high-resolution carbon chemostratigraphy with the paragenetic sequence and the outcrop-and-gamma-ray based sequence stratigraphy to provide better age control and to enhance the sequence stratigraphic correlation of the Cyrenaican Miocene Ar-Rajmah Group carbonate platform. This study also compares the regional and global Miocene $\delta^{13}C$ curves, trends, and values to those of the Miocene Carbonate platform of the Cyrenaica (Figs 20 and 21).

Geological Setting

Global tectonic events set the stage for the transition from the Mesozoic greenhouse to Cenozoic icehouse conditions (Potter, and Szatmari, 2009). Conditions were enhanced when the northward moving continents detached from Antarctic in the southern hemisphere followed by continental concentration in the northern hemisphere associated with equatorial collisions, epiorogenic events in the northern high latitudes, and continental detachment close to the north-pole circle (Potter, and Szatmari, 2009). In the southern hemisphere, the detachment of south America and Australia from Antarctic opened the Drake Passage, and the Tasmanian Sea, two oceanic gateways and created the cold water Circumpolar Antarctic Current and the expansion of the east Antarctic sheet into the west Antarctic. In the equatorial and northern low latitudes, the collisions of the Indian and the African continents with the Eurasian continent led to the closure of

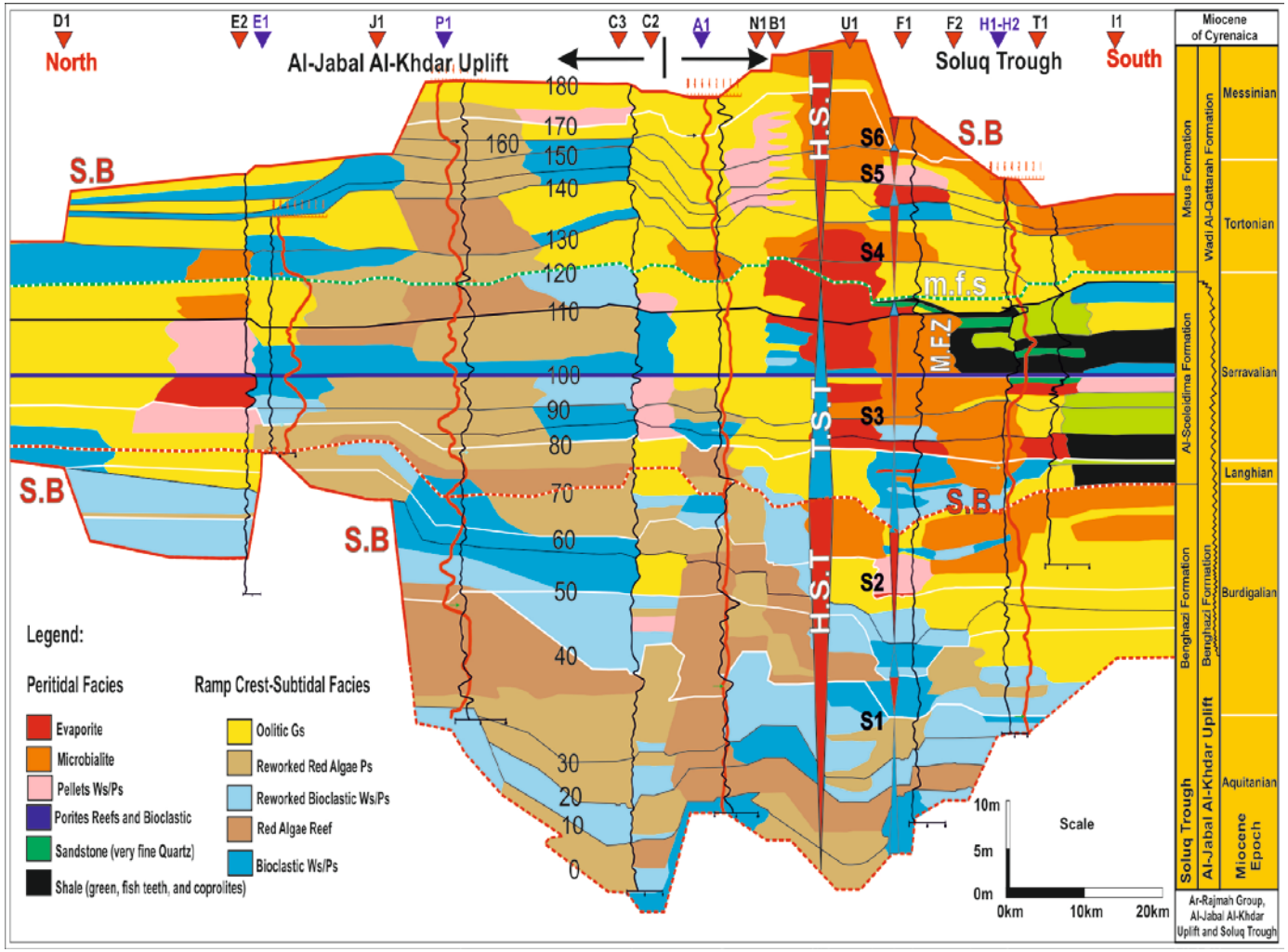

Figure 18. Sequence Stratigraphic framework of the Miocene, Ar-Rajmah Group, Cyrenaica, NE Libya (Amrouni et al., 2013). The locations of measured sections are marked at the top by inverted triangles. The blue triangles indicate sections sampled for chemostratigraphy .Thin black curves are gamma ray, and the thick red curves are carbon isotopes curves.

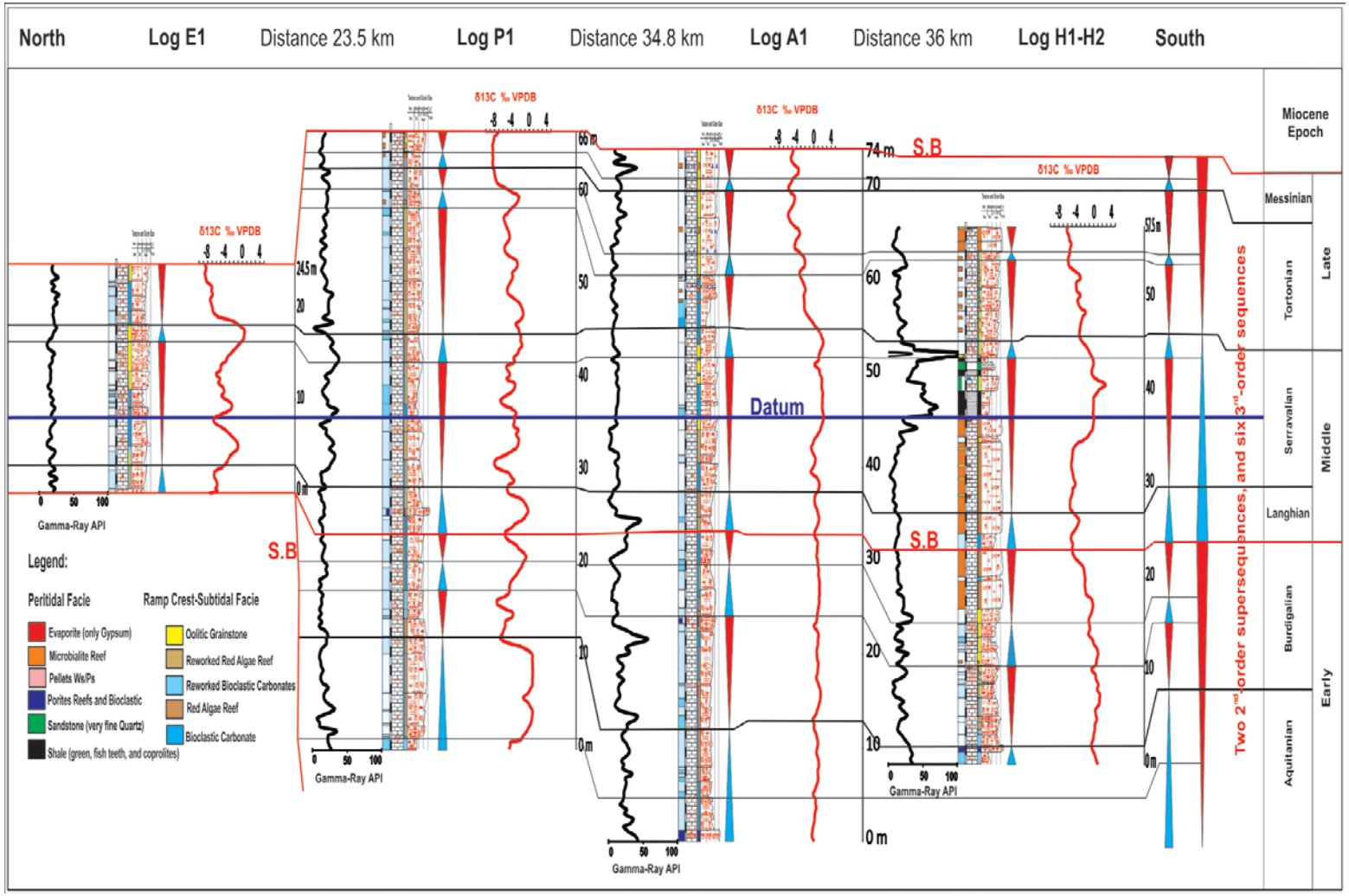

Figure 19. Chemostratigraphic correlation between carbon stable isotope curves of the Cyrenaican Miocene carbonate sequence, Ar-Rajmah Group.

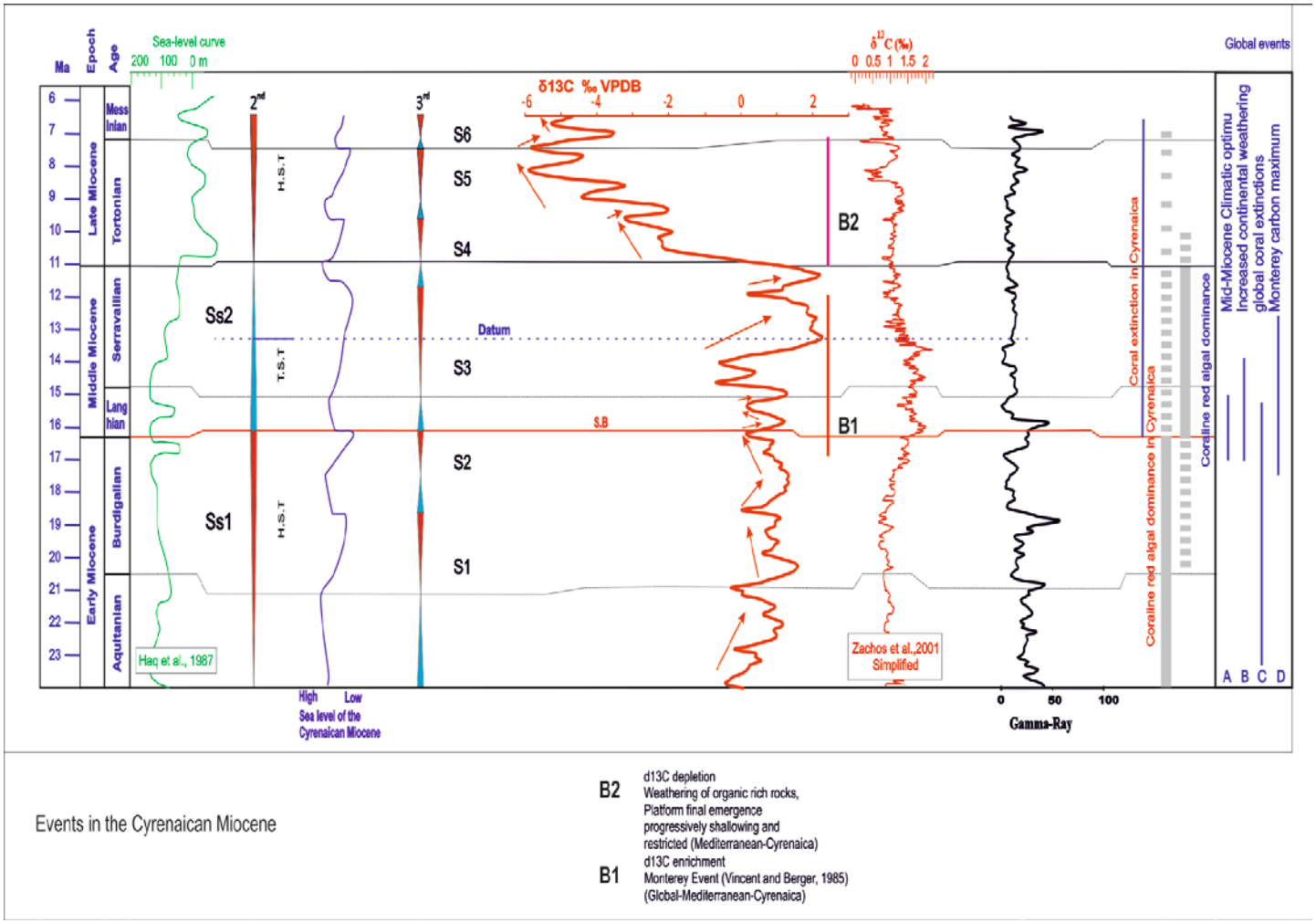

Figure 20. Chemostratigraphic comparison between the Ar-Rajmah Group Cyrenaican Miocene and the global carbon curves, besides the comparison between the Ar-Rajmah Cyrenaican Miocene and the global and sea level. Global events listed in this figure are defined in (A) Zachos et al. (2001), (B) John et al. (2003), (C) Halfar and Mutti (2005), and (D) Vincent and Berger (1985).

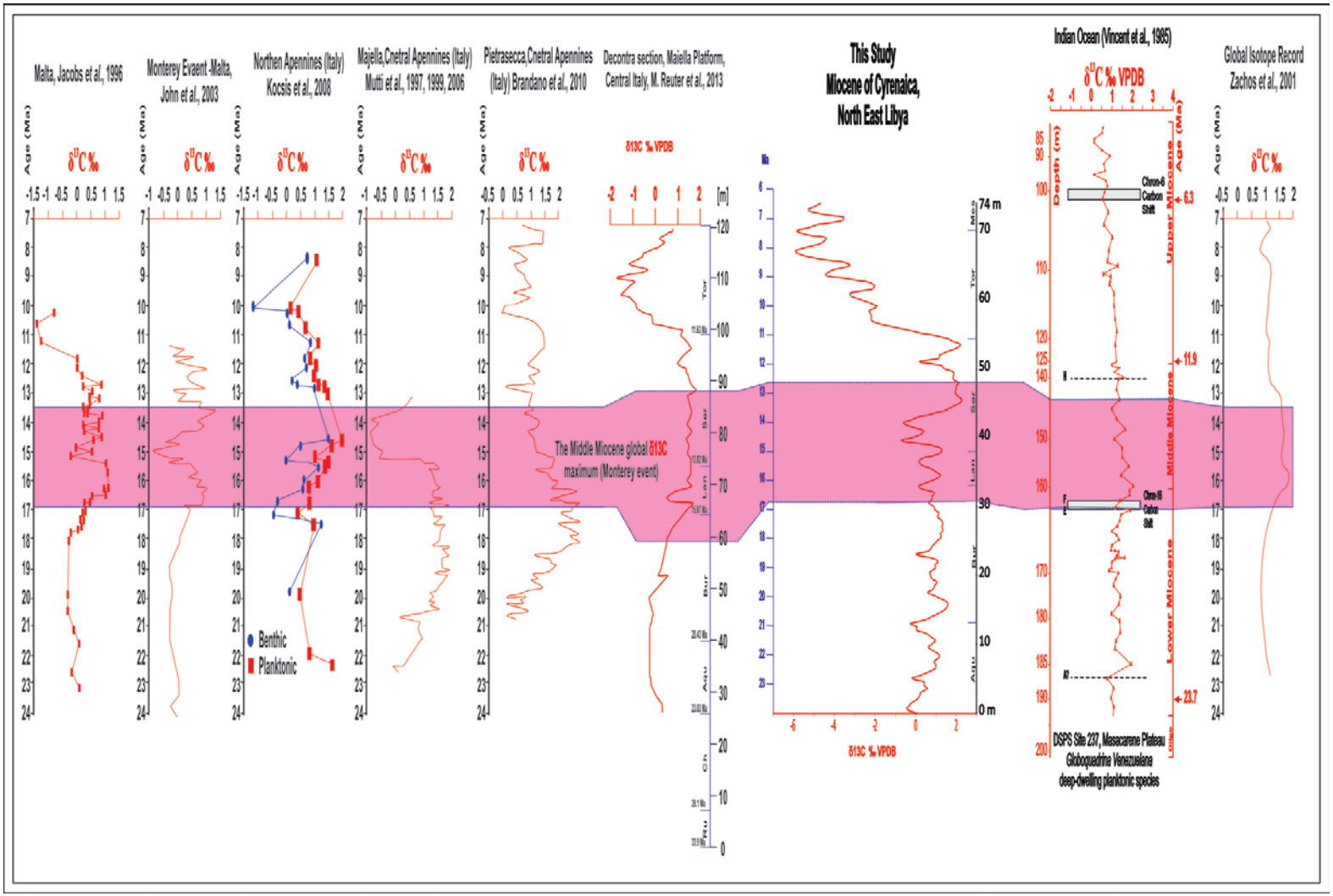

Figure 21. Comparison between the Ar-Rajmah Group Cyrenaican, Mediterranean, Indian Ocean, and the global carbon Miocene curves.

the main gateways of the equatorial east-west flowing warm water Tethys Ocean. From east to west, the Indonesian Pacific-Indian gateway closed first, followed by the closure of Arabian-Asian Indian-Mediterranean gateway, then the Gibraltar Mediterranean-Atlantic gateway, and finally the Isthmus Panama Atlantic-Pacific gateway. At this stage the global equatorial flow through the Tethys Ocean stopped. In high latitudes, continental collision and epiorogenic uplift reactivated the 13,000 km Eurasian belt and the 16,000 km Andean–Cordilleran belt. Continental Ice-sheets expanded along these high mountain ranges to enhance the icehouse cooling conditions, and created vast deserts in mountains-shadow interior areas. In the north Atlantic, the detachment of the Greenland–Scotland Ridge allowed the deep, cold, Arctic water to modify the global oceanic system (Potter and Szatmari, 2009).

The Cyrenaica area of northeast Libya includes two major tectonic provinces, the Al-Jabal Al -Khdar Uplift to the north and the Cyrenaica Platform in the south. Additionally, the Soluq and Marmarica Troughs represent western and eastern indentations on the margin of the Cyrenaica Platform (Hallett, 2002). The stratigraphy and structure of the Cenozoic Cyrenaica Platform is unique in onshore Libya, as it formed within a splay wedge that escaped significant post-depositional tectonism (Hallett, 2002).

Al Jabal Al-Khdar anticlinorium represents the southern portion of the Neo-Tethys basin that formed as an extensional trough or basin during the Middle Jurassic (El Hawat and Shelmani, 1993). Maximum subsidence of this area occurred during the Cretaceous; however, coincident with the opening of North Atlantic at the end of the Cretaceous Al-Jabal Al-Khdar was in a dextral compressional duplex due to the persistent north-northwest movement of Africa towards Europe and the acceleration of the Alpine Orogeny (El Hawat and Shelmani, 1993). Later, subsidence of the Al-Jabal Al-Khdar trough ceased and it was inverted to form the Al-Jabal Al-Khdar uplifted anticlinorium (El Hawat and Shelmani, 1993). Al-Jabal Al-Khdar was tectonically uplifted during the Early Pliocene during the re-opening of the Mediterranean connection to the Atlantic Ocean, and the opening of the Red Sea to the Indian Ocean

(El Hawat and Shelmani, 1993); it has remained subaerially exposed since the Early Pliocene.

The exposed surface rocks on the Cyrenaican platform range from Cretaceous to Late Miocene (El-Hawat and Abdulsamad, 2004). The Eocene to Late Miocene rocks of Cyrenaica are sub-divided into five unconformity-bounded sequences (El Hawat and Shelmani, 1993; El-Hawat and Abdulsamad, 2004). The exposures in the Al-Jabal Al-Khdar are mainly shallow to deep marine carbonate rocks. However, the Soluq Trough Miocene outcropping strata are mixed shallow marine carbonate and siliciclastic rocks.

The Oligocene-Miocene boundary is an erosional surface everywhere in Libya (El Hawat and Shelmani, 1993). Subduction of the European plate under the African plate during the Late Oligocene-Early Miocene elevated a series of Cretaceous-Early Tertiary islands forming the Al-Jabal Al-Khdar anticlinorium during the Miocene (El Hawat and Shelmani, 1993). The Early Miocene Al-Faidyah Formation is characterized by glauconite at its basal contact overlain by marly wackestone to packstone, and re-worked Nummulite fichteli from underlying Oligocene rocks (Pietersz, 1968; Rohlich, 1974; El-Hawat and Shelmani, 1993; Abdulsamad et al, 2009). Shallow marine facies of the Middle Miocene Benghazi Formation record a transgression that covered almost the entirety of the Cyrenaica Platform (El Hawat and Shelmani, 1993). Subsequently, a regional disconformity surface formed as sea level fell during the separation between the Tethys and the Paratethys (El Hawat and Shelmani, 1993). The Late Miocene sequence of Al-Jabal Al-Khdar is composed of Tortonian oolitic shoals overlain by Messinian carbonate and evaporite rocks (El Hawat and Shelmani, 1993).

The Middle Miocene Ar-Rajmah Formation (Desio, 1935 a and b) was later sub-divided into the Benghazi and Wadi Al-Qattarah Members (Klen,1974; Rohlich 1974). Subsequently, in the southern part of Cyrenaica the Ar-Rajmah Formation was raised to Group status comprised of the Benghazi, Msus and Sceleidima formations (Francis and Issawi, 1977; Mazhar and Issawi; 1977; Swedan and Issawi, 1977). Based on sedimentology and sequence stratigraphy in the northern part of Cyrenaica, the

Benghazi and Wadi Al-Qattarah Members were raised to formations and the Ar-Rajmah Formation was raised to Ar-Rajmah Group in Cyrenaica (El-Hawat and Abdulsamad, 2004).

The Middle Miocene (Langhian-Serravalian) Benghazi Formation is an open marine facies association of skeletal wackestone and coral boundstone (El-Hawat and Abdulsamad, 2004; El-Hawat and Salem, 1987). The Benghazi Limestone was named and its age was determined as Middle Miocene (Gregory, 1911; and Banerjee, 1980) based on marine microfaunal assemblages (e.g. *Borelis melo.* and other forams).

The Late Miocene (Tortonian-Messinian) Wadi Al-Qattarah Formation was first delineated for the youngest Tertiary deposits in Al-Jabal Al-Khdar (Klen, 1974). The Tortonian unit is cross bedded oolitic and bioclastic grainstone shoals of barrier islands with Messinian back barrier lagoonal mudstone, stromatolite and interbedded evaporite.

The Wadi Al-Qattarah Formation lateral equivalents are the Al-Sceleidima Formation and Msus Formation. The Al-Sceleidema Formation is stratigraphically overlain by the Msus Formation and both are shallow marine deposits. The Al-Sceleidema Formation is mixed carbonate and siliciclastic composed of sandstone, calcareous sandstone, claystone, gypsum and limestone. The Msus Formation is mostly bioclastic and oolitic limestone with lesser amounts of gypsum (Francis and Issawi, 1977). Benthic foram biostratigraphy of the Miocene rocks of northeast Libya indicates that the Ar-Rajmah Group records the entire Miocene (Abdulsamad and El-Zanati, 2013).

Methods/Data

This chemostratigraphic study began by determining the detailed regional facies relationships from field work and lab observations. 29 stratigraphic sections were measured bed-by-bed over a distance of 130 km (Fig. 18 and 19), 14 spectral gamma-ray profiles were constructed using a hand-held gamma-ray scintillometer at 0.5 m intervals,

and annotating facies distributions on panoramic digital photomosaics. The lab work included petrographic and diagenetic studies of 503 hand samples and their thin sections, bulk stable isotope ($\delta^{18}O$ and $\delta^{13}C$) analyses, and XRF element analysis of 148 samples.

Thin sections were analyzed to indentify the main skeletal and non-skeletal components, cements and diagenesis. 148 samples were analysed for trace and common elements by using XRF Niton-XL3t-950-Gold+, calibrated at 330 seconds with four different energy levels for filtering.

The 503 whole-rock stable isotope samples were collected at four measured sections (E1, P1, A1, H1-H2) using a 0.5 m sampling interval. The samples were micro-drilled for the $\delta^{18}O$ and $\delta^{13}C$ isotopic analysis by Isotope-ratio mass spectrometry (IRMS) and Kiel automated carbonate device in the Stable Isotope Geosciences Facility at Texas A&M University. The samples are calibrated to VPDB using standard NBS-19 (N=17, $\delta^{13}C$ = 1.95 ‰, $\delta^{18}O$ = -2.20 ‰). For these samples the precision is 0.04 ‰ and 0.08 ‰ for $\delta^{13}C$ and $\delta^{18}O$ respectively.

The carbon and oxygen stable isotopes values were plotted individually then a curve of the data was constructed using a weighted five points running average .The datum at the base of the maximum flooding zone in the Middle Miocene that has both high gamma ray values and a positive carbon isotope excursion. The oxygen and carbon stable isotopes curves were tied to the field measured outcrop stratigraphic sections and gamma ray vertical profiles. The Cyrenaican Miocene carbon isotope curve is compared with coeval regional and global Miocene carbon curves (Figs. 20 and 21).

Results

Depositional Facies of the Cyrenaican Miocene Ar-Rajmah Group

The Ar-Rajmah Group depositional profile records a shallowing upward gently dipping ramp with nine carbonate and two siliciclastics facies that are grouped into peritidal (Table 8 and Figs. 18 and 22), ramp crest, and subtidal facies (Table 9 & Figs. 18 and 22, Amrouni et al., 2013). The peritidal facies include: 1) evaporite, 2) microbialite (stromatolites, thrombolites, and laminites), 3) pelletal wackestone/packstone, 4) Porites reefs and bioclastic packstone, 5) very fine to fine quartz sandstone, and 6) green shale. The ramp crest facies is oolitic grainstone. The subtidal facies include: 1) bioclastic wackestone/packstone, 2) reworked bioclastic wackestone/packstone, 3) red algae reefs, 4) and reworked red algae packstone. Depositional facies of Ar-Rajmah Group are dominantly carbonate that shallow upwards, with siliciclastic influx only in the Middle Miocene interval. All of the Ar-Rajmah Group carbonate facies were sampled for oxygen and carbon stable isotopes analysis.

Peritidal facies

Evaporite

Yellow swallow tail gypsum lenses (Table 8 and Figs. 18 and 22) are up to 15 m thick and tens of meters wide. The evaporite lenses consist of 10 cm to 50 cm thick beds, of chevron or lozenge shape gypsum crystals growing perpendicular to bedding planes. These evaporite lenses are encased laterally and vertically within either microbialite or sandstone or shale units. In the southern part of the study area section F1 there is a 1.5 m thick bed of rippled white gypsum containing reworked coarse sand and

Table 8. Peritidal Cyrenaican Miocene facies of the Ar-Rajmah Group.

Lithofacies	Characteristics	Interpretation
EvaPorites	Lenses up to 15 m thick and various in widths with sharp top and bottom surfaces; bed thickness ranges 10 cm to 50 cm. Yellow, crystalline swallow tail selentic gypsum in fresh outcrops with Internal chevron or lozenge shape crystals. Some white in color with reworked coarse crystals and rippled. The evaporite lenses usually are encased in microbialite or siliciclastic facies.	Restricted Lagoonal evaporite facies
Microbialites reefs	Microbialites form mounds up to 12 m thick; the beds thicknesses range is from few centimetres up to 3 m with sharp top surfaces that usually have mudcracks. The microbialites are cryptalgal Laminites, stromatolites, and massive domal thrombolites. Internal structure is laminated, massive, or pelletal. Fenestral porosity is common. Have some fossils, ooid, or enriched in quartz grains. Microbialites usually intercalated thin beds of bioclastics or ooids.	Intertidal-supratidal back barrier
Pelletal wackestone /Packstone	Form units of up to 7 m thick, the beds thickness range is 0.5 m up to 2 m. The beds surfaces are sharp or sharp erosional. Laminated, and well bedded mostly associated with microbial or oolitic grainstone facies, however, occasionally associated with reworked red algae and Porites corals facies.	Intertidal back barrier
Bioclastic Porites reefs	Up to 21 m thick units of white massive and branched Porites with very large macro-bivalves, oysters, echinoids, and gastropods and microscopic forams and pellets. Lenticular beds thickness range is 1.5 m to 3 m. Channelled and channels fill is pelletal bioclastics at base that fines up to bioclastic wackestone to mudstone. Reddish brown chert nodules are common in this facies.	Lagoonal bioclastic porite reefal facies
Quartz sandstone	Up to 1 m thick Friable, well rounded, polycrystalline, yellowish to greyish white very fine to fine quarts sandstone with no fossils neither sedimentary structure observed. It reaches 6 m thick as mixed bio-oo-quartz sandstone, cross-bedded, laminated and cross laminated and occasionally bioturbated at the top surface. Fossils are leached bivalves and gastropods.	Estuary mouth
Green Shale	Up to 3.5 m thick, friable, locally laminated green shale with coprolites and fish teeth. Beds thickness range is 0.5 m to 2 m. Contains silt size quartz grains besides gypsum crystals at the base.	Estuary mouth

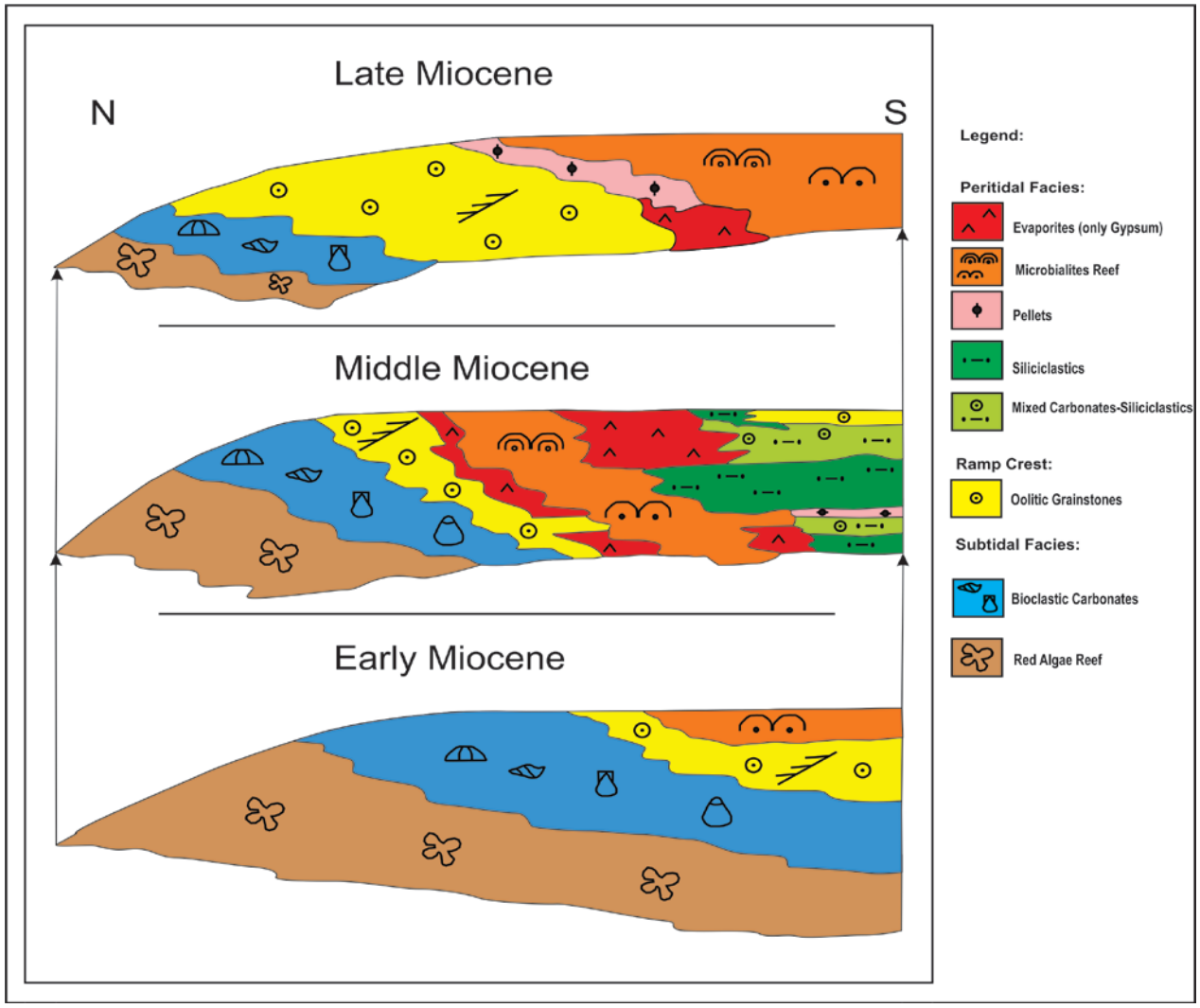

Figure 22. Simplified 2D evolutionary depositional models of the Miocene Cyrenaican carbonate platform, Ar-Rajmah Group, NE Libya.

Table 9. Ramp crest-subtidal Cyrenaican Miocene facies of the Ar-Rajmah Group.

Lithofacies	Characteristics	Interpretation
Oolitic grainstone facies	Form packages of up to 21 m thick, Channelled, Laminated, x-laminated, well bedded, X-bedded, graded bedding, and 4 m thick unidirectional clinoforms. Beds thickness ranges from 0.5 m to 7 m. Rare fossils that are mostly dwarfed bivalves, gastropods, and forams. Intercalated with microbialites.	Subtidal-intertidal oolitic barrier
Bioclastic mudstone /packstone	Form units of up to 8 m thick, massive, well bedded, cross bedded, laminated, and cross-laminated with bivalves, gastropods, bryozoans, oysters, echinoids, some red algae, and microscopic forams and occasionally corals. Beds thickness range is 0.5 m to 3 m with sharp top and bottom surfaces. Occasionally beds bioturbated at the basal part.	Subtidal open marine facies
Reworked Bioclastic packstone	Piles of up to 8 m thick, well bedded, cross bedded, laminated, cross laminated and channelled with dominantly broken shells of bivalves, gastropods, bryozoans, oysters, echinoids, some red algae, occasional fragmented corals and microscopic forams. Beds thickness range is 0.5 m to 3 m with sharp top and bottom surfaces.	Subtidal open marine facies
Red algal coralline reef	Reefs up to 26 m thick units, with lenticular beds of 1 m to 3 m thick that contain massive bodies contain baseball size heads of coralline red algae with bivalves, gastropods, bryozoans, oysters, echinoids, and microscopic forams with some occasional corals occurrences. The beds basal to top surfaces are sharp. The beds show graded bedding due to changes in fossil sizes. They form bidirectional clinoforms in some localities.	Subtidal open marine facies
Reworked red algal	Form units of up to 11.5 m thick. The beds are of 0.5 m to 3 m thick, well bedded, graded bedding and occasionally massive with sharp base and top surfaces. Most fossils are fragmented red algae with broken shells of bivalves, gastropods, bryozoans, oysters, echinoids, and microscopic forams and occasional coral fragments.	Subtidal open marine facies

conglomerate clasts of yellow and white gypsum crystals. The bedded gypsum is interpreted to have formed in restricted tidal ponds. Dissolution and silica replacement of gypsum are its most prominent diagenetic features with gypsum crystals being fragmented and reworked into sand and conglomerate beds.

Microbialite

The microbialite facies (Table 8 and Figs. 18 and 22) comprises cryptalgal laminite, stromatolite, and thrombolite beds of a few centimeters up to 3 m thick, reaching a maximum thickness of 12 m. The microbialite beds are bounded by sharp surfaces, and their upper surface commonly has mud cracks.

Rip-up clasts occur in the base of a few thrombolite beds. Microbialite facies commonly contain fenestral and vuggy pores. Massive thrombolite domes are the most dominant microbial component. Stromatolite has elongated laterally linked domes. Laminites occur either at the basal part of the stromatolite beds or as separate, thinly laminated beds intercalated with yellow gypsum. Some dwarf bivalves and gastropods, and composite ooid "grapestones" occur within the microbialite facies.

The microbialite facies increase in thickness, size and frequency towards the Soluq Trough in the southern part of the study area. They change from microbialite patch reefs, 20 cm to 50 cm diameter in the northern part of the study area into elongated mounds of more than 1.5 m diameter in the southern part. In addition, laminites dominate the northern part (Al-Jabal Al-Khdar Uplift), stromatolites dominate the central part, usually intercalated with oolitic grainstone, and thrombolites dominate the southern part (Soluq Trough). The microbialite facies commonly are intercalated with oolitic grainstone, evaporite, and pelletal wackestone/packstone. Diagenetic chert nodules are common in the microbialite facies.

The amount and size of the quartz sand grains within the microbialite facies increase upwards and towards the south. Micritization, recrystallization, and dissolution are the dominant diagenetic features in the microbialite facies. Replacement with

gypsum and then silica is common, and there is only minor dolomitization. Dissolution seams are associated with fractures. The microbialite facies are interpreted to have formed in restricted peritidal settings adjacent to and landward of the ooid shoals.

Pelletal wackestone/packstone

Pelletal wackestone and packstone units (Table 8 and Figs. 18 and 22) are up to 7 m thick, laminated, cross laminated, locally cross bedded, and have normal and reverse graded bedding. Facies associated with the pelletal wackestone/packstone are microbialite, oolitic grainstone, re-worked red algae, and Porites coral. Pelletal wackestone/packstone beds range from 0.5 m to 2 m thick. The pelletal facies commonly contains ooids and very fine to fine quartz sand grains in the southern part of the study area. Diagenetic chert nodules occur where pellets are associated with ooid grainstone and microbialite.

The pelletal wackestone/packstone facies commonly are fossil-rich containing small forams, small bivalves, fragmented red algae, Porites, and microbialites. The pelletal wackestone/packstone facies is interpreted to have formed in a shallow lagoon between the microbialite and ooid grainstone shoals.

Bioclastic Porites reefs

The bioclastic Porites reef facies form white mounds up to 21 m thick. The mounds have internally branched thick Porites blocks with white mud matrix supporting bioclastic grains of very large bivalves, gastropods, oysters, echinoids, *Borils melo* and *miliolids* forams, and pellets. The beds are 1.5 m to 3 m thick, and lenticular in shape. This facies contains channels, 1.5 m – 3 m deep and up to 5 m wide, that are filled with pelletal grainstone/packstone that fine up into bioclastic wackestone and mudstone. Diagenetic reddish brown chert nodules are common in the bioclastic Porites reefs. The

bioclastic Porites facies is interpreted to have formed irregular patch reefs within a lagoon that developed between the ooid shoal ramp crest and coeval tidal flats.

Quartz sandstone

The quartz sandstone (Table 8 and Figs. 18 and 22) commonly occurs as beds of 1 m maximum thickness, yellowish to greyish white friable very fine to fine quartz sandstone. However, it reaches up to 6 m thick when interbedded with ooids and bioclastic grains to form bioclastic-ooid-rich quartz sandstone. The bioclastic-ooid-rich sandstone is laminated, cross laminated, cross bedded, and has graded bedding. Fossils including small bivalves and gastropods occur only in the mixed bioclastic-ooid-rich quartz sandstone, and are mostly leached due to dissolution. The quartz sandstone forms a tongue interpreted to have formed by filling in an estuary.

Green Shale

The green shale (Table 8 and Figs. 18 and 22) is friable, and locally laminated, and reaches a maximum thickness of 3.5 m, with beds being 0.5 to 2 m thick. Coprolites and fish teeth occur in the green shale facies (Francis and Issawi, 1977). The basal part of the green shale commonly contains some gypsum crystals. Some silt size quartz grains occur within the green shale. The green shale also is interpreted to have formed in an estuary environment.

Ramp crest facies

Oolitic grainstone

The oolitic grainstone (Table 9 and Figs. 18 and 22) reaches up to 21 m thick and has a variety of sedimentary structures such as channels, lamination, cross-lamination, cross-bedding, and normal and reverse graded bedding. The oolitic grainstone beds range from 0.5 m to 7 m thick with sharp erosional upper and lower surfaces. The oolitic grainstone contains large unidirectional clinoforms up to 4 m thick that are cut by small channels up to 1.5 m deep containing soft sediment deformation structures. Occasional diagenetic chert nodules, and bands of chert up to 20 cm thick, occur in some horizons especially where ooid grainstone is associated with microbialite. At the southern part of the study area, ooid grainstone contains some very fine to fine sand size quartz grains in the matrix.

Fossils are rare in the oolitic grainstone and include: forams, small bivalves, and small gastropods. Ooid grainstone beds are intercalated with microbialites throughout the study area. The abundance of the microbial intercalations and oolitic grapestones increase in the southern part of the study area. Ooid grainstone facies is interpreted to have formed as a continuous high energy shoal that separated the restricted lagoon from open marine shallow subtidal facies.

Shallow subtidal facies

Bioclastic mudstone /packstone

Bioclastic mudstone/wackestone and packstone (Table 9 and Figs. 18 and 22) is up to 8 m thick, with beds ranging from 0.5 m to 3 m thick. These beds are massive, laminated, cross laminated, graded, or locally bioturbated. In addition, packstone beds

are either fining upward into bioclastic wackestone or coarsening upward into bioclastic grainstone. Fossils in the bioclastic mudstone/packstone facies include bivalves, gastropods, bryozoans, oysters, echinoids, horn corals, red algae, and forams. Fossil sizes vary from very large to dwarf. Some bioclastic units are dominated by one large size fossil type such as oysters or echinoids. The oyster beds usually form as fining upward channel fill within evaporite beds. Yellow, marly bioclastic wackestone and packstone occurs locally. Marly packstone is dominated by large echinoids with less common bivalves and gastropods, whereas the marly wackestone is dominated by bivalves and gastropods. Diagenetic chert nodules occur in this facies where it is associated with corals. The bioclastic mudstone/packstone facies was deposited in a shallow open marine subtidal setting.

Re-worked bioclastic packstone/grainstone

Re-worked bioclastic packstone (Table 9 and Figs. 18 and 22) is up to 8 m maximum thickness, with beds ranging from 0.5 to 3 m thick. Re-worked bioclastic grainstone occurs in the upper part of many re-worked bioclastic packstone beds. The reworked bioclastic packstone facies is cross bedded, graded, and forms occasional channels. The common fossils in the reworked bioclastic packstone are broken shells of bivalves, gastropods, bryozoans, oysters, echinoids, red algae, local horn corals, and forams. *Borils melo* is a very common foram in this facies. Marly reworked bioclastic packstone is dominated by large echinoids with fragmented bivalves and gastropods. The fossils in these facies vary from large to dwarfed. Diagenetic chert nodules occur where this facies contains corals. The re-worked bioclastic packstone/grainstone formed in a shallow subtidal setting.

Coralline red algal reefs

Coralline Red algal reefs (Table 9 and Figs. 18 and 22) are up to 26 m thick, and are composed of lenticular shaped beds 1 to 3 m thick. Bidirectional clinoforms occurring in this facies are massive and consist of 10 cm diameter heads of *in situ* coralline red algae with some large bivalves, gastropods, bryozoans, oysters, echinoids, horn corals, and forams. *Borils melo* forams are very common in this facies. Graded bedding is evident due to rapid changes in fauna sizes even within the same bed. The coralline red algal facies formed isolated reefs basinward of the ooid shoal.

Re-worked red algae

The re-worked coralline red algal facies (Table 9 and Figs. 18 and 22) is up to 11.5 m thick, with 0.5 m to 3 m thick beds. This facies has graded bedding, and occasionally is massive. Locally, the re-worked red algae form bidirectional clinoforms of up to 4 m high. In this facies fossils are very common, dominantly fragmented red algae, bivalves, gastropods, bryozoans, oysters, echinoids, and microscopic forams such as *Borils Melo*. The biota and their fragments vary in size from large to dwarf. The dominant depositional texture is packstone, but the very top part of some beds is grainstone. The reworked coralline red algal facies formed in an open marine shallow subtidal setting.

Sequence Stratigraphy

The sequence stratigraphic framework is based on the integration of the sedimentological analysis, correlation of stratigraphic time surfaces and vertical stratigraphic sections, stable isotope profiles, and gamma-ray logs (Table 10 &Figs. 18 and 19). The Ar-Rajmah Group Miocene carbonate rocks record two 2nd-order

Table 10. Summary of sequence stratigraphy of the Cyrenaican Miocene, Ar-Rajmah Group.

2nd Order Sequence	2nd Order systems Tracts	3rd Order Sequences	Para-sequences	Occurrence	Thickness	SB	TST	MFS	HST
SS2	HST 25 m	S6	PS20 - PS19	Covers the Messinian age	2 to 5 m thick (not fully preserved because the top surface is the present day exposure surface)	Sharp surface at the top of microbialites, oolitic grainstone, bioclastic packstone, and red algal packstone facies	1 to 2 m thick deepening upward unit of reworked red algal packstone, oolitic grainstone, and pelletal packstone facies	Placed at the top of the oolitic grainstone facies, within microbialites facies, pelletal packstone facies, oolitic grainstone facie, and reworked red algae packstone facies	2.5 to 4 m thick shallowing upward unit of microbialites facies, pelletal packstone facies, oolitic grainstone facies, and reworked red algal packstone facies
		S5	PS18 - PS17	Covers the Tortonian age	5 to 11 m thick	Sharp surface at the top of microbialites, oolitic grainstone, bioclastic packstone, and red algal packstone facies	1 to 2 m thick deepening upward unit of reworked red algal packstone, bioclastics packstone, oolitic grainstone, pelletal packstone, ,and evaporite facies	Placed at the top of the evaporite facies, within pelletal packstone facies, oolitic grainstone facie, and reworked red algae packstone facies	2 to 10 m thick shallowing upward unit of microbialites facies, pelletal packstone facies, oolitic grainstone facies, bioclastic packstone facies, and reworked red algal packstone facies
		S4	PS16 - PS13		5 to 13 m thick	Sharp surface at the top of microbialites, oolitic grainstone, bioclastic packstone, and red algal packstone facies	1 to 6 m thick deepening upward unit of reworked red algal packstone, reworked bioclastics packstone, oolitic grainstone, pelletal packstone, green shale facies, sandstone facies, and reworked evaporite facies	Placed at the top of the evaporite facies, the green shale facies, bioclastic packstone facies, red algal packstone facies within evaporite facies, oolitic grainstone facie, and reworked red algae packstone facies	6 to 11 m thick shallowing upward unit of evaPorites facies, microbialites facies, pelletal packstone facies, oolitic grainstone facies, bioclastic packstone facies, and reworked red algal packstone facies
	TST 26 m	S3	PS12 – PS6	Covers the Middle Miocene, Langhian and Serravallian ages	13 to 22 m thick	Sharp surface at the top of microbialites, oolitic grainstone, bioclastic packstone, and reworked red algal packstone facies, and bioclastic packstone coral Porites facies	2 to 8 m thick deepening upward unit of red algal packstone, bioclastics, oolitic grainstone, pelletal packstone, and microbialites facies.	Placed at the top of the evaporite facies, the green shale facies, within microbialites facies, pelletal packstone, bioclastic packstone, and reworked red algae facies	13 to 16 m thick shallowing upward unit of evaPorites facies, microbialites facies, pelletal packstone facies, sandstone facies, green shale facies, oolitic grainstone facies, bioclastic packstone facies, and reworked red algal packstone facies
SS1	HST 46 m	S2	PS5 - PS3	Covers the Burdigalian age	5 to 15 m thick ,	Sharp erosional surface at the top of echinoid dominated bioclastic packstone facies	1 to 4 m thick deepening upward unit of red algal packstone, bioclastic packstone, oolitic grainstone and bioclastic packstone coral Porites facies	Placed at the top of and within red algal packstone facies bioclastic packstones facies, and oolitic grainstone facies	5 to 12.5 m thick shallowing upward unit of microbialites facies, pelletal packstone facies, oolitic grainstone, reworked (bioclastic packstone, red algal packstone), and bioclastic packstone coral Porites facies
		S1	PS2 - PS1	Covers the Aquitania age and lower part of the Burdigalian age	3 to 30.5 m thick	Sharp surface at the top of Eocene Numulitic Packstone	2 to 28 m thick deepening upward unit of bioclastic packstone and red algal packstone , and bioclastic packstone coral Porites facies	Placed at the top and within the deep facies red algal packstone, beneath echinoid dominated bioclastic packstone facies	3 to 10 m thick shallowing upward unit of echinoid dominated bioclastic packstone facies), red algae packstone, oolitic grainstone, and bioclastic packstone coral Porites facies

supersequences (97 m maximum thickness), containing six 3rd-order sequences, and 20 parasequences (Fig. 18, and Amrouni et al., 2013). The older 2nd-order supersequence is incomplete and only the shallowing upward highstand systems tract (HST) is preserved, whereas the younger 2nd-order supersequence is complete and both the deepening upward transgressive systems tract (TST), and the shallowing upward highstand systems tract (HST) are preserved. The TST of the younger 2nd-order supersequence is separated by a sharp disconformity surface from the underlying HST, and by a maximum flooding zone from the HST of the younger 2nd-order supersequence. The HST of the older 2nd-order supersequence is correlative to the Early Miocene Benghazi Formation, the TST and HST of the younger 2nd-order supersequence is the Middle and Late Miocene Wadi Al-Qattarah Formation. The HST of the older 2nd-order supersequence includes two 3rd-order sequences (S1 and S2) that are composed mainly of coral reefs, Porites, red algae (rhodoliths), and open marine skeletal packstone containing large bivalves, gastropods, oysters, and echinoids. The TST of the younger 2nd-order supersequence includes only one 3rd-sequence (S3) containing re-worked red algae fragments at its base, shallowing upward into bioclastic grainstone, capped by cross-bedded oolitic grainstone. Microbialite, and evaPorites associated with pelletal mudstone, pelletal packstone, interbedded with fine to very fine quartz sandstone and green shale only in the southern part of the field area mark the upper part of this 3rd-order sequence. The HST of the younger 2nd-order supersequence includes three 3rd-order sequences (S4, S5, and S6). This HST is dominated by continuous bodies of oolitic grainstone and microbialite associated with some bioclastic carbonate, red algae, and pelletal packstone.

The 3rd-order sequences are composed of shallowing upward parasequences ranging in thickness from 1 m to more than 8 m. In the study area, the peritidal and ramp crest facies are thicker in the south, whereas the subtidal facies are thicker in the north. Also, the peritidal and ramp crest facies are dominant in the younger sequences, whereas the subtidal facies dominate the older sequences.

Carbon and Oxygen Isotopes

The Miocene Ar-Rajmah Group $\delta^{18}O$ data ranges from -9.2 to +9.7 ‰ VPDB, and the $\delta^{13}C$ data ranges from -10.1 to +7.6 ‰ VPDB (Fig. 19 and 20, and Tables 11 and 12). Except for measured section A1, there is a positive covariance between oxygen and carbon values that is considered a record of diagenetic alteration (e.g. Bathurst, 1975), where carbon and oxygen curves track each other. Thus, section A1 is considered the reference section of the study area since its carbon and oxygen curves have less diagenetic alteration.

The Ar-Rajmah Group is composed of peritidal, ramp crest, and subtidal facies (Fig. 23 and Tables 11). The peritidal facies evaporite (only gypsum), $\delta^{18}O$ data is -7.3 ‰ VPDB, and the $\delta^{13}C$ data is 0.0 ‰ VPDB. The microbialite $\delta^{18}O$ data ranges from -8.1 to +4.2 ‰ VPDB, and its $\delta^{13}C$ data range from -6.9 to 3.0 ‰ VPDB. The stromatolites have positive values of $\delta^{18}O$ data +4.3 ‰ VPDB, and the $\delta^{13}C$ data +3.0 ‰ VPDB. Pelletal wackestone/packstone, $\delta^{18}O$ data ranges from -5.9 to -4.3 ‰ VPDB, and the $\delta^{13}C$ data ranges from -9.9 to -0.5 ‰ VPDB. Porites reefs and bioclastic packstone, $\delta^{18}O$ data ranges from -7.3 to -5.0 ‰ VPDB, and the $\delta^{13}C$ data ranges from -8.4 to -0.7 ‰ VPDB. Very thin carbonate beds within the very fine to fine quartz sandstone, $\delta^{18}O$ data ranges from -7.2 to +9.7 ‰ VPDB, and its $\delta^{13}C$ data ranges from -4.6 to +7.6 ‰ VPDB. Very thin carbonate beds within the green shale, $\delta^{18}O$ data ranges from +3.1 to +3.9 ‰ VPDB, and the $\delta^{13}C$ data ranges from -2.4 to -0.5 ‰ VPDB

The ramp crest oolitic grainstone, $\delta^{18}O$ data ranges from -9.2 to +2.9 ‰ VPDB, and the $\delta^{13}C$ data ranges from -9.3 to +3.0 ‰ VPDB. The subtidal facies bioclastic carbonate, $\delta^{18}O$ data ranges from -7.6 to +3.3 ‰ VPDB, and the $\delta^{13}C$ data ranges from -8.9 to +2.1 ‰ VPDB. Re-worked bioclastic carbonate, $\delta^{18}O$ data ranges from -7.1 to +3.3 ‰ VPDB, and the $\delta^{13}C$ data ranges from -9.8 to +2.5 ‰ VPDB. Red algae reefs, $\delta^{18}O$ data ranges from -7.7 to +3.7 ‰ VPDB, and the $\delta^{13}C$ data ranges from -9.5 to +2.1 ‰ VPDB. Re-worked red algae, $\delta^{18}O$ data ranges from -6.4 to +3.7 ‰ VPDB, and the $\delta^{13}C$ data ranges from -10.1 to +2.3 ‰ VPDB.

Table 11. The Ar-Rajmah Group depositional facies ranges of the oxygen and carbon isotopic values of the Cyrenaican Miocene.

Maximum ‰		Minimum ‰		Average ‰		Facies	Depositional Facies
$\delta^{13}C$ VPDB	$\delta^{18}O$ VPDB	$\delta^{13}C$ VPDB	$\delta^{18}O$ VPDB	$\delta^{13}C$ VPDB	$\delta^{18}O$ VPDB		
0.0	-7.3	0.0	-7.3	0.0	-7.3	EvaPorites	Peritidal
3.0	4.3	-6.9	-8.0	-3.5	-3.2	Microbialites	
-0.4	-4.3	-8.9	-5.9	-4.1	-5.1	Pelletal Pack/Wackestone	
-0.7	-5.0	-8.4	-7.3	-6.1	-6.5	Porites bioclastic packstone	
7.5	9.7	-4.6	-7.2	-0.8	1.1	Sandstone	
-0.5	3.8	-2.4	3.1	-1.5	3.5	Green Shale	
3.0	2.8	-9.3	-9.2	-2.4	-4.4	Oolitic grainstone	Ramp Crest
2.1	3.3	-8.9	-7.6	-2.8	-2.9	Bioclastic Packstone	Subtidal
2.5	3.3	-9.8	-7.1	-2.0	-2.1	Reworked Bioclastic Packstone	
2.1	3.7	-9.5	-7.7	-0.4	0.0	Red algal Packstone	
2.3	3.7	-10.0	-6.4	-3.9	-2.2	Reworked Red algal Packstone	

Table 12. The Ar-Rajmah Group ages ranges of the oxygen and carbon isotopic values of the Cyrenaican Miocene.

Maximum ‰		Minimum ‰		Average ‰		Miocene
$\delta^{13}C$ VPDB	$\delta^{18}O$ VPDB	$\delta^{13}C$ VPDB	$\delta^{18}O$ VPDB	$\delta^{13}C$ VPDB	$\delta^{18}O$ VPDB	Ages
-1.4	-2.7	-9.3	-7.4	-6.6	-4.6	Messinian
3.0	4.3	-9.3	-9.2	-4.0	-4.2	Tortonian
7.5	9.7	-8.9	-7.4	-1.8	-3.2	Serravallian
2.4	3.3	-10.0	-6.3	-3.1	-2.4	Langhian
2.5	3.7	-9.8	-7.9	-1.5	-1.7	Burdigalian
1.8	3.6	-9.2	-5.5	-0.2	0.5	Aquitanian

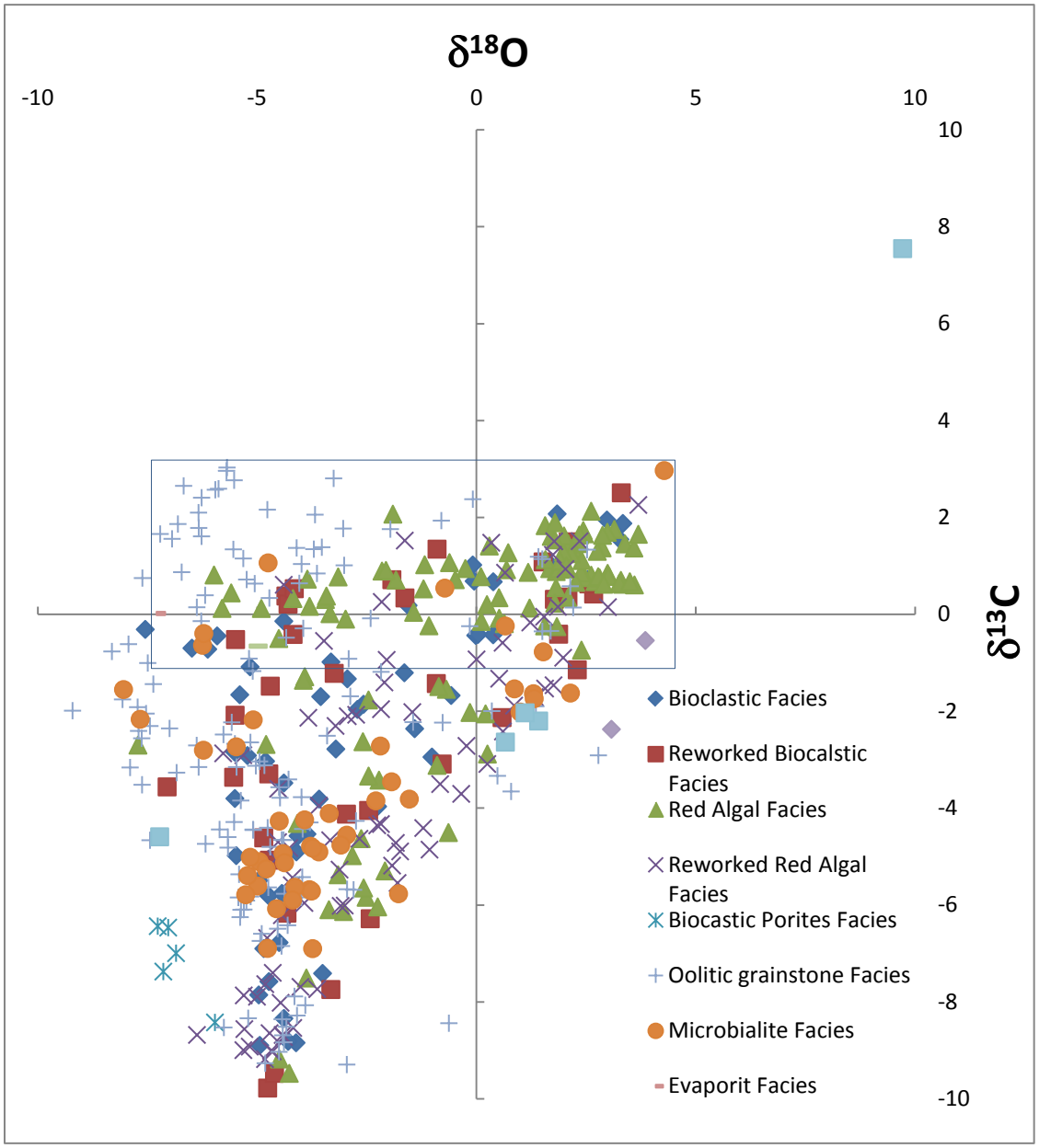

Figure 23. Age based oxygen and carbon cross-plot of the Cyrenaican Miocene carbonate platform, Ar-Rajmah group, NE Libya.

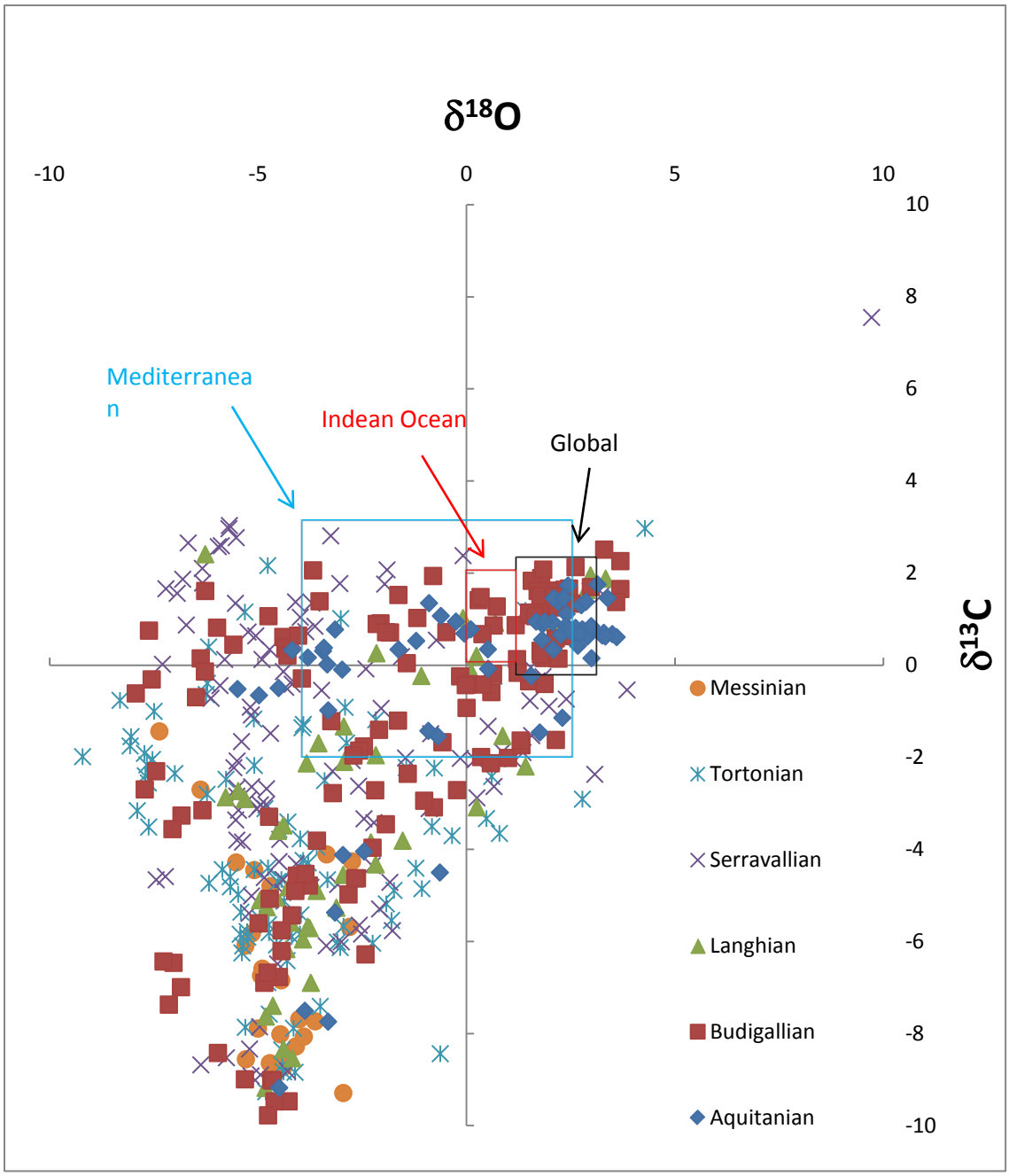

Figure 24. Facies based oxygen and carbon cross-plot of the Cyrenaican Miocene carbonate platform, Ar-Rajmah group, NE Libya.

The Ar-Rajmah Group carbonate sequence is dominated by coralline red algae and bioclastic packstone in the Early Miocene, a mix of coralline red algae, bioclastic packstone, oolitic grainstone, microbialite, and evaporite in the Middle Miocene, and oolitic grainstone, microbialite and evaporite in the Late Miocene. The Early Miocene is relatively enriched in both $\delta^{18}O$ and $\delta^{13}C$ values. The Middle Miocene is relatively depleted in $\delta^{18}O$, but enriched in $\delta^{13}C$ values. The Late Miocene is depleted in both $\delta^{18}O$ and $\delta^{13}C$ values (Fig. 24 and Table 12).

Carbon Isotope Record

The correlation between the Cyrenaican carbon isotope curves and the outcrop based-gamma-ray-profiles and sequence stratigraphic analysis led to the delineation of two 2nd-order supersequences that include six 3rd-order sequences. In the Cyrenaican platform sections the carbon isotope values are depleted at, or below, the 3rd-order sequence boundaries. The carbon isotope values trend gradually increases from sequence 1 to the top of sequence 2, and then there is a sharp increase in the upper part of the Middle Miocene sequence 3. On the contrary, there is a sharp decrease in the carbon isotope values from sequence 4 to sequence 5, followed by a gradual increase in carbon isotope values trend through sequence 6. The maximum carbon isotope enrichment occurred in Middle Miocene 3rd-order sequence 3 that coincides with a high gamma ray zone, and minimum carbon isotope depletion occurred in the Tortonian 3rd-order sequence 5.

Discussion

Ramp Geometry

The depositional profile of the Miocene Ar-Rajmah Group depositional facies includes nine carbonate facies and two siliciclastics facies that are grouped into peritidal facies (Table 8 & Figs. 18 and 19), ramp crest facies and subtidal facies (Table 9). The spatial arrangement of these depositional facies (Figs. 18 and 19) from landward peritidal facies to seaward ramp crest and relatively deeper marine subtidal facies indicates deposition occurred along a carbonate ramp (Ahr, 1973; Read, 1985; Tucker, 1996; and Schlager, 2005).

The muddy subtidal lagoonal facies landward of the ramp crest facies were poorly developed in 3rd-order sequences S1 and S2, and very well developed in 3rd-order sequences S3- S6. The subtidal lagoonal facies in sequences S1 and S2 were dominated by Porites coral behind the bioclastic barrier. Temporal development of the lagoonal facies indicates that the oolitic ramp crest facies in sequences S1 and S2 were not producing enough accommodation space to create a muddy subtidal lagoon. However, in sequences S3-S6 the oolitic ramp crest facies were thicker and created enough accommodation space for the muddy subtidal lagoonal facies to develop.

Climate

The global Miocene paleoclimate

During the last 65 Ma, the Earth's climate shifted from warm, ice-free poles to a colder climate with continental ice-sheets and polar ice caps (Zachos et al., 2001). The warmest climate in the Cenozoic was in the period between Middle Palaeocene to Early Eocene that followed by long term cooling from the Middle Eocene to Middle-

Late Oligocene. From the Late Oligocene to Middle Miocene there was a relatively warming trend with decrease in oxygen isotopic values and reduced extent of the Antarctic ice cap that associated with brief periods of glaciation. After the Middle Miocene warm climate optimum (17 to 15 Ma), there was gradual global cooling with increased oxygen isotopic values, that resulted from the re-establishment of the major Antarctic ice-sheet by 10 Ma (Zachos et al., 2001). Cooling increase continued into the early Pliocene due to the expansion of the west-Antarctic and Arctic ice-sheets (Zachos et al., 2001).

The Mediterranean region Miocene paleoclimate

The Miocene climate record of the Mediterranean area indicates there was a long-term coupling between atmospheric CO_2 and climate, so that the major glaciations were associated with low CO_2, whereas the warmer intervals were associated with elevated CO_2 (500 ppmv) (Kurschner, 2008). The Early Miocene climate of the Central Mediterranean was arid with strong seasonality and low sedimentation rate (John et al., 2003). The Middle Miocene of the Mediterranean was a period of a subtropical/warm-temperate humid climate with a trend of slightly decreasing temperatures (Ivanov et al., 2002; and John et al., 2003). The Late Miocene was characterized by more diverse climatic conditions. The beginning of this period is marked by a slight cooling and a significant drying, followed by fluctuations of all paleoclimate parameters indicating cycles of humid/dryer and warmer/cooler conditions (Ivanov et al., 2002).

The Mediterranean Miocene coral reefs reflect a global cooling trend associated with a decrease in coral diversity. The environmental conditions during this period change from open marine, humid tropical to land-locked semi-arid and marginally subtropical (Esteban, 1996).

During the Aquitanian the Mediterranean climate became tropical to sub-tropical with sea level fall during a global climatic minimum (Hallam, 1981). The

Mediterranean was an open ocean with extensive rhodalgal and highly diverse coral reefs, but evaPorites were deposited in the shallower areas (Esteban, 1996).

Sea level fall and increased Antarctic glaciation led to global cooling that coincides with Early Miocene Arabian-Turkish plates collision (Barron and Keller, 1982). The Early Burdigalian cool climate allowed only the temperate rhodalgal and foramol carbonate facies to dominate (e.g. Lees and Buller, 1972; Carannante et.al. 1988). Organic-rich marl and diatomaceous sediments were deposited in the basin (Esteban, 1996).

The Late Burdigalian and Langhian were dominated by a warmer climate that allowed moderately diverse corals to develop extensive carbonate platforms in the Mediterranean region (Purser et al, 1996; Buchbinder et al 1993, and 1996; Permanyer and Esteban, 1973; Orszag-Sperber and Piolt, 1976; Lietz and Schwarzbach, 1970; Chevalier, 1961; Wijsman-Best and Boekschoten, 1982; Esteban, 1996). An unconformity surface separates the two coral reef units of the upper most Burdigalian and Langhian in the Mediterranean region. *Stylophora*, *Porites*, and *Tarbellastraea* are the dominant Langhian coral reefs constituents (Esteban, 1996).

The Serravallian was dominated by a colder climate and poor subtropical to temperate fauna associated with thick evaporite deposits in the Mediterranean (Esteban, 1996). This event is called “Serravallian crisis” (Rogl et al, 1978; Demarcq, 1984, 1985), where its depositional facies relationships are similar to those during Messinian evaporite deposition (Rouchy, 1982a, b).

During the latest Serravallian the previously collided Arabian and Turkish plates were uplifted producing a major global sea level fall (Esteban, 1996). The Mediterranean ocean became semi-closed, disconnected completely from the Indo-Pacific in the east, but still connected with a narrow shallow seaway with the Atlantic Ocean in the west. The eastern part of the Mediterranean was dominated by red beds and evaPorites, whereas the central and western parts were dominated by open marine facies and coral reefs during global highstands (Esteban, 1996).

During the Tortonian and Messinian coral reefs developed becoming larger in the Messinian. The Mediterranean during the Messinian was gradually isolated from the Atlantic Ocean, thick and extensive evaPorites were precipitated, due to repeated tectonic uplifts and sea level falls. The evaPorites interbedded with marine, restricted marine, brackish, and hypersaline sediments (Esteban, 1996).

The Cyrenaican Ar-Rajmah Group Miocene paleoclimate

The paleoclimate of the Cyrenaican Miocene platform can be deduced from its carbonate components and depositional facies. The Early Miocene is dominated by open marine coralline red algal facies, bioclastic packstone facies, and lagoonal bioclastic Porites coralline facies. The Middle and Late Miocene were dominated by the oolitic grainstone, microbialite, and evaporite facies that gradually replaced the open marine facies.

The Cyrenaican climate during the Early Miocene was warm to allow the coralline red algae facies to dominate and coral Porites to grow. However, during the Middle and Late Miocene the climate became colder and semi-arid that led to the gradual displacement of the coralline facies by the microbialite facies and the evaPorites facies, and the deposition of siliciclastic facies.

The Miocene Cyrenaican succession is a carbonate dominated system with observable siliciclastic influence in the Middle Miocene. A switch from Burdigalian carbonate dominated system to siliciclastic dominated succession in the Late Burdigalian-Serravallian surrounding the Mediterranean region (John et al., 2003 referred to the maps in Esteban, 1996). In addition, the carbonate platform in the North Nicaraguan Rise as part of the Tethys Ocean recorded a general increase in the siliciclastic influx from the Burdigalian through the Serravallian (Mutti et al., 2005).

Cyrenaican Stable Isotope Patterns, Interpretations, and Comparison with Regional and Global Coevals

The $\delta^{13}C$ stable isotope curves constructed for the Miocene Ar-Rajmah Group of Cyrenaica, NE Libya, are compared with the regional Mediterranean, Indian Ocean, and global Miocene curves patterns (Fig. 21). The $\delta^{13}C$ stable isotope curve is notably similar to the Indian Ocean, and regional Mediterranean curves. However, the amplitudes of the stable isotope excursions in the Cyrenaican Miocene are much greater. The similarity of stable isotope curve of the Cyrenaica region with those records indicates this succession preserves nearly the entire Miocene period, as indicated also by benthic forams (Abdulsamad and El-Zanati, 2013).

The seawater oxygen and carbon isotopic composition varies through time in the geological record (Veizer et al., 1999; and Grossman, 2012a). Therefore, it is a must to know the original secular isotopic composition of the Miocene marine carbonate rocks to correlate them globally. The benthic-foram-based global Miocene stable isotope curve (Zachos et al., 2001) has $\delta^{18}O$ values ranging from 1.6 to 3.2 ‰ VPDB, and the $\delta^{13}C$ values ranges from -0.1 to 2.2 ‰ VPDB. The planktonic-foram-based Miocene Indian Ocean stable isotope curve (Vincent et al., 1985) has $\delta^{18}O$ values ranges from 0.0 to 1.6 ‰ VPDB, and the $\delta^{13}C$ values ranges from 0.1 to 2.0 ‰ VPDB. The fossil-and-bulk-rock-based Mediterranean region Miocene stable isotope curves (Jacobs et al., 1996; John et al., 2003; Kocsis et al., 2008, Mutti et al., 1997, 1999, 2006; Brandano et al., 2010, and Reuter et al., 2013) have $\delta^{18}O$ values ranging from -3.8 to 2.5 ‰ VPDB, and $\delta^{13}C$ values ranging from -1.8 to 2.8 ‰ VPDB. The whole-rock stable isotope values of the Cyrenaican Miocene Ar-Rajmah Group carbonate record a broader range of values from -9.2 to +9.7 ‰ VPDB for $\delta^{18}O$, and range from -10.1 to +7.6 ‰ VPDB for $\delta^{13}C$ (Fig. 21).

The Cyrenaican Miocene Ar-Rajmah Group $\delta^{13}C$ values are mostly lighter than the isotopic signatures of the regional Mediterranean Miocene, the Indian Ocean,

and the global Miocene records. The most depleted $\delta^{13}C$ values (Fig. 23) are associated with the ramp crest facies and the peritidal facies of the Cyrenaican Miocene rocks.

Depletion in the $\delta^{13}C$ values of the Cyrenaica Miocene Ar-Rajmah Group relative to other curves can be attributed to ^{13}C-depleted-fresh-water diagenesis (e.g. Simms and Ruffell, 1990; Immenhauser et al., 2003), its restricted depositional environments and "aging" (e.g. Patterson and Walter 1994; Holmden et al., 1998; Swart et al., 2009) dominated by peritidal facies and ramp crest facies associated with evaPorites. Oxidization of organic matter in soil zones or water "aging" lead to the accumulation of CO_2 enriched in C_{12} (Allan and Matthews, 1982; Lohmann, 1988; Immenhauser, 2003) that produced carbonate materials depleted in $\delta^{13}C$ values. Also, basin upwelling of the oxidized isotopically-light-organic-carbon can lead to the depletion of the $\delta^{13}C$ values in waters of normal salinity (Patterson and Walter 1994; Immenhauser et al., 2003).

The enrichment in the $\delta^{13}C$ values of the Cyrenaica Miocene Ar-Rajmah Group relative to the other curves can be attributed to either local primary productivity or the preservation of the admixture of aragonite and calcite. The local productivity may have enriched the $\delta^{13}C$ by removing the ^{12}C from the seawater dissolved inorganic carbon (DIC) (Broecker, 1982; Kump and Arthur, 1999; Panchuk et al., 2006; Grotzinger et al., 2011; Hajikazemi et al., 2012). The preservation of organic-rich sediments indicates local high productivity. In the Cyrenaica Miocene carbonate sequence the green shale unit with fish teeth and coprolites, records the highest gamma ray levels in the area, and its U-gamma ray values are higher than the K-Th-gamma ray values. For the aragonite-calcite admixture, the depositional aragonitic sediments record the original marine signature and are enriched in ^{13}C values relative to the successor calcitic sediments (Swart, 2008; and Swart et al., 2009).

Isotopes and Depositional Facies

The marine isotopic signature might be altered or not preserved, if there was a strong correlation between the depositional facies and their isotopic values (Kaufman and Knoll, 1995). The Cyrenaican Miocene carbon-oxygen stable isotope values were plotted as facies (Fig. 24) to define the relationship between the depositional facies and their isotopic values.

Most of the $\delta^{13}C$ and $\delta^{18}O$ isotopic values of the Cyrenaican Miocene carbonate platform were influenced by fresh water diagenesis that led to the depletion of $\delta^{13}C$ and $\delta^{18}O$ data. However, even the well preserved $\delta^{13}C$ and $\delta^{18}O$ data shows a notable depositional facies control due to the correlation between the isotopic values and their facies (Kaufman and Knoll, 1995). For instance, the peritidal facies is more abundant in the positive $\delta^{18}O$ data than the positive $\delta^{13}C$ data due to the evaporation effect to be enriched in $\delta^{18}O$ than $\delta^{13}C$, during the deposition of the evaPorites. Also, the ramp crest facies $\delta^{13}C$ data is likely enriched due to the preservation of the original marine signatures besides the high productivity effect, during deposition of the high gamma ray green shale. In addition, subtidal facies are positively enriched in both $\delta^{18}O$ and $\delta^{13}C$ due to better preservation of the original marine signatures in their original aragonite-calcite mineralogies. The subtidal facies are dominated with fossil that have aragonitic skeletons such as red algae, and bivalves.

Isotope Correlation and Relative Sea-Level Changes

Local sea level changes can result in lateral variations in the $\delta^{13}C$ values in the stratigraphic record due to mixing of open marine water with restricted shallow waters (Immenhauser et al., 2002; Immenhauser et al., 2003; and Fanton and Holmden, 2007). During a high relative sea level rise, carbonate platforms are flooded and carbonate production started (Swart and Elberli, 2005). Enrichment of the $\delta^{13}C$ values can be associated with TSTs and relative sea level rises, whereas depletion of the $\delta^{13}C$ values

can be associated with HSTs and relative sea level falls (Immenhauser et al., 2003; and Fanton and Holmden, 2007). Also, marginal marine areas can have locally enriched $\delta^{13}C$ values when they experienced high organic matter deposition. However, if these marginal organic-rich deposits are eroded and oxidized during the next sea level fall, the deposited deep basinal facies will be depleted in $\delta^{13}C$ values because of the enrichment of ^{12}C (Broecker, 1982; Hajikazemi et. al., 2012; and Vincent et.al., 1985). Thus, relative sea level changes can be directly related to the relative variation in the $\delta^{13}C$ values.

Carbon isotope curves of the Miocene Ar-Rajmah Group succession were tied with the detailed sequence stratigraphic framework (Amrouni et al., 2013). The datum of the sequence stratigraphic interpretation is the base of the maximum flooding zone that is characterized by high gamma-ray values. The correlation of the Cyrenaican Miocene carbon isotope curves (Figs. 18 and 19) defined approximate ages and durations for the Cyrenaican 2nd-order sequences (SS1 and SS2) and 3rd-order sequences S1-S6).

The preserved section of SS1 represents the HST and it has $\delta^{13}C$ values commonly >0, enrichment trend, with a relative depletion of $\delta^{13}C$ below its upper sequence boundary (Figs. 18 and 19). The HST of SS1 is dominated by marine subtidal facies of coralline red algae and bioclastic carbonates. The TST of SS2 has enriched $\delta^{13}C$ values >0, enrichment trend, whereas the HST of SS2 has a trend of sharp depletion in the $\delta^{13}C$ values, and there is a relative enrichment of $\delta^{13}C$ values beneath the top boundary of each system tract. The TST of SS2 is dominated by ramp crest facies and peritidal facies that associated with subtidal facies, whereas the HST of SS2 is dominated by ramp crest facies and peritidal facies.

In addition, there are cyclic changes and trends (Fig. 20) associated with the 3rd-order sequences (S1-S6). For the Early Miocene S1 and S2, there are trends of enrichment in $\delta^{13}C$ values in consistence with the TSTs, and there are trend of depletion in $\delta^{13}C$ values in consistence with the HSTs. The 3rd-order sequences S1 and S2 have a relative depletion in $\delta^{13}C$ beneath sequences boundaries, and are dominated by open marine subtidal facies.

For the Middle Miocene S3, there is a trend of enrichment in $\delta^{13}C$ values that interrupted with a sudden depletion in the middle of the TST. The $\delta^{13}C$ values have a trend of sharp enrichment that is not in consistence with the HST. The 3rd-order sequence S3 has a relative depletion in $\delta^{13}C$ below the sequence boundary, and is dominated by a mixture of subtidal facies in the basin center that shallows vertically and laterally into ramp crest and peritidal facies. The HST-S3 enrichment in the $\delta^{13}C$ values is attributed to the increase of the primary organic productivity, where the depletion was due to meteoric water diagenesis or oxidation of the organic carbon.

For the Middle-Late Miocene S4, there is enrichment in $\delta^{13}C$ values in consistence with the TST, and a sharp depletion trend in $\delta^{13}C$ values in consistence with the HST. The 3rd-order sequence S4 has a relative depletion in $\delta^{13}C$ below the sequence boundary. It is dominated by ramp crest and peritidal facies with some localized and mostly reworked subtidal facies in the basin center.

The Late Miocene S5 and S6 have enrichment trend in $\delta^{13}C$ values consistent with the TST. Also, they have sharp depletion trend in $\delta^{13}C$ values consistent with the HST. The 3rd-order sequences S5 and S6 have relative depletion in $\delta^{13}C$ below the sequence boundary. They are dominated by shallowing upward ramp crest and peritidal facies with some localized and mostly reworked basal subtidal facies.

Stable isotope data analysis of variations and patterns of the Cyrenaican Miocene $\delta^{13}C$ values of the 2nd order supersequences shows partial similarity to the regional Mediterranean, Indian Ocean, and to the global Miocene coeval patterns. Due to local factors such as fresh water diagenesis, local primary organic productivity, and environmental depositional settings the $\delta^{13}C$ patterns of the 3rd-order Cyrenaican Miocene sequences shows less similarity to their regional Mediterranean, Indian Ocean, and the global Miocene counterparts. Therefore, the patterns and variations in Cyrenaican Miocene $\delta^{13}C$ curves represent a long term global isotopic signature overprinted by shorter term locally and regionally altered isotopic signatures. The Cyrenaican Miocene stable isotopic curve expresses more locally controlled alteration rather than global marine signatures, as it is the case with many shallow marine

carbonate platforms (Holmden et al., 1998; Immenhauser et al., 2003; Patterson and Walter, 1994; Hajikazemi et al., 2012; Swart and Eberli, 2005).

Cyrenaican Miocene events

The whole-rock $\delta^{13}C$ values can be used as proxies for $\delta^{13}C$ of ocean water, because, in contrast to the $\delta^{18}O$, the $\delta^{13}C$ is more resistant to the diagenetic alteration and required high water/rock ratios to change the carbonate sediments $\delta^{13}C$ values significantly during diagenesis (Banner and Hanson, 1990; Banner, 1995; Jacobsen and Kaufman, 1999; Veizer et al., 1999; and Grotzinger et al, 2011). The Cyrenaican Miocene, the regional Mediterranean, the Indian Ocean, and the global $\delta^{13}C$ curves show enrichment trends during Early Miocene followed by enrichment in the Middle Miocene, and then depletion in the Late Miocene (Fig. 21). In addition, the Late Miocene $\delta^{13}C$ curves show sharp and sudden depletion in the Cyrenaican and the Mediterranean region, where they show generally gradual depletion in the Indian Ocean, and the global curves. The exception is the very upper part of the Late Miocene where all curves reversed a gradual enrichment in the $\delta^{13}C$ values.

The Middle Miocene enrichment in S3 of the Cyrenaican $\delta^{13}C$ curve (Fig. 20) represent a global ^{13}C-maximum, Monterey event, (Vincent and Berger, 1985) that is recorded in all Miocene curves (Fig. 21). In addition, in the Cyrenaican platform the Serravallian Tortonian boundaries (S4-S6) show a sudden marked decrease in the $\delta^{13}C$ (Fig. 21). The Tortonian $\delta^{13}C$ depletion pattern occurs in Mediterranean region (Reuter et al., 2013), in the Indian Ocean (Vincent et al, 1985), and in the global (Zachos et al., 2011) curve. However, the Cyrenaican and Mediterranean $\delta^{13}C$ depletion is very large in amplitude compared to the planktonic record of the Indian Ocean (Vincent et al., 1985), and global record (Zachos et al., 2001). The increased amplitude of this fluctuation in the progressively restricted, shallowing upward Cyrenaican carbonate platform is interpreted as the expression of carbonate platform emergence (e.g. Reuter et.al, 2013; Patterson and Walter, 1994).

The Cyrenaican Middle Miocene interval is dominated by peritidal facies associated with some subtidal facies and abundant ramp crest oolitic grainstone facies. The dominant peritidal facies specifically include evaPorites, and siliciclastic green shale that enriched in fish teeth and coprolites. The evaporation is main factor of $\delta^{18}O$ enrichment, and the high primary organic productivity that stored as organic green shale is the main factor of $\delta^{13}C$ enrichment.

In the central Mediterranean a deepening upward sequence started in the Early Miocene, and then shallowed upward in the Late Miocene (Jacobs et al, 1996). However, the Cyrenaican platform mostly does not record the deepening due to the continuous uplifting/resistance to subsidence, instead having an aggradtional facies stacking pattern during the Middle Miocene. The Late Miocene in Cyrenaican is both aggradational and progradational (Amrouni et al, 2013).

Conclusions

The Cyrenaican Miocene $\delta^{13}C$ and $\delta^{18}O$ chemostratigraphy is established through the analysis of the Ar-Rajmah Group carbonate platform rocks. The integration of the stable isotope data with the detailed gamma-ray profiles-outcrop-based sequence stratigraphy defines two 2^{nd}-order supersequences (SS1-SS2) and six 3^{rd}-order sequences (S1-S6) in the Cyrenaican Miocene section. Due to resistance to subsidence, the Cyrenaican platform Middle Miocene deepening signature is aggradation thick shallow facies rather than deepening upward facies as in coeval Mediterranean sequences. These sequences are identified based on facies analysis, stacking patterns, stratigraphic surfaces, gamma-ray signatures, field observations, and pattern of the stable isotopes. The subtidal coralline red algae dominated only the whole Early Miocene and gradually replaced by the shallower restricted facies in the Middle Miocene and Late Miocene.

The Miocene Ar-Rajmah Group $\delta^{18}O$ data ranges from -9.2 to +9.7 ‰ VPDB, and the $\delta^{13}C$ data ranges from -10.1 to +7.6 ‰ VPDB. The $\delta^{18}O$ and $\delta^{13}C$ values of the Miocene Ar-Rajmah Carbonate Group have a wider range than the regional

Mediterranean, the Indian Ocean, and the global Miocene $\delta^{18}O$ and $\delta^{13}C$ values. The $\delta^{13}C$ and $\delta^{18}O$ curves of the Cyrenaican Ar-Rajmah Group indicate this succession spans much of the Miocene as indicated previously by foram biostratigraphy.

The Cyrenaican Miocene isotopic values represent a long term marine global isotopic signature overprinted by shorter term locally and regionally alterations due to environmental facies control, diagenesis, and local high organic productivity. The enrichment of the values $\delta^{13}C$ is associated with an organic-rich green shale deposits, the enrichment of $\delta^{18}O$ values is associated with the peritidal evaporite deposits, and the depletion of $\delta^{13}C$ and $\delta^{18}O$ values are associated with meteoric water diagenesis.

The positive carbon isotope excursion of the Cyrenaica platform in late Early Miocene and Middle Miocene records the global Monterey event. The amplified Tortonian negative carbon isotope shift records the emergence of the upward restricted shallow-water Cyrenaican platform.

CHAPTER IV

SEQUENCE STRATIGRAPHY AND DIAGENESIS IN THE CYRENAICAN MIOCENE CARBONATE SUCCESSIONS, AL-JABAL AL-KHDAR UPLIFT AND SOLUQ TROUGH, NR LIBYA

Overview

Four measured sections of the Miocene Ar-Rajmah Group carbonate rocks in Cyrenaica, northeast Libya, each 25-75 m thick, spanning 94 km in length, and were sampled every 0.5 m for sequence stratigraphy, stable isotope ($\delta^{18}O$, $\delta^{13}C$) chemostratigraphy, XRF elements analysis, and diagenesis. Petrographic study of the samples identifying facies based on texture, grain types, mud content, cements, porosity types and amount, dolomitization, dedolomitization, gypsification, silicification, and recrystallization. Combined the sequence stratigraphy, chemostratigraphy, and petrography indicates the Ar-Rajmah Group records two sequences separated by a sequence boundary and two different diagenetic patterns.

The chemostratigraphic data of the Ar-Rajmah Group suggests this unit preserves the entire Miocene as indicated by previous microfossil-based paleontological studies. The stable isotope data indicates the Early Miocene is generally enriched in both $\delta^{18}O$ and $\delta^{13}C$, the Middle Miocene is enriched in $\delta^{13}C$ but depleted in $\delta^{18}O$, and the Late Miocene is depleted in both $\delta^{18}O$ and $\delta^{13}C$.

The petrographic analysis shows two distinct lithological, textural and paragenetic patterns above and below a sequence boundary corresponding roughly to the Middle Miocene Langhian-Serravallian boundary. The older Miocene interval (Langhian and older) is dominated by silicified dedolomitized bioclastic-rich, bryozoan, and red algal packstone beds. The younger Miocene interval (Serravallian and younger)

is dominated by silicified and recrystallized oolitic grainstone, and microbial-bioclastic-oolitic grainstone.

The main porosity types in the Miocene Ar-Rajmah Group sequences are oomoldic, fenestral, dolomoldic, frame-growth, biomoldic, fracture, vuggy, cavernous, and intercrystalline. However, the dolomoldic and frame-growth porosity dominates in the older dedolomitized Miocene interval, whereas the oomoldic and fenestral porosity is dominant in the younger recrystallized Miocene interval. The Late Miocene has the lowest average porosity values, whereas the Middle Miocene has the highest average porosity values, and the Early Miocene has medial average porosity values.

The paragenetic sequence in the Ar-Rajmah Group is: 1) micritization, 2) symmetrical rim cement, 3) asymmetrical rim cement, 4) initial pore filling cement, 5) initial dissolution , 6) secondary pore filling cement, 7) recrystallization, 8) dolomitization, 9) dedolomitization, 10) secondary dissolution, 11) geopetal infill, 12) initial fracturing, 13) dissolution seems, 14) gypsum replacement, 15) silicification, 16) fracture filling cement , 17) a second period of fracturing, and 18) a third episode of dissolution.

Introduction

The diagenetic history of carbonate rocks can be deduced through indentifying the diagenetic events, and their paragenetic sequence. The diagenesis study of the Cyrenaican Miocene ramp outcrops will serve as good analogue for similar subsurface ramp reservoirs such as Jurassic Smackover Formation, Little Cedar Field, southwest Alabama (Tonietto and Pope, 2013; Al Haddad and Mancini, 2013; and Benson and Mancini, 1984), and Permo-Triassic Khuff Formation, Ghawar Field, Saudi Arabia (Al-Dukhayyil, and Read, 2012). The main objectives of this work are to define microscopically the diagenetic events and processes that occurred during and after the deposition of the Miocene carbonate sequence of Cyrenaica, NE Libya (Fig. 25). A step further is to establish the paragenetic succession framework for the Cyrenaican Miocene

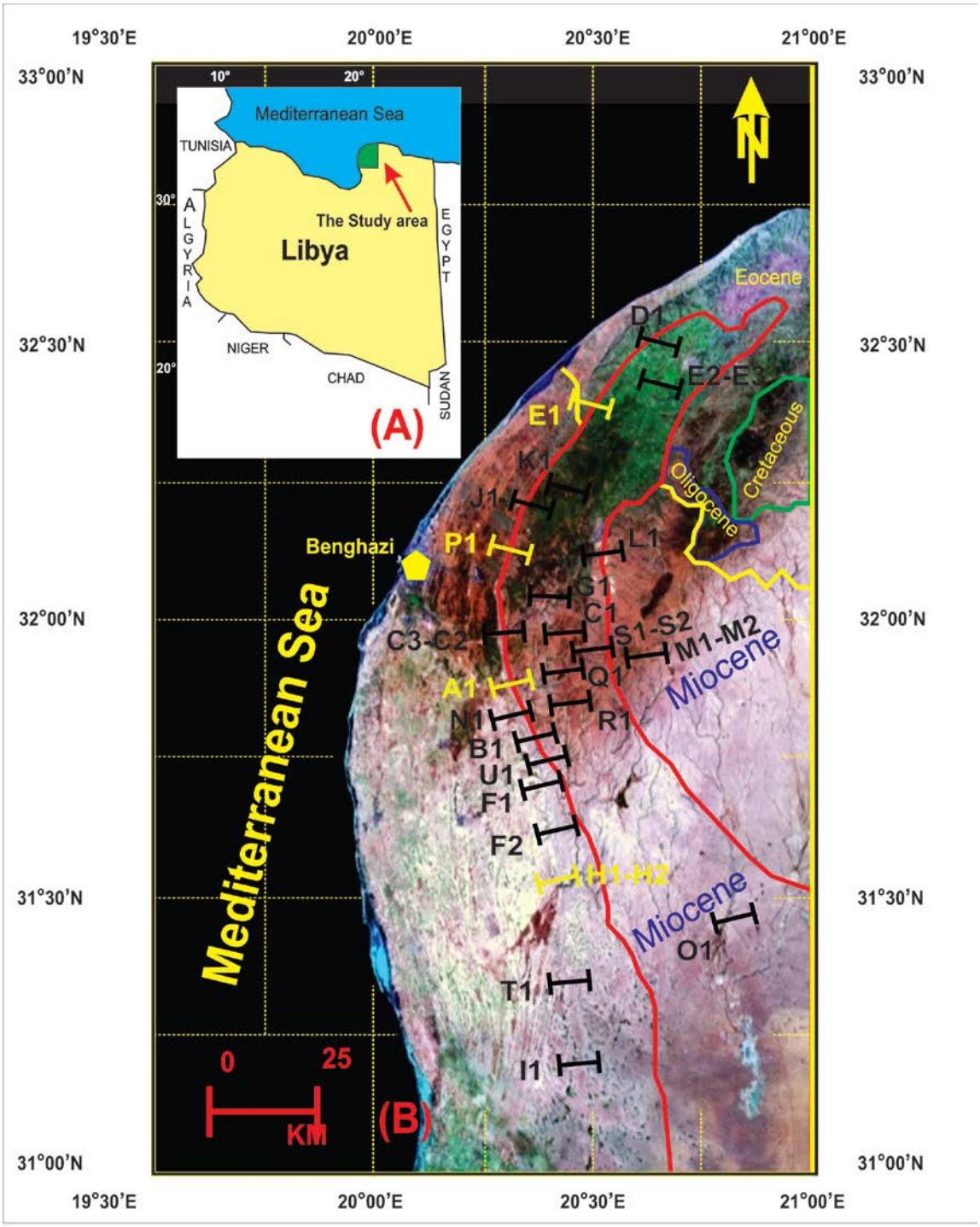

Figure 25. (A) Location map of the study area in northeastern Libya. (B) Landsat image of NE Libya showing the geological boundaries of Cretaceous- Tertiary rocks. The geological boundaries are based on the IRCs sheet-Benghazi (Klen, 1974) and sheet-Soluq (Franci Francis and Issawi, 1977) that were later modified by (El-Hawat et al., 1987).

carbonate ramp. The final step is to tie the paragenetic sequence with the chemostratigraphy and the outcrop-and-gamma-ray based sequence stratigraphy for the Cyrenaican Miocene shallow Carbonate platform.

Geological Setting

Cyrenaica, northeast Libya is dominated by two major tectonic provinces, the Al-Jabal Al -Khdar Uplift north and the Cyrenaica Platform south. Additionally, the Soluq and Marmarica Troughs are two indentations into the margin of the Cyrenaica Platform (Hallett, 2002). The Cyrenaica Platform is stratigraphically and structurally different than the rest of onshore Libya, as it formed within a tectonic splay wedge and escaped significant post-depositional tectonism (Hallett, 2002).

The Al Jabal Al-Khdar anticlinorium is the southern limb of the Neo-Tethys basin. The Mediterranean syncline formed during the Middle Jurassic as an extensional trough or basin. It reached its maximum subsidence during the Cretaceous. However, coincident with the opening of North Atlantic at the end of the Cretaceous Al-Jabal Al-Khdar was in a dextral compressional duplex due to the persistent north-northwest movement of Africa towards Europe and the acceleration of the Alpine Orogeny (El Hawat and Shelmani, 1993). Later, subsidence of the Al-Jabal Al-Khdar trough ceased and it was inverted to form the Al-Jabal Al-Khdar anticlinorium (El Hawat and Shelmani, 1993).

Sedimentologically, the surface rocks of Al-Jabal Al-Khdar are subdivided into seven cycles of sedimentation, ranging in age from the Middle Eocene to Middle Miocene (Rohlich, 1980). The Eocene to Late Miocene rocks of Cyrenaica are subdivided into five unconformity-bounded sequences (El Hawat and Shelmani, 1993; El-Hawat and Abdulsamad, 2004).

The exposed surface rocks on the Cyrenaican platform range from Cretaceous to Late Miocene (El-Hawat and Abdulsamad, 2004). Except for rare cases that have transitional contacts, all these units are bounded at their base and top by disconformities.

The exposures in the Al-Jabal Al-Khdar, north Cyrenaica, are mainly shallow to deep marine carbonate rocks. However, in the Soluq Trough rocks are solely Miocene mixed shallow marine carbonate and siliciclastic rocks exposed on the surface.

The Oligocene-Miocene boundary is an erosional surface everywhere in Libya (El Hawat and Shelmani, 1993). Subduction of the European plate under the African plate during the Late Oligocene-Early Miocene elevated a series of Cretaceous-Early Tertiary islands that form the core the Al-Jabal Al-Khdar anticlinorium during the Miocene (El Hawat and Shelmani, 1993). The Nummulite fichteli of the structurally uplifted Oligocene rocks were eroded and redeposited as littoral to neritic Early Miocene rocks (El Hawat and Shelmani, 1993). Shallow marine facies of the Middle Miocene Benghazi Formation record a transgression that covered most of the Cyrenaica Platform (El Hawat and Shelmani, 1993). Subsequently, a regional disconformity surface formed during a major regression coincident with the separation between the Tethys and the Paratethys, and the Messinian salinity crisis of the Mediterranean (El Hawat and Shelmani, 1993). The Late Miocene sequence of Al-Jabal Al-Khdar is composed of Tortonian oolitic shoals overlain by Messinian interbedded carbonate and evaporite rocks (El Hawat and Shelmani, 1993).

Al-Jabal Al-Khdar was tectonically uplifted during the Early Pliocene with the reopening of the Mediterranean connection to the Atlantic Ocean, and the opening of the Red Sea to the Indian Ocean (El Hawat and Shelmani, 1993). It has remained subaerially exposed since that time.

The Early Miocene Al-Faidyah Formation is characterized by a basal glauconitic coarse sand sized black grains overlain by marly skeletal wackestone to packstone with abundant reworked Nummulite fichteli from underlying Oligocene rocks (Pietersz, 1968; Rohlich, 1974; El-Hawat and Shelmani, 1993; Abdulsamad et al, 2009). The Middle to Late Miocene Ar-Rajmah Group comprises the Middle Miocene Benghazi Formation and the Late Miocene Wadi Al-Qattarah Formation and its equivalents the Msus and Sceleidima Formations (Francis and Issawi, 1977; El-Hawat and Abdulsamad, 2004).

The Ar-Rajmah Group was initially designated a single Middle Miocene Formation (Desio,1935 a and b) and it was later sub-divided into the Benghazi Member and Wadi Al-Qattarah Member in Al-Jabal Al-Khdar (Klen, 1974; and Rohlich, 1974). Subsequently, in the Soluq Trough area the Ar-Rajmah was raised to Group status comprised of three Formations Benghazi, Msus and Sceleidima (Francis and Issawi, 1977; Mazhar and Issawi; 1977; Swedan and Issawi, 1977). Later the Benghazi and Wadi Al-Qattarah Members in Al-Jabal Al-Khdar area were raised to Formations and the Ar-Rajmah was raised to a Group in Cyrenaica based on sedimentological and sequence stratigraphic field observations (El-Hawat and Abdulsamad, 2004).

The Middle Miocene (Langhian-Serravalian) Benghazi Formation is an open marine facies association of skeletal wackestone and coral boundstone (El-Hawat and Abdulsamad, 2004; El-Hawat and Salem, 1987). The unit was named Benghazi Limestone and its age was determined as Middle Miocene (Gregory, 1911; Banerjee, 1980) based on marine microfaunal assemblages (e.g. Borelis melo. and other forams).

The Late Miocene (Tortonian-Messinian) Wadi Al-Qattarah Formation was first delineated for the youngest Tertiary deposits in Al-Jabal Al-Khdar (Klen, 1974). The Tortonian unit is cross bedded oolitic and bioclastic grainstone shoals of barrier islands with Messinian back barrier lagoonal mudstone, stromatolite and evaporite.

The Wadi Al-Qattarah Formation lateral equivalents are the Al-Sceleidima Formation and Msus Formation. The Al-Sceleidema Formation is stratigraphically overlain by the Msus Formation and both are shallow marine deposits. The Al-Sceleidema Formation is mixed carbonate and siliciclastic composed of sandstone, calcareous sandstone, claystone, gypsum and limestone. The Msus Formation is mostly bioclastic and oolitic limestone with lesser amounts of gypsum (Francis and Issawi, 1977).

In spite of the difference in their tectonic settings, the Late Miocene exposures of the Al-Jabal Al-Khdar in northeast Libya and the Sirt Basin in central Libya are both composed of oolitic grainstone shoals and barrier islands with back barrier lagoonal mudstone and evaporite (Amrouni, 2000, 2006). However, the Late Miocene oolitic

shoals of the Al-Jabal Al-Khdar have tidal sedimentary structures (e.g. herringbone cross-bedding and reactivation surfaces) that are absent in coeval Sirt Basin units (Amrouni, 2000, 2006).

Methods/Data

The petrographic lab work involves an intensive study of 503 hand samples and their thin sections. 148 samples from the measured field section A1 were analysed for trace and common elements using XRF Niton-XL3t-950-Gold+, calibrated at 330 seconds with four different energy levels for filtering.

Blue dye was inserted into the epoxy of all thin sections to enhance porosity identification. Alizarin Red-S stain was used to distinguish between calcite and dolomite minerals, and potassium ferricyanide stain was used to differentiate ferroan from non-ferroan carbonate minerals (Dickson, 1965, 1966).

For the petrographic work, a three part thin section description scheme was established and followed. It includes: 1) quantitative analysis, 2) qualitative analysis, and 3) diagenetic process. The quantitative part involved determining the type and percentage of grains, matrix, cement, and pores. The qualitative studies rock textures (fabrics and grain size), sedimentary structures (primary and secondary), and trace fossils. Diagenetic processes includes micritization, dissolution/leaching (pore creations), cementation (pore destruction), compaction (mechanical and chemical), and neomorphism (recrystallization, inversion, and replacement).

For describing the original depositional texture of carbonate rocks Dunham classification (1962) that modified by Embry and Klovan (1971) was used. The crystalline dolomitized limestone textures were described using Randazzo and Zachos classification (1983), Amthor et al. (1993), Sibley & Gregg (1987), and Tucker (1996). Cements types and fabrics were identified and described using schemes provided by Flügel (2004).

The grain contacts and compaction were described in accordance with Taylor (1950). Porosity was described as in (Choquette and Pray, 1970) and using the genetic porosity classification (Ahr, 2011; Humbolt and Ahr, 2008; and Ahr et al., 2005).

Results

The field and petrographic work of the Cyrenaican Miocene carbonate platform of the Ar-Rajmah Group, NE Libya, indicates deposition occurred on a low relief carbonate ramp. The ramp consists of eleven depositional facies were subjected to eighteen diagenetic events produced by six diagenetic processes that left their print over on these rocks.

The depositional facies includes nine carbonate facies and two siliciclastic facies. The carbonate facies include: 1) oolitic grainstone, microbialite (stromatolite, thrombolite, and cryptalgal-laminite), 3) pelletal wackestone/packstone, 4) gypsum, 5) bioclastics packstone Porites reefs, 6) bioclastic carbonates wackestone/packstone, 7) reworked bioclastic carbonates wackestone/packstone, 8) red algae reefs, 9) reworked red algae packstone. The siliciclastic facies are: 10) Very fine to fine quartz sandstone, and 11) green shale with fish teeth and coprolites.

The six main diagenetic processes that altered the Cyrenaican Miocene platform are: 1) micritization, 2) dissolution, 3) cementation, 4) recrystallization, 5) replacement, and 6) compaction (chemical and mechanical). These diagenetic processes produced a microscopically identifiable succession of alteration events. The paragenetic sequence (Fig. 26) of the Ar-Rajmah Group is: 1) micritization, 2) symmetrical rim cement, 3) asymmetrical rim cement, 4) initial pore-filling cement, 5) initial dissolution , 6) secondary pore filling cement, 7) recrystallization, 8) dolomitization, 9) dedolomitization, 10) secondary dissolution, 11) geopetal infilling, 12) initial fracturing, 13) dissolution seems, 14) gypsum replacement, 15) silicification, 16) fracture filling cement , 17) a second period of fracturing, and 18) a third episode of dissolution.

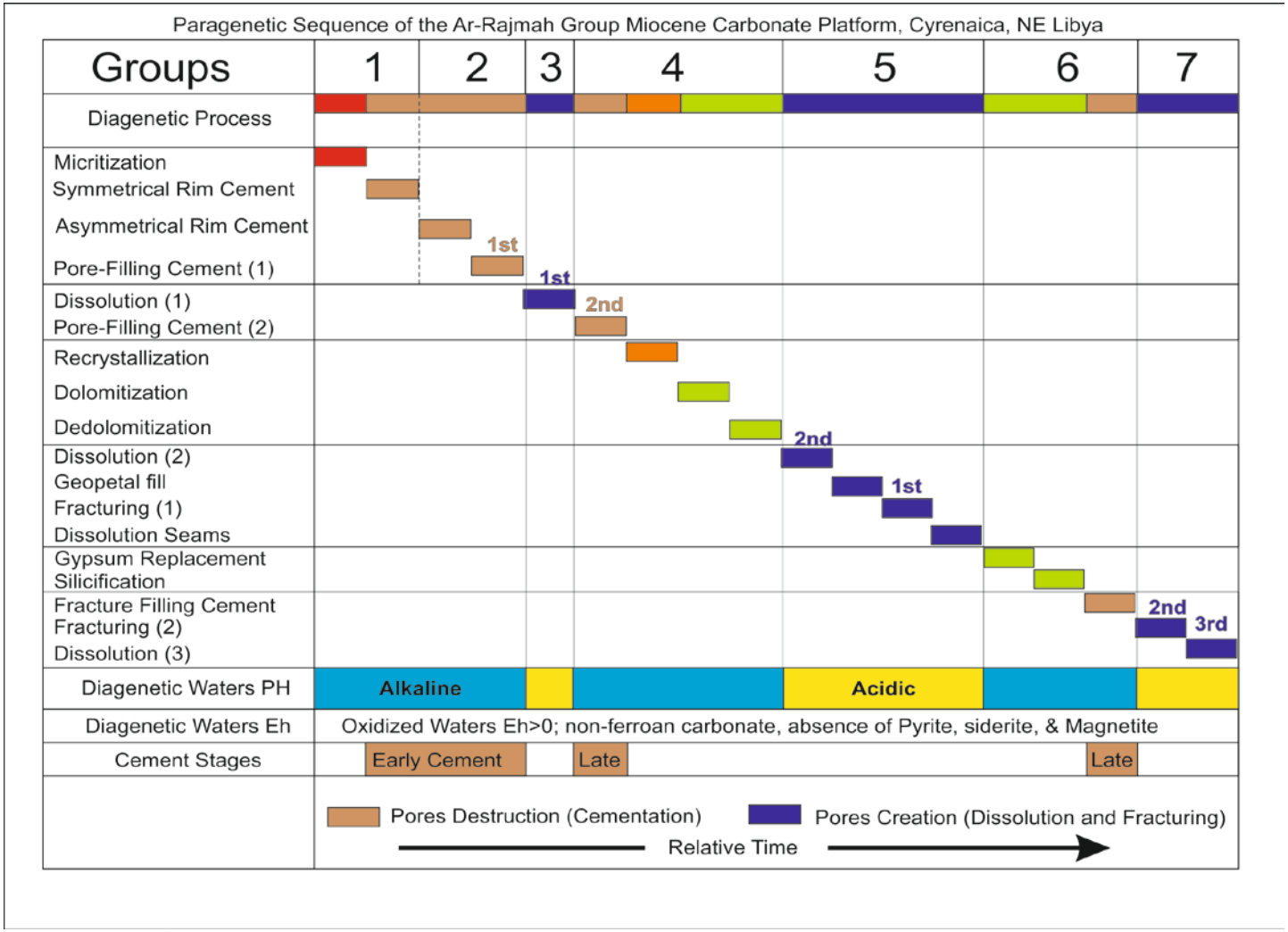

Figure 26. Paragenetic sequence of the Ar-Rajmah Group carbonate platform, Cyrenaica, NE Libya.

Micritization is common in the Cyrenaican Miocene carbonate ramp rocks (Fig. 27 A and B). The micritization affected both skeletal and non-skeletal grains.

Cementation is a common feature in the Ar-Rajmah Group Cyrenaican Miocene rocks. The observed cement types are: symmetrical rim cements (Fig. 28 A and B), asymmetrical rim cement (Fig. 29 A and B), pore-filling cement (Fig. 30 A and B), fracture filling cement (Fig. 31 A), and large cement structures (Fig. 31 B). The identified symmetrical rim cements are: fibrous, bladed, dogtooth, and circum-granular. The asymmetrical rim cements are: the gravity or dripstone, and meniscus.

The pore-filling cements occur either between grains as intergranular cement or inside leached grains intragranular cement (Fig. 30 A and B). They include drusy and blocky sparite. The fracture filling cements are various. The small fractures are filled with microcrystalline silica, whereas the large fractures are filled by dolomite cement (Fig. 31 A). The large cement structures are of three forms: crust, fan-shape, and botryoid (Fig. 31 B).

Dissolution is the dominant diagenetic feature that occurred at three different times during the diagenetic sequence of the Cyrenaican Miocene carbonate rocks. Leaching the Cyrenaican carbonate rocks led to the formation of the intercrystalline and dolomoldic porosity (Fig. 32 A and B), oomoldic and biomoldic porosity (Fig. 33 A and B), channel, and vuggy secondary porosity (Fig. 34 A and B). Also, geopetal structures in the oolitic grainstone facies were formed after the dissolution processes (Fig. 33 A).

Recrystallization is very dominant in the matrix and cements, but rare in the grainy component of the Cyrenaican carbonate rocks. The matrix crystals are enlarged in size and their crystal form and shape changed to form sand-size crystalline mosaic (Fig. 35 A).

Compaction is a notable diagenetic feature in the Cyrenaican Miocene carbonate rocks forming fractures and dissolution seams (Figs. 35 B, and 36 A and B). Fractures are more common in the Early and Middle Miocene strata than in the Late Miocene rocks. There are two phases of fracturing. The early fractures are partially filled with microcrystalline quartz and/or dolomite cements (Fig. 35 B), where the late fractures are

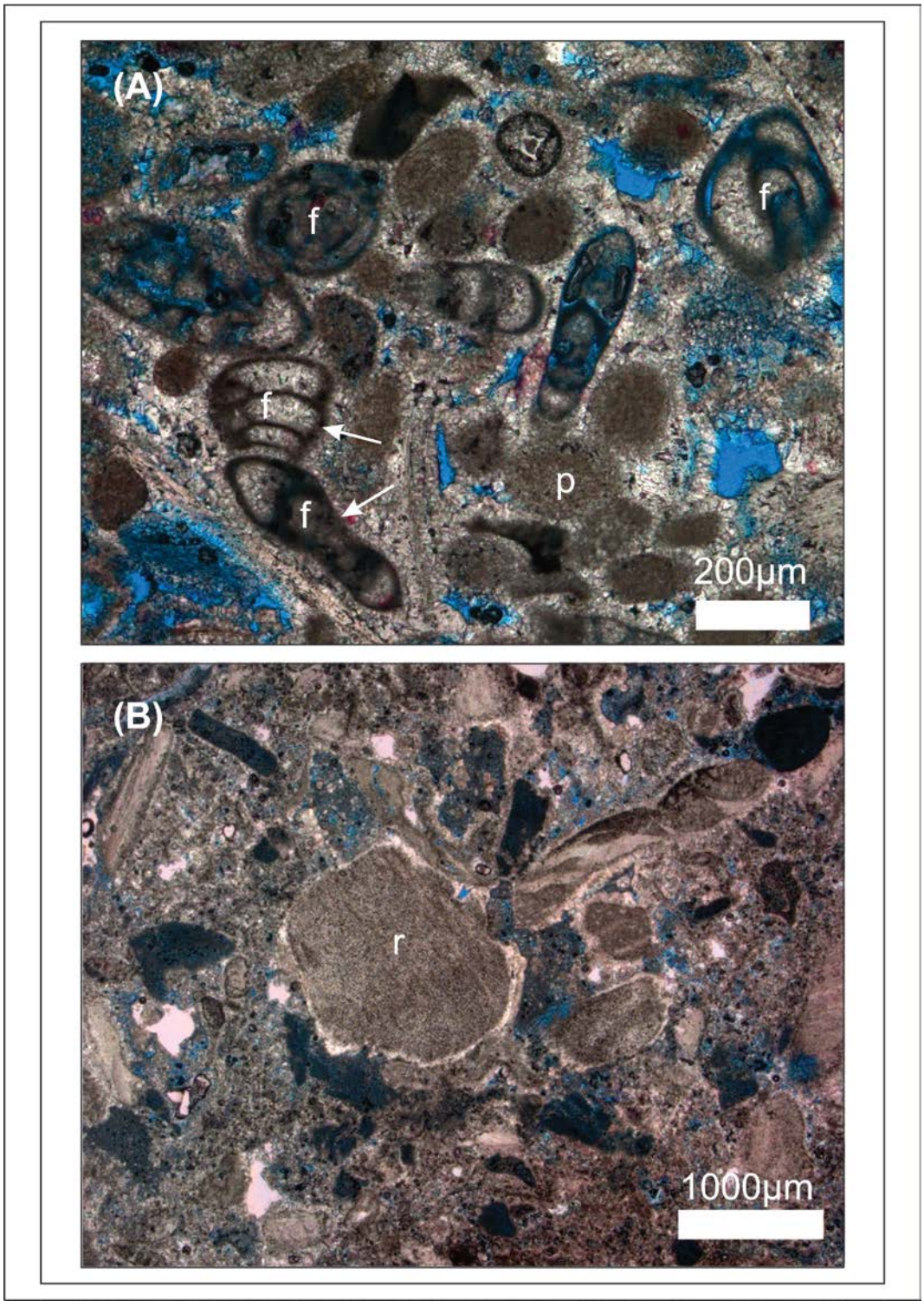

Figure 27. Photomicrographs of the micritization (A) Micrite envelopes around the forma fossils in pelletal-bioclastic grainstone, (f) forams and (p) pellets. (B) Micritized grains in red algal facie, (r) red algae fragments.

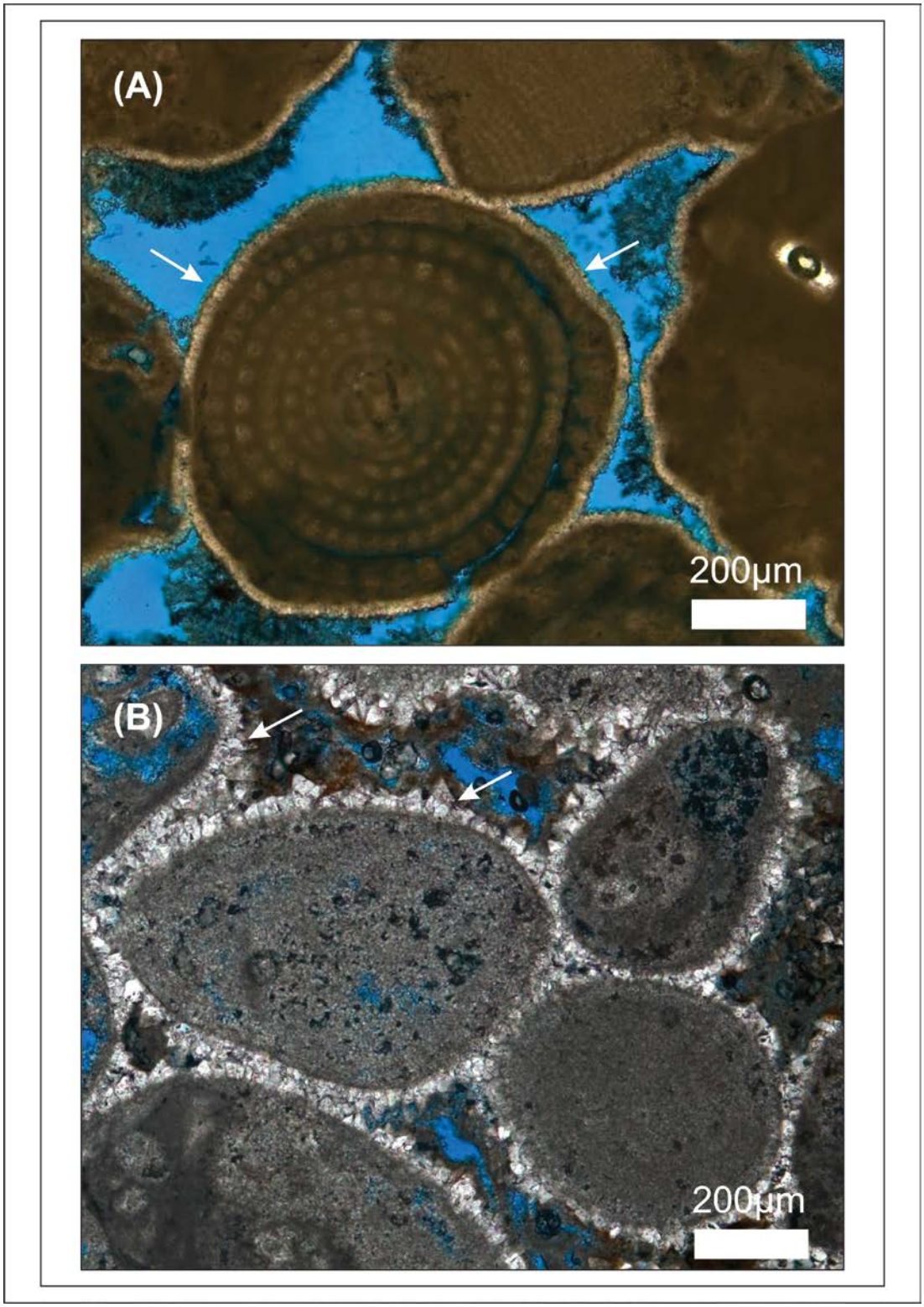

Figure 28. Photomicrographs of symmetrical asymmetrical rim cements. (A) Fibrous symmetrical rim cement in bioclastic grainstone facies. (B) Dogtooth symmetrical rim cement in oolitic grainstone facies.

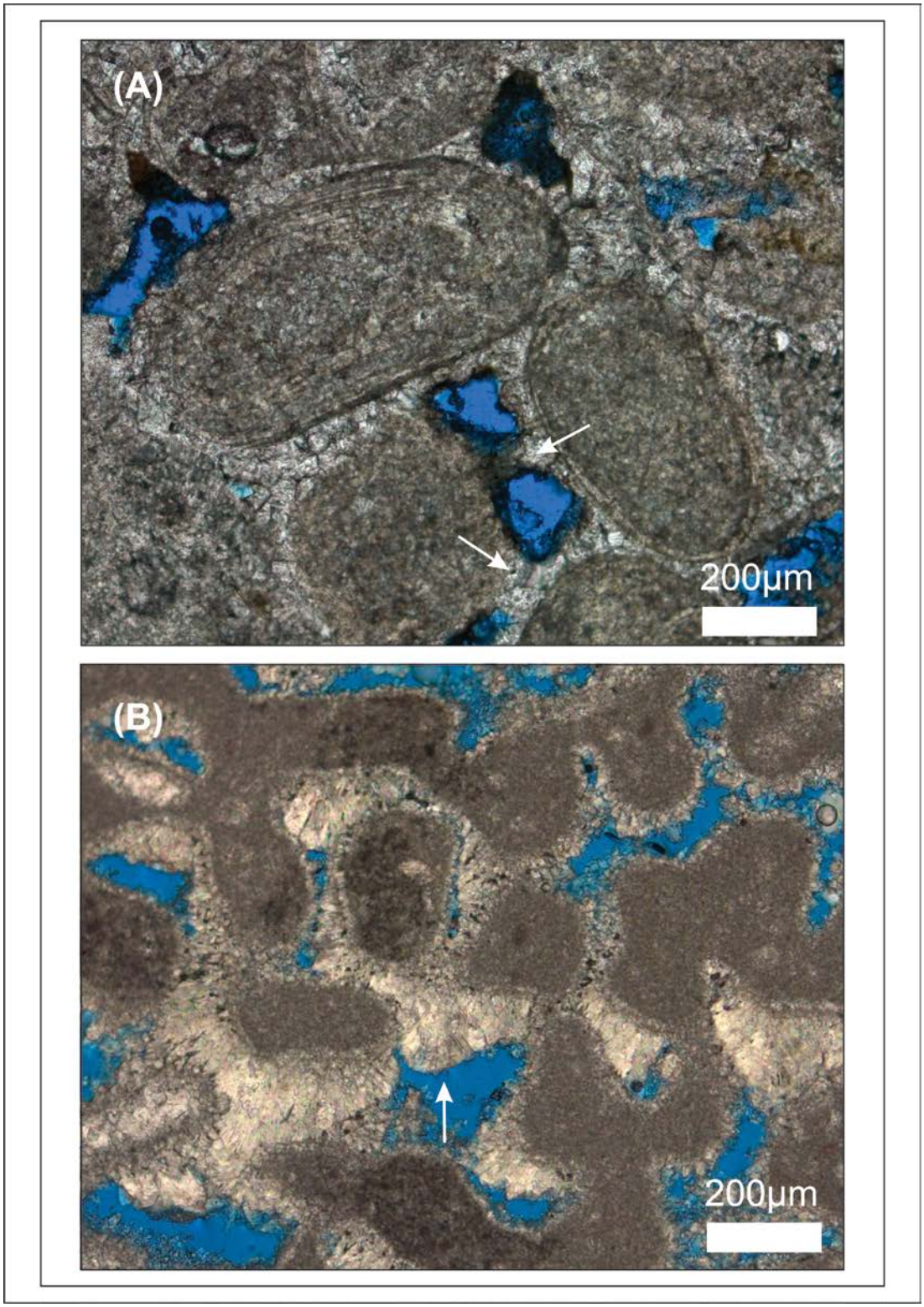

Figure 29. Photomicrographs of asymmetrical rim cements. (A) Meniscus asymmetrical rim cement in oolitic grainstone facies. (B) Gravity/Pendant asymmetrical rim cement in bioclastic facies.

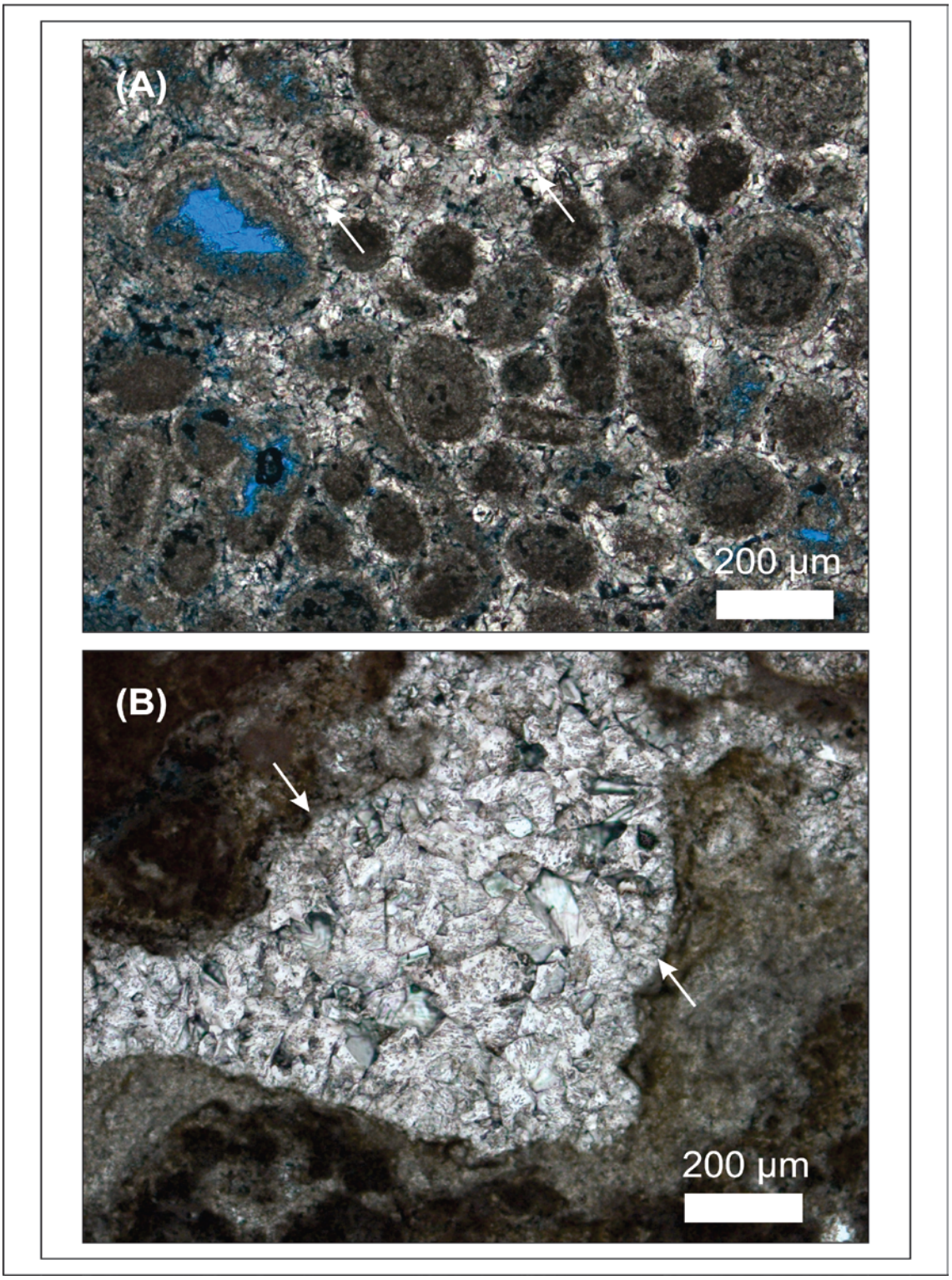

Figure 30. Photomicrographs of the pore-filling cements. (A) Intergranular pore fill cement in oolitic grainstone facie. (B) Drusy and blocky cement in red algal facies.

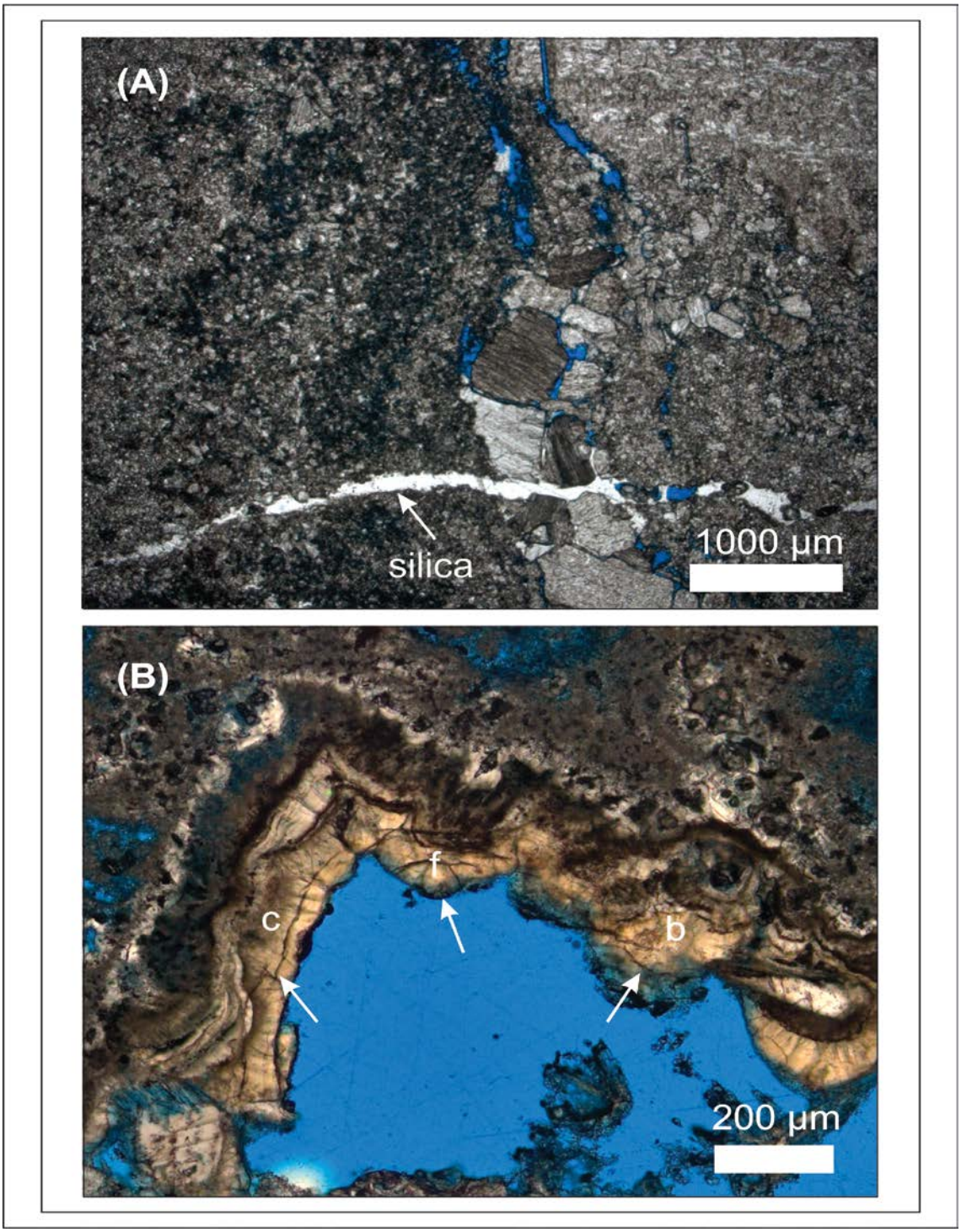

Figure 31. Photomicrographs of the dolomite and silica fracture fill cements and Thick crust cements. (A) Dolomite cement filled vertical fracture and silica cement filled the horizontal fracture. (B) Thick cement layer show on the left side crust cement and on the right side a combination of fan-shape and botryoid cements in red algal facies, (c) crust cement, (f) fan shape cement, and (b) botryoid cement.

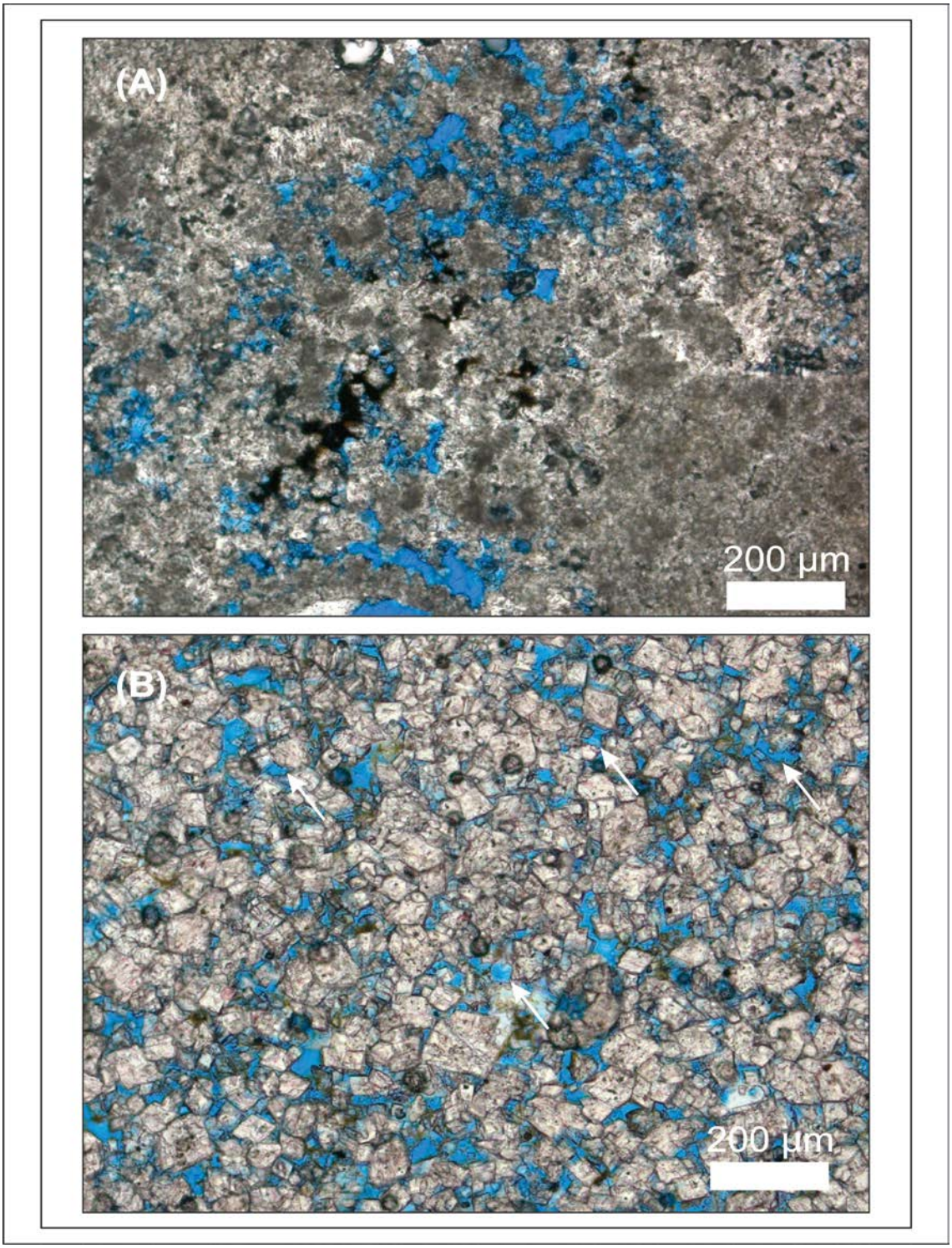

Figure 32. Photomicrographs of the secondary diagenetic pores. (A) Intercrystalline porosity in red algal facies. (B) Dolomoldic porosity in red algal facies.

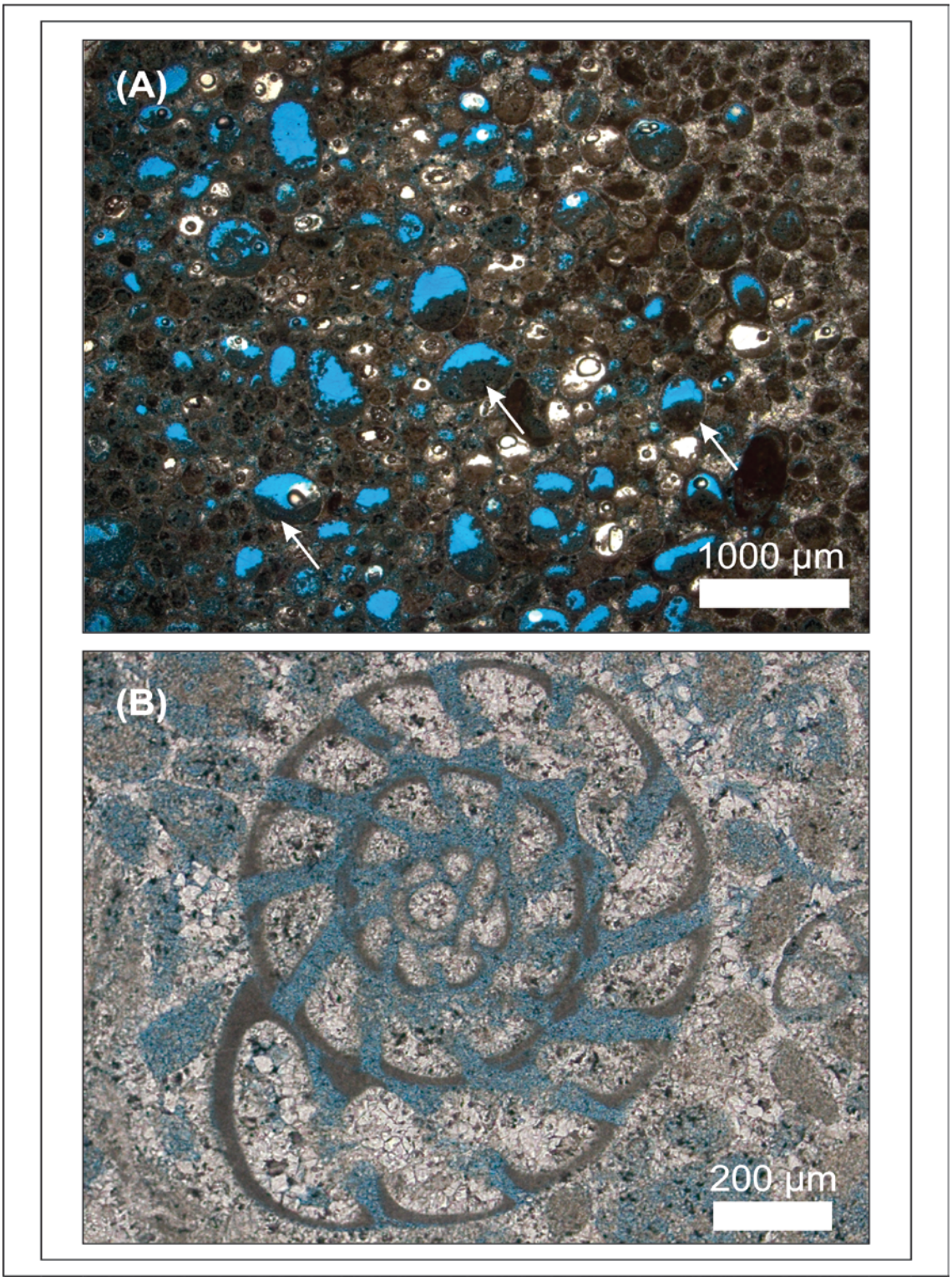

Figure 33. Photomicrographs of the secondary diagenetic pores. (A) Oomoldic porosity and geopetal dissolution structure in oolitic grainstone facies. (B) Biomoldic porosity bioclastic grainstone facies.

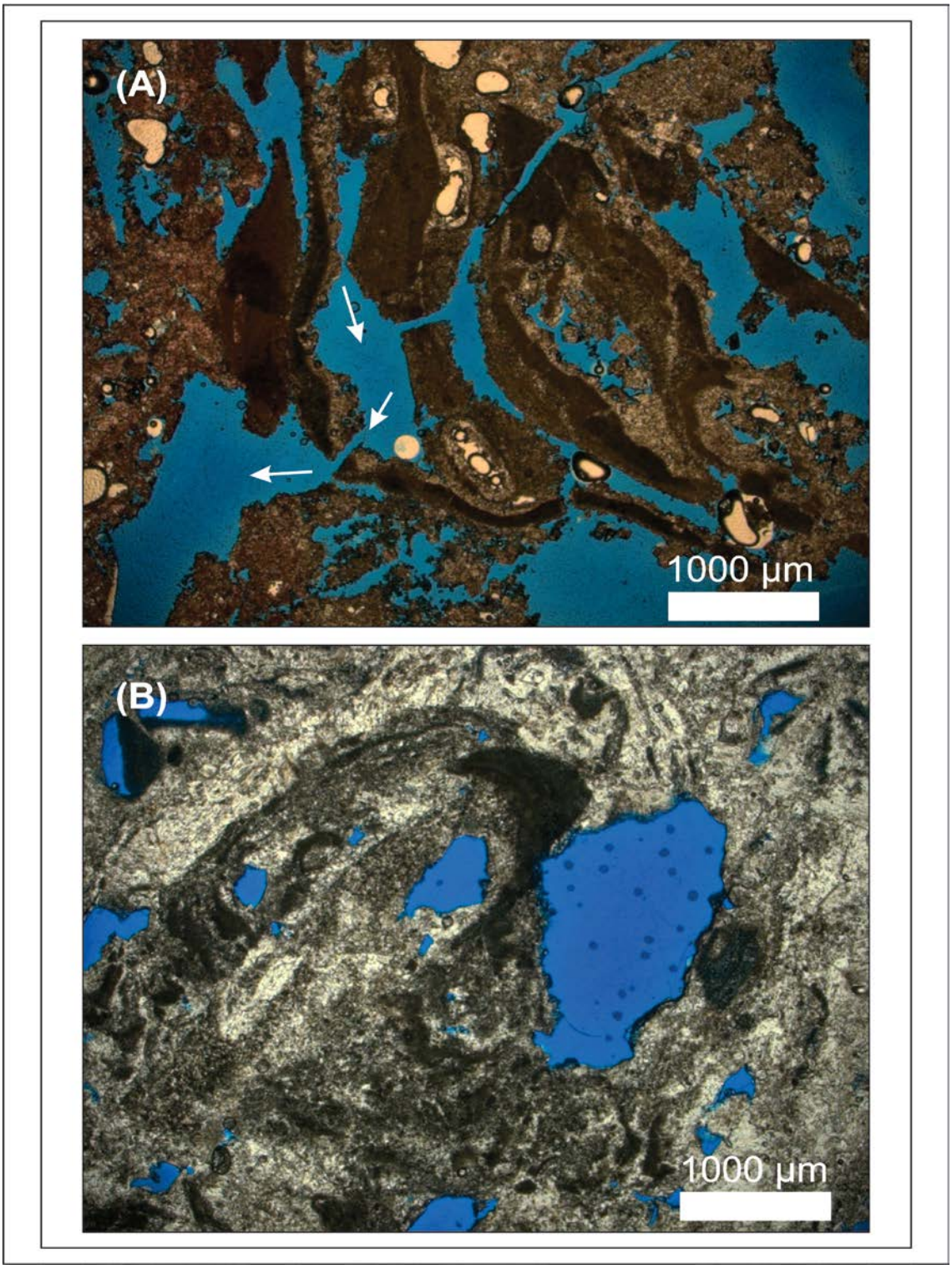

Figure 34. Photomicrographs of the secondary diagenetic pores. (A) Channel Porosity in red algal facies. (B) Vuggy porosity in red algal facies.

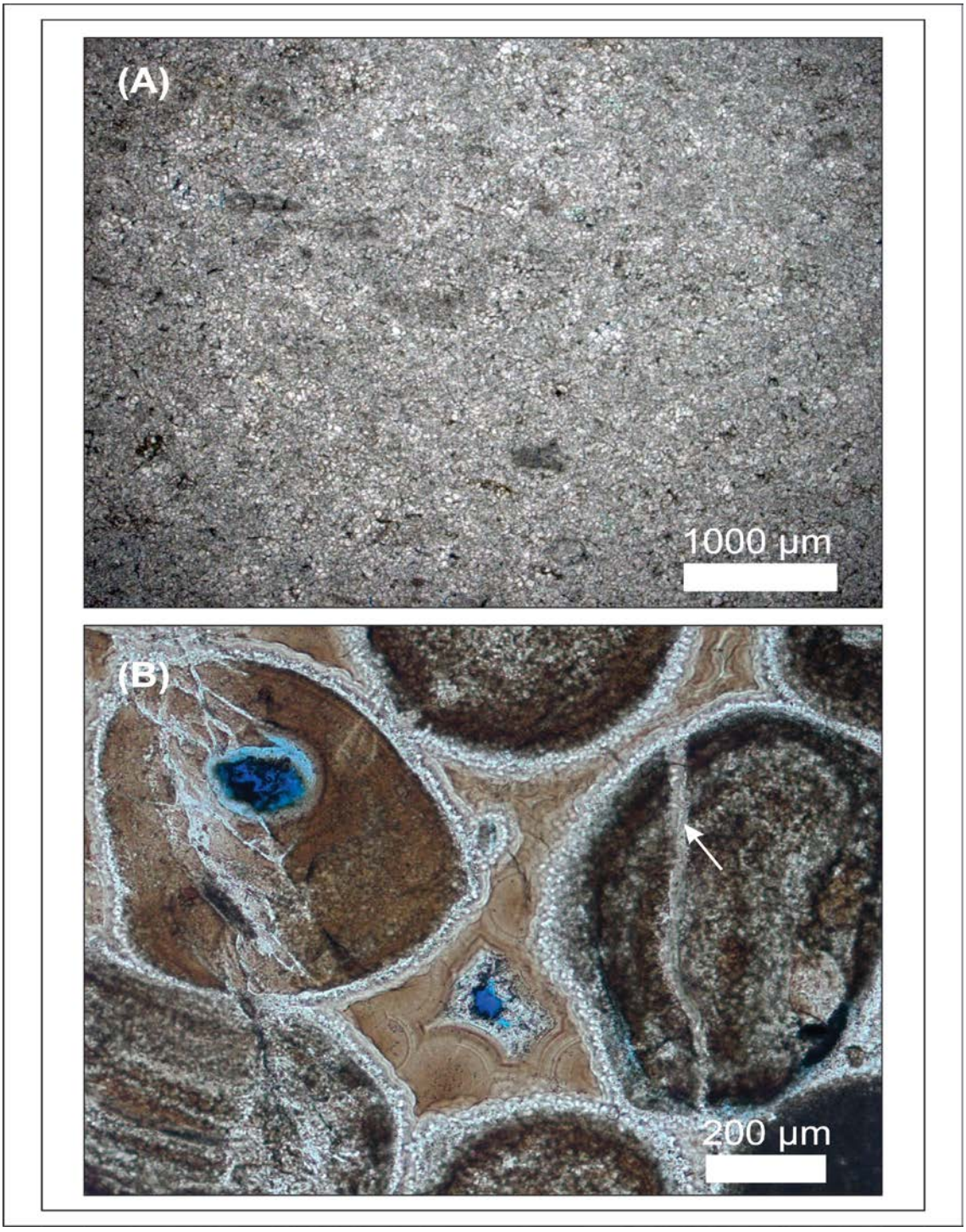

Figure 35. Photomicrographs of the recrystallization and 1st compaction phase. (A) Recrystallization of the mud matrix caused crystals growth in microbialite facies. (B) 1st Phase fractures were filled with microcrystalline quartz that was later leached at some places in oolitic grainstone facies. Later pores were filled with botryoid chalcedony.

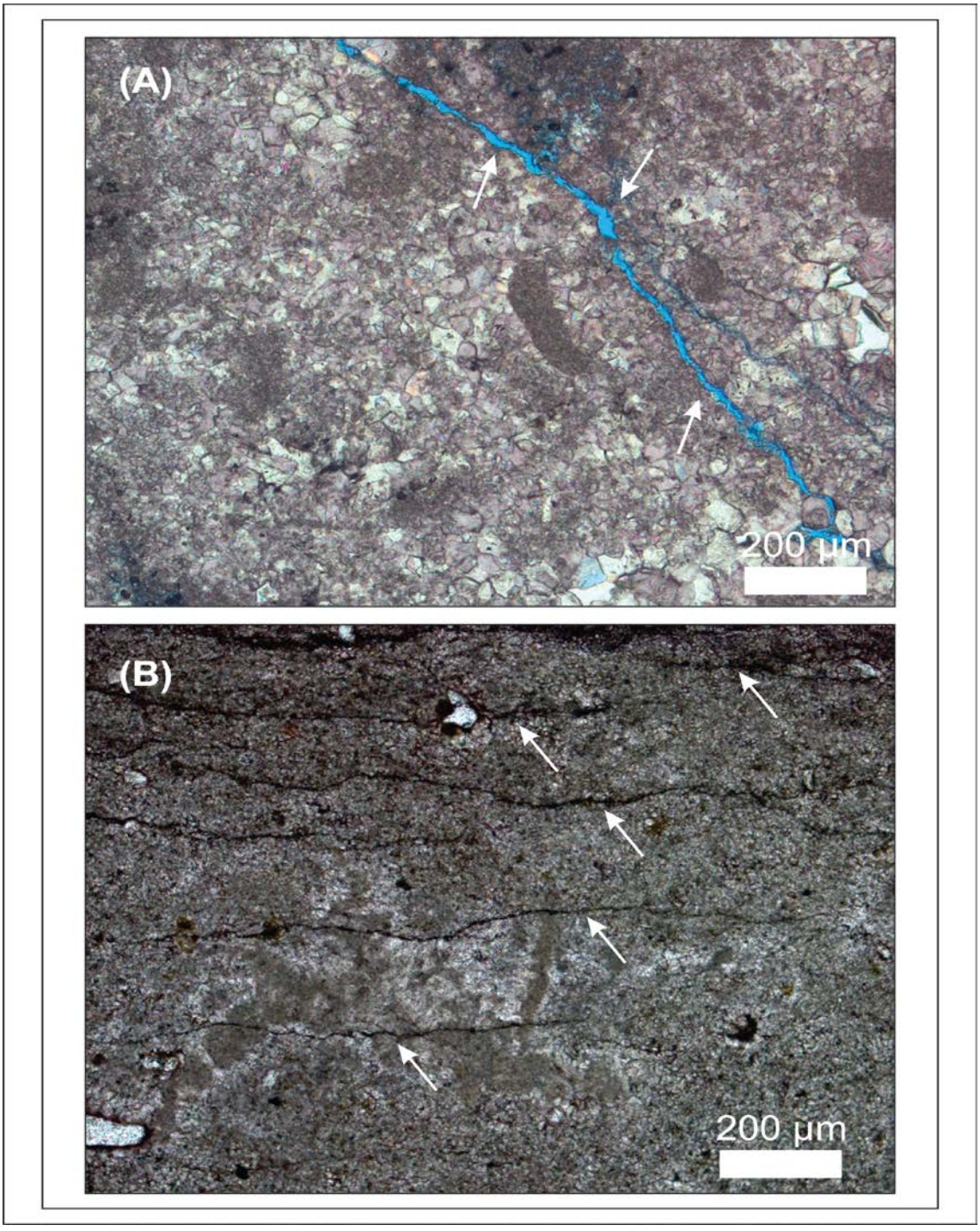

Figure 36. Photomicrographs of the compaction types. (A) 2nd phase fractures are open and free of cement in red algal facies. (B) Dissolution seams in microbial facies occur due to chemical compaction and always associated with fractures.

open and unfilled (Fig. 36 A). The dissolution seams are very common in the fractured zones associated with microbialites facies (Fig. 36 B).

Replacement processes are very intensive for the dolomitization and dedolomitization, but limited in volume for gypsum replacement and silicification. All stained thin sections of the studied Cyrenaican Miocene carbonate rocks are non-ferroan limestone, dolomite and dedolomite. The dolomitization and dedolomitization processes are dominant in the lower Miocene strata, whereas recrystallization and dissolution seams are dominant in the younger Miocene rocks. Type-1, Type-2, and Type-3 dolomites (Figs. 37 A and B, and 38 A) were observed in the thin sections. The Type-3 dolomite, the dominant dolomite type, has porphyrotopic texture, polymodal crystals, which are both fabric destructive and fabric selective. Commonly this dolomite is dedolomitized (Fig. 38 B) because it turned to pink to red-brown when treated with Alizarin Red-S stain, having planar crystal boundaries, euhedral to subhedral crystal shapes, and crystal sizes from 15-180 μm.

Occasionally, in the Cyrenaican Miocene, carbonate rocks are partially replaced by gypsum then by silica in quartz-rich thrombolite facies (Fig. 39 A). In other cases, the silica replaced the lozenge shape gypsum crystals (Fig. 39 B). The Chalcedony forms some silica cement. Silicification occurs throughout the sections, but the amount decreases significantly in the younger Miocene interval. Moreover, the amount of silicification increases drastically along some 3rd-order sequence boundaries. Some pore-filling-cements are dedolomitized drusy and blocky cements with occasional chalcedony silica filling pores.

The petrographic analysis shows two distinct lithological, textural and paragenetic patterns above and below the Middle Miocene Langhian-Serravallian boundary. The older Miocene interval (Langhian and older) is dominated by silicified dedolomitized bioclastic-rich, bryozoan, and red algal packstone. The younger Miocene interval (Serravallian and younger) is dominated by silicified and recrystallized oolitic grainstone, and microbial-bioclastic-oolitic grainstone.

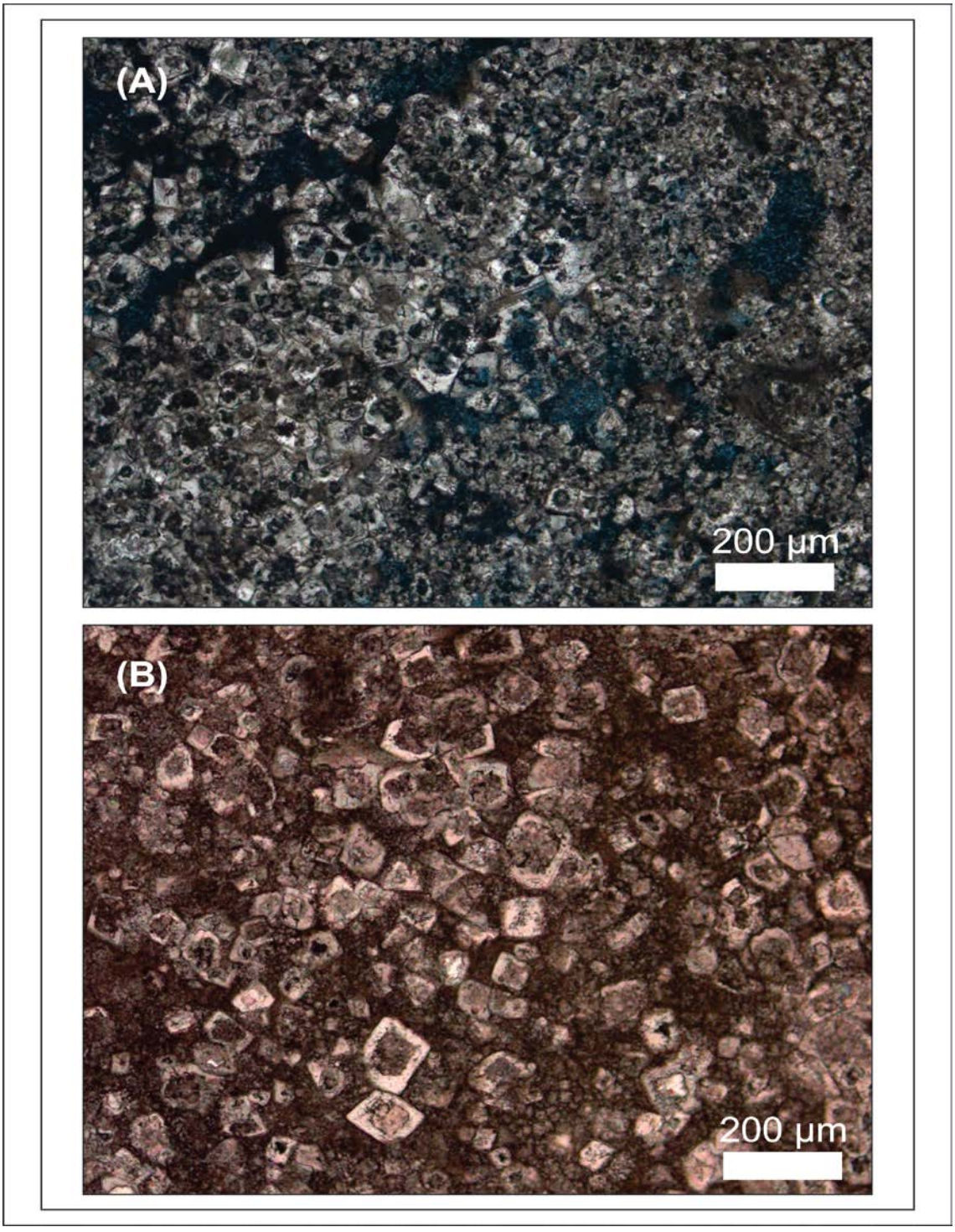

Figure 37. Photomicrographs of the diagenetic replacement events. (A) Mixed Type-1 subhedral medium size mosaic dolomite and Type-2 coarse mosaic, cloudy core and clear rim dolomite in red algal facies. (B) Type-2 coarse mosaic clear rim dolomite in red algal facies

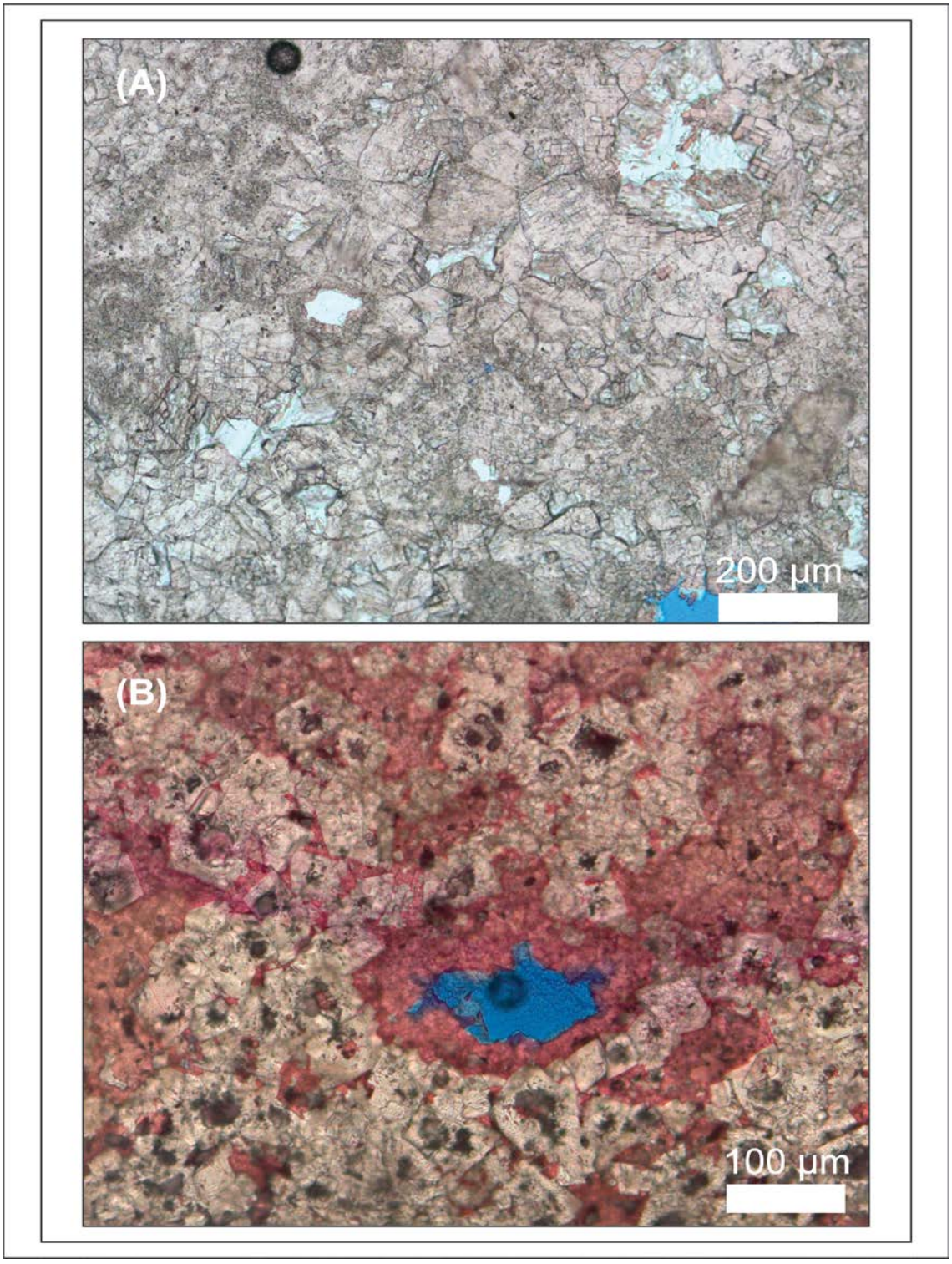

Figure 38. Photomicrographs of the diagenetic replacement events. (A) Type-3 coarse clear crystals dolomite in red algal facies. (B) Dedolomitization when dolomite replaced by calcite in red algal facies.

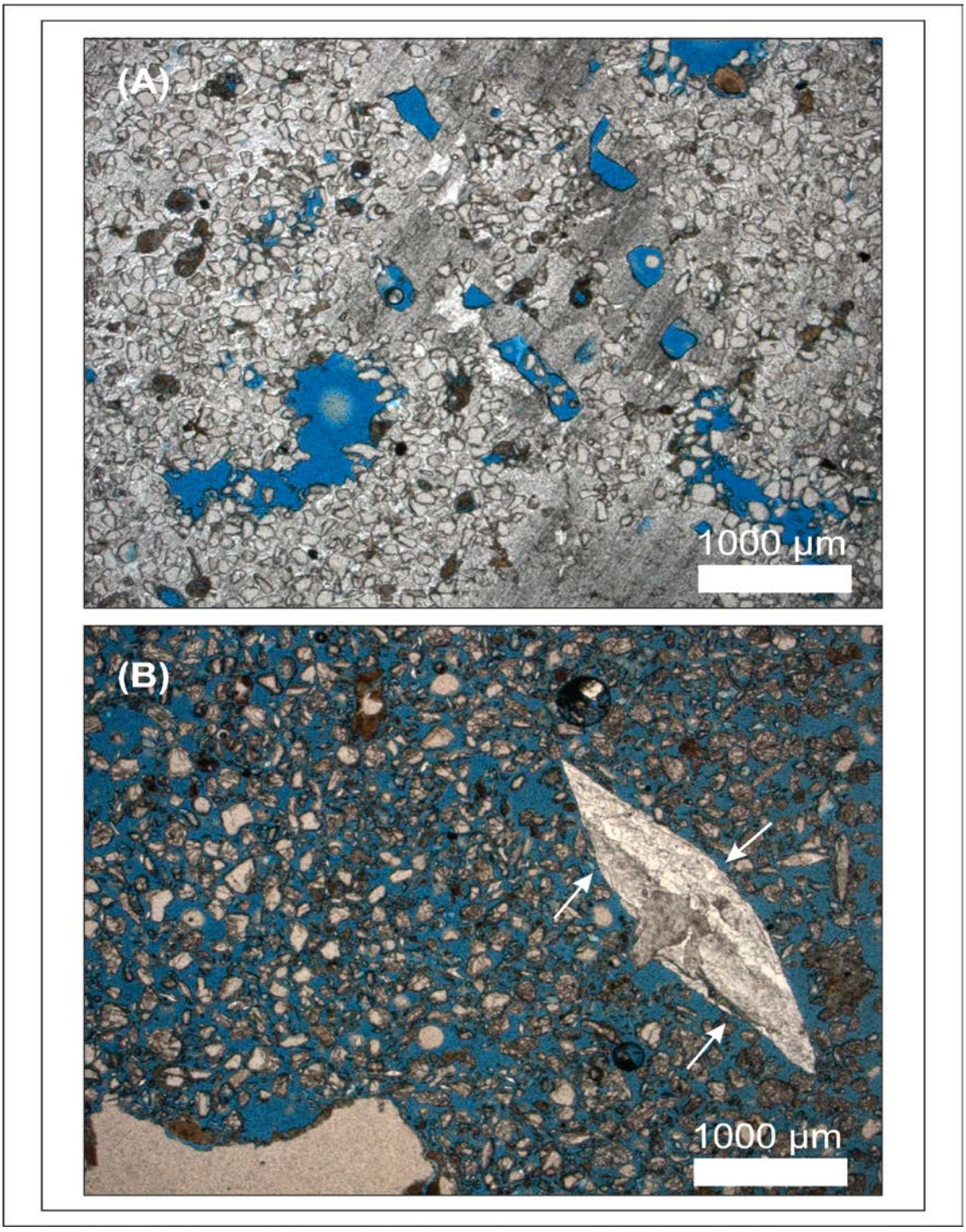

Figure 39. Photomicrographs of the diagenetic replacement events. (A) Quartz-rich thrombolite replaced by gypsum then by silica. (B) Gypsum crystal replaced by silica in siliciclastic facies.

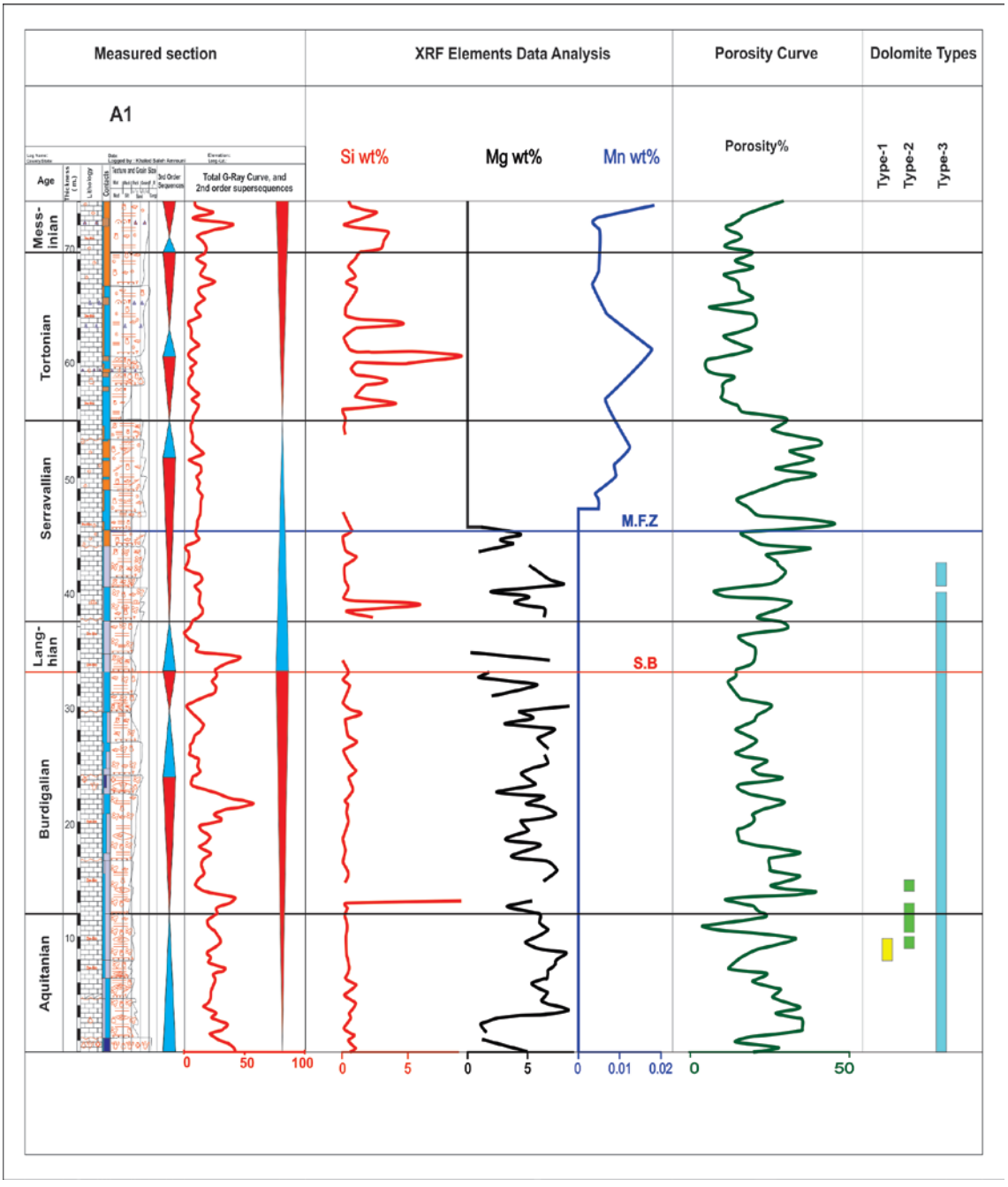

Figure 40. Measured field section A1, two 2nd-order supersequences, six 3rd-order sequences, total Gamma Ray profile, Si wt% , Mg wt%, Mn wt%, and porosity% curves, and dolomite types plotted as columns. The time lines are delineated based on the $\delta^{18}O$ and δ13C stable isotopes correlation, the 2nd-order supersequence boundary is the denoted as S.B, and the maximum flooding zone is denoted as M.F.Z.

The main porosity types in the Miocene sequences are oomoldic, fenestral, dolomoldic, frame-growth, biomoldic, fracture, vuggy, cavernous, and intercrystalline. However, the dolomoldic and frame-growth porosity is dominant in the older dedolomitized Miocene interval, whereas the oomoldic and fenestral porosity is dominant in the younger recrystallized Miocene interval. Geopetal filling structures are restricted to the oolitic grainstone facies, and the dissolution seams are restricted to the microbial facies. The Late Miocene has the lowest average visually estimated porosity values, whereas the Middle Miocene has the highest average porosity values, and the Early Miocene has medial average porosity values (Fig. 40).

The Si, Mg, and Mn element curves from the XRF data have three different patterns (Fig. 40). The Si element curve shows a spiky increase of the silica amount at some 3rd-order sequences boundaries, above some time boundaries between Miocene ages. The Mg element curve is continuous throughout the lower part of the Miocene, but absent in the upper part of the Miocene section. The Mn% element curve is absent in the lower part of the Miocene, occurring only in the upper part of the Miocene.

Discussion

The Cyrenaican Miocene carbonate platform is shallow marine ramp setting that includes peritidal facies, ramp crest facies, and subtidal facies. The peritidal facies include microbialites, pelletal wackestone/packstone, gypsum, bioclastic Porites reefs, green shale, and sandstone. The ramp crest facies is the oolitic grainstone. The subtidal facies includes the coralline red algae packstone, reworked red algae packstone, bioclastic wackestone/packstone, and reworked bioclastic packstone (Amrouni et al., 2013).

The Cyrenaican Miocene carbonate rocks were subjected to several diagenetic events some of which occurred more than once (e.g. micritization, cementation, dissolution, recrystallization, dolomitization, dedolomitization, gypsum replacement, silicification, and compaction). It is very obvious that the Cyrenaican Miocene carbonate

rocks had been through different stages of diagenesis as indicated by the superposition of the many different mineral phases and different cement minerals (e.g. Braithwaite, 1993 and 1986).

Cross cutting relationships were utilized in the petrographic part of this study to define the relative timing of each diagenetic event and then to build the paragenetic history of the Cyrenaican Miocene shallow carbonate rocks. The paragenetic sequence of the Cyrenaican Miocene consists of 18 diagenetic events that are lumped into 7 groups. Group 1 includes micritization and symmetrical rim cements. Group 2 includes asymmetrical rim cements and the 1st phase of pore-filling cement. Group 3 is the 1st phase of dissolution. Group 4 consists of 2nd phase of pore-filling cements, recrystallization, dolomitization, and dedolomitization replacement processes. Group 5 includes the 2nd phase of dissolution, geopetal fill, 1st phase of fracturing, and dissolution seams. Group 6 is made up of gypsum replacement, silica replacement, and fracture filling cement. Group 7 includes 2nd phase of fracturing, and 3rd phase of dissolution.

Micritization, fibrous, bladed, and dogtooth symmetrical cements are early phreatic-marine cements (e.g. Flügel, 2004; and Tucker 2009). Micritization (Fig. 27 A-B) was the first transformation process. Carbonate rocks micro-boring activity by endolithic cyanobacteria and then refilling leads to the formation of dense dark micrite (Tucker, 1996, 2009). The Micritization process affected skeletal grains and non-skeletal grains in the Cyrenaican rocks.

The symmetrical rim cements (Fig. 28 A-B) represent the second and third stages of diagenesis in the Cyrenaican. They are formed as fibrous, bladed, dogtooth, and circum granular during early marine conditions. The asymmetrical rim cement formed as gravity cement.

Meniscus, pendant asymmetrical rim cements and intergranular 1st pore-filling cement are the components of Group 2. They commonly form in the vadose-meteoric environment (e.g. Flügel, 2004). The asymmetrical rim cements are formed as meniscus, and pendant (Fig. 29 A-B). They represent the third stages of diagenesis in the Cyrenaican Miocene rocks. The asymmetrical rim cements dominantly form in the

vadose-meteoric environment, although they could form in the vadose-marine environment too (e.g. Flügel, 2004). The fourth stage of diagenesis is 1st pore-filling cement that filled the intergranular pores. This cement was originally clear crystals of spary calcite that filled intergranular depositional pore space (Fig. 30 A).

Group 3 is the 1st phase of meteoric water dissolution. The fifth stage of diagenesis is represented by the 1st dissolution of grains and cements. In this stage the calcium under saturated meteoric waters (e.g. Flügel, 2004; Scholle and Ulmer-Scholle, 2003; and Tucker, 1996) leached some grains and cements to create secondary intragranular, biomoldic and oomoldic porosity (Fig. 33 A-B).

2nd phase of Blocky and drusy pore-filling cements, recrystallization, dolomitization, and dedolomitization replacement processes are Group 4**.** The 2nd pore-filling cements that filled the secondary pore spaces represent the sixth stage of diagenesis. These pore-filling cements (Fig. 30 B) are drusy and blocky sparite cements of large sizes crystals that form in vadose meteoric water.

The seventh stage of diagenesis in the Cyrenaican Miocene carbonate rocks is the recrystallization (Fig. 35 A). In this stage matrix crystals grew, and changed their crystals shape and form without any change in their mineralogy (e.g. Flügel, 2004; Scholle and Ulmer-Scholle, 2003; Bathurst, 1972 and 1975; Tucker, 1996; and Folk, 1965).

Dolomitization and dedolomitization are the two diagenetic replacement processes that came as stages eight and nine (Figs 37 A-B, and 38 A-B). Dolomite formed by replacing the original calcite mineral. The dolomitization process affected grains, matrix and cements. There are three types of dolomite in the Cyrenaican carbonate rocks. Dolomite types 1 and 2 are replacement dolomite, whereas type-3 is dolomite cement (e.g. Amthor et al., 1993). The dolomitization process could either enhance or reduce the porosity (Ahr, 2008). The dedolomitization is the subsequently replacement process that transformed the dolomite again to calcite. Most of the dolomite rhombs in the study area turned to pink-reddish brown when treated with the Alizarin Red-S (e.g. Dickson, 1965 and 1966). In the case of Ar-Rajmah group the seepage-

reflux and the sabkha evaporation dolomitization models (e.g. Flügel, 2004;and Tucker, 199) could explain the formation of the dolomite in the shallowing upward Cyrenaican Miocene carbonate succession that dominated by peritidal facies associated interbedded with evaporite deposits.

The 2nd phase of dissolution, geopetal fill, 1st phase of fracturing, and dissolution seams are Group 5. The 2nd dissolution and geopetal dissolution structures are the tenth and eleventh stages of diagenesis in the Cyrenaican Miocene carbonate rocks. The meteoric water 2nd dissolution phase leached some of the cements, matrix, and grains (e.g. Flügel, 2004; Scholle and Ulmer-Scholle, 2003) to create the secondary intercrystalline, and dolomoldic porosity, to enhance the biomoldic and oomoldic, and to create vuggy and channel porosity (Figs 32 A-B, 33 A-B, 34 A-B). Geopetal meteoric water dissolution structure (Fig. 8 A) formed when the insoluble residue in the void space accumulated at the base of the secondary pore space.

The twelfth and thirteenth stages are mechanical and chemical compaction (Fig. 29 B-D). The mechanical compaction is the 1st fracturing that cut through grains and matrix. The chemical compaction is dissolution seams in the Cyrenaican Miocene that are mostly associated with the fractured rocks that have muddy matrix such as microbialite. Mechanically induced stylolites could result in porosity reduction (Braithwait, 1986). However, stylolites may also act as permeable zones and enhance the reservoir quality (Carozzi and Bergen, 1987).

Group 6 is made up of gypsum and silica replacement, and fracture filling cement. The replacement processes by gypsum and then by silica are the fourteenth and fifteenth stages of diagenesis (Fig. 39. A-B). The replacement gypsum and silica are very common in the microbial facies in the Cyrenaican Miocene. The diagenetic gypsum was always replaced by silica. In addition, there are cases where the depositional gypsum crystals also were replaced by silica. Silica types are chalcedony, microcrystalline quartz and megaquartz. The chalcedonic silica is length slow, which indicates the association of the silica with the evaPorites (e.g. Tucker, 1996).

The fracture filling-cement is the stage sixteen in the diagenetic sequence in the Cyrenaican Miocene. Some fractures are filled with microcrystalline quartz cement and some others are open and unfilled (Figs. 31 A, and 35 B).

Group 7 is the 2nd phase of fracturing, and 3rd phase of dissolution. The seventeenth stage of diagenesis is a second phase of mechanical compaction. The 2nd fracturing events cut through grains and matrix and sometimes cross cutting previously cemented fractures (Figs 35 B, and 36 A). The last stage of diagenesis is the 3rd phase of meteoric water dissolution that represents the eighteenth event. In this stage the meteoric diagenetic water leached some silica cements that replaced calcite cements and silica cements that filled fractures (Figs. 31 A, and 35 B). Also, it enhanced the intercrystalline, dolomoldic, biomoldic, and oomoldic porosity.

The stable isotopes and XRF Data of the Cyrenaican Miocene strata support the petrographic observations (Figs. 26 and 40). The $\delta^{18}O$ and $\delta^{13}C$ stable isotopes cross-plot shows a trend of depletion from older to younger Miocene rocks. This general trend indicates that the younger Miocene intervals were subjected to more meteoric water alteration than the older one (e.g. Simms and Ruffell, 1990; Banner and Hanson, 1990; Banner, 1995; Jacobsen and Kaufman, 1999; Veizer et al., 1999; Immenhauser et al., 2003; and Grotzinger et al, 2011). The XRF data shows that the amount of the Mn element is very low and only occurs in the Upper Miocene interval. The Mn element content increase is an indicator of diagenesis alteration (e.g. Brand and Veizer, 1980; Veizer, 1983; Banner, 1995), and supports the petrographic and isotopic data that the upper part of the Cyrenaican Miocene subjected to intensive meteoric water diagenesis. Also, the absence of the Mg element, dolomite component, in the upper part of the Cyrenaican Miocene is evidence that some dolomitized intervals that show pseudo-dolomite rhombic crystals in the upper part of the Cyrenaican Miocene were recalcitized due to the meteoric water diagenesis.

To sum up, the Cyrenaican Miocene ramp carbonate rocks had been through eighteen diagenetic events. These events started with micritization then rim cements and 1st pore-filling cements that partially reduced the primary porosity. Next, the 1st

dissolution event that created secondary intercrystalline, biomoldic, and oomoldic porosity, and then followed by the 2nd pore-filling cement that again reduced the porosity. Recrystallization that led to enlargement of matrix crystals led to the reduction of the intercrystalline porosity. Dolomitization and dedolomitization replacement events happened next and they may either have negative or positive effect on the porosity. The 2nd dissolution followed and again enhanced the secondary porosity to a large extent. The first fracturing event enhanced the porosity and permeability by cutting through gains and matrix. The dissolution seems that followed they may have either positive or negative impact to the porosity. The next stage was replacement by gypsum and silica followed by the fracturing fill cement that cause minor growth of silica into pore spaces that might cause minor reduction of the porosity. The following 2nd fracturing event and the following 3rd dissolution events played a major role in enhancing the secondary porosity and the permeability of the Cyrenaican Miocene carbonate ramp rocks.

Porosity in the Miocene is still facies controlled, in spite of the diagenetic enhancement and creation of secondary porosity. The highest porosity values are in the Middle Miocene that dominated with the high energy oolitic grainstone facies, the medial porosity values are in the Early Miocene that dominated by coralline red algae facies, and the lower porosity values are in the Late Miocene associated with the low energy microbial-oolitic grainstone.

The XRF and δ18O and δ13C stable isotopes data proved that the Cyrenaican Miocene rocks had been through meteoric diagenesis that led to substantial elimination of the trace elements, and the depletion of the δ18O and δ13C stable isotopes and. This elemental and chemical data analysis supports the thin sections petrographic analysis.

Conclusions

The Cyrenaican Miocene ramp has nine shallow marine carbonate tidal to subtidal depositional facies intercalated with a siliciclastic tongue of quartz sandstone and green shale. Six diagenetic processes produced a succession of eighteen diagenetic

events. The lower part of the Cyrenaican Miocene carbonate sequence has different depositional texture and diagenetic pattern than the upper part. The boundary between the two paragenetic successions in the study area ties roughly with the chemostratigraphic and the outcrop sequence stratigraphic surfaces.

The analysis of the petrographic, XRF-elements and δ18O and δ13C stable isotopes data of the Cyrenaican Miocene carbonate rocks indicates the multiple phases of diagenetic alteration. Also, it shows that the upper part of the Cyrenaican Miocene sequence is affected by the meteoric water diagenesis more than lower part. The diagenetic processes enhanced the total porosity, although porosity is still showing depositional facies control trends.

CHAPTER V

CONCLUSIONS

The Ar-Rajmah Group of the Cyrenaica Platform is a ramp system with irregular palaeotopography. The platform has two 2nd-order supersequences that include six 3rd order sequences. The oldest 2nd-order supersequences made of HST, where the youngest 2nd order supersequence made of TST, and HST. The TST is separated by a sharp unconformity surface from the older HST, and by a maximum flooding zone from the younger HST. The HST of the older 2nd-order supersequence represents the Benghazi Formation of the Early Miocene. The TST and HST of the younger 2nd-order supersequence represent the Wadi Al-Qattarah Formation and its lateral equivalents Al-Sceleidima Formation and Msus Formation. The shallowing upward 3rd-order sequences range in thickness from 3.5 m to more than 22.5 m. The Early Miocene ramp system is dominated by red algal and bioclastic facies, the Middle and Late Miocene ramp system is dominated by microbial-oolitic grainstone facies in association with evaPorites. The Porites corals are only present in the Early Miocene, whereas the siliciclastic facies are only present in the Middle Miocene. This outcrop study of the Ar-Rajmah Group extends for more than 130 km along a dip profile and its excellent 3-D exposure makes it an analogue for ooid grainstone, microbial carbonate, and red algae reservoirs in the subsurface within the Mediterranean region and globally.

The Cyrenaican Miocene $\delta^{13}C$ and $\delta^{18}O$ chemostratigraphy is established through the analysis of the Ar-Rajmah Group carbonate platform rocks. The integration of the stable isotope data with the detailed gamma-ray-outcrop-based stratigraphic section resulted in defining two 2nd order supersequences (SS1-SS2) and six 3rd order sequences (S1-S6) in the Cyrenaican Miocene section. These sequences are identified based on facies analysis, stacking patterns, stratigraphic surfaces, gamma-ray signatures, field observations, and pattern of the stable isotopes.

The Miocene Ar-Rajmah Group $\delta^{18}O$ data ranges from -9.21 to +9.72 ‰ VPDB, and the $\delta^{13}C$ data ranges from -10.05 to +7.55 ‰ VPDB. The $\delta^{18}O$ and $\delta^{13}C$ values of the Miocene Ar-Rajmah Carbonate Group have a wider range than the regional Mediterranean, the Indian Ocean, and the global Miocene $\delta^{18}O$ and $\delta^{13}C$ values. The $\delta^{13}C$ and $\delta^{18}O$ curves of the Cyrenaican Ar-Rajmah group sections contain the whole Miocene as indicated by the previous study of the forams biostratigraphy.

The Cyrenaican Miocene isotopic values represent a long term marine global isotopic signature overprinted by shorter term locally and regionally alterations due to environmental facies control, diagenesis, and local high organic productivity. The enrichment of the values $\delta^{13}C$ is associated with an organic green shale deposits that characterized by high gamma-ray signature, the enrichments of $\delta^{18}O$ is associated with the peritidal evaporite deposits, the depletion of $\delta^{13}C$ and $\delta^{18}O$ is associated with meteoric water diagenesis.

The positive carbon isotope excursion of the Cyrenaica platform in late Early Miocene and Middle Miocene records the global Monterey event. The amplified Tortonian negative carbon isotope shift records the emergence of the upward restricted shallow-water Cyrenaican platform.

The Cyrenaican platform is a carbonate dominated system with an observable siliciclastic influx in the Middle Miocene that associated with high gamma ray, 2nd order transgressive system tract, and enrichment in the δ13C. Due to resistance to subsidence, the Cyrenaican platform Middle Miocene deepening signature is aggradation thick shallow facies rather than deepening upward facies as in the Mediterranean coeval sequences.

The subtidal coralline red algae dominated only the whole Early Miocene and gradually replaced by the shallower restricted facies in the Middle Miocene and Late Miocene. The Porites corals are not dominant in the Cyrenaican platform, and only restricted to the Early Miocene sequence.

The Cyrenaican Miocene ramp has nine shallow marine carbonate tidal to subtidal depositional facies intercalated with a siliciclastic tongue of quartz sandstone

and green shale. Six diagenetic processes produced a succession of eighteen diagenetic events. The lower part of the Cyrenaican Miocene carbonate sequence has different depositional texture and diagenetic pattern than the upper part. The boundary between the two paragenetic successions in the study area ties roughly with the chemostratigraphic and the outcrop sequence stratigraphic surfaces.

The analysis of the petrographic, XRF-elements and δ18O and δ13C stable isotopes data of the Cyrenaican Miocene carbonate rocks indicates the multiple phases of diagenetic alteration. Also, it shows that the upper part of the Cyrenaican Miocene sequence is affected by the meteoric water diagenesis more than lower part. The diagenetic processes enhanced the total porosity, although porosity is still showing depositional facies control trends.

REFERENCES

Abdulsamad, E., and Bu-Argoub, F., 2006, Sedimentary facies and Foraminifera of the Miocene carbonates of the Ar Rajmah Group in Cyrenaica, NE-Libya: Petroleum Research Journal, v. 19, p. 49-60.

Abdulsamad, E., Bu-Argoub, F., and Tmalla, A., 2009, A stratigraphic review of the Eocene to Miocene rock units in the al Jabal al Akhdar, NE Libya: Marine and Petroleum Geology, v. 26, p. 1228-1239.

Abdulsamad, E.O., 2000, Contribution to the Nummulites taxonomy from the Palaeogene sequences of Al Jabal al Akhdar (Cyrenaica, NE Libya): Revue de Paléobiologie, v. 19, p. 19-45.

Abdulsamad, E.O., and Barbieri, R., 1999, Foraminiferal distribution and palaeoecological interpretation of the Eocene–Miocene carbonates at Al Jabal al Akhdar (northeast Libya): Journal of Micropalaeontology, v. 18, p. 45-65.

Abdulsamad, E.O., and El Zanati, S.M., 2013, Miocene benthic foraminifera from the Soluq area, ne Libya: biostratigraphy and environmental significance: Journal of Mediterranean Earth Sciences, v. 5, p. 245-256

Abdusamad, E., 1999, Stratigraphy and paleobiogeography of Tertiary larger foraminifera from Al Jabal al Akhdar (Cyrenaica, NE Libya): Giornale di Geologia, ser, v. 3, p. 75-98.

Abreu, V.S., and Anderson, J.B., 1998, Glacial eustasy during the Cenozoic: sequence stratigraphic implications: AAPG bulletin, v. 82, p. 1385-1400.

Ahr, W.M., 1973, The carbonate ramp: an alternative to the shelf model: Transactions, Gulf Coast Association of Geological Societies, v. 23, p. 221-225.

Ahr, W.M., 2011, Geology of carbonate reservoirs: the identification, description and characterization of hydrocarbon reservoirs in carbonate rocks, John Wiley & Sons.

Ahr, W.M., Allen, D., Boyd, A., Bachman, H.N., Smithson, T., Clerke, E., Gzara, K., Hassall, J., Murty, C., and Zubari, H., 2005, Confronting the carbonate

conundrum: Oilfield Review, v. 17, p. 18-29.

Al Haddad, S., and Mancini, E.A., 2013, Reservoir characterization, modeling, and evaluation of Upper Jurassic Smackover microbial carbonate and associated facies in Little Cedar Creek field, southwest Alabama, eastern Gulf coastal plain of the United States: AAPG bulletin, v. 97, p. 2059-2083.

Al Haddad, S., and Mancini, E.A., 2013, Reservoir characterization, modeling, and evaluation of Upper Jurassic Smackover microbial carbonate and associated facies in Little Cedar Creek field, southwest Alabama, eastern Gulf coastal plain of the United States: AAPG bulletin, v. 97, p. 2059-2083.

Al-Dukhayyil, R., and Read, J.F., 2012, Permo-Triassic Upper Khuff Carbonate Sequences, Ghawar Field, Saudi Arabia, GEO 2012.

Allan, J., and Matthews, R., 1982, Isotope signatures associated with early meteoric diagenesis: Sedimentology, v. 29, p. 797-817.

Amrouni, K.S., 2006, Sedimentology and Sequence Stratigraphy of Late Miocene Sequence (Wadi Yunis Member, Al Khums Formation),Sirt Basin, Libya. MSc Thesis submitted to the Department of Earth Sciences in partial fulfillment to the requirement for the Master degree of Science in Geology The University of Garyounis, Benghazi, Libya, p. 245.

Amrouni, K.S., 2000, Geology of the area between Wadi Al-Abuad and Wadi Zazah, Cyrenaica, NE Libya. BSc Thesis submitted to the Department of Earth Sciences in partial fulfillment to the requirement for the degree of Bachelor of Science in Geology, the University of Garyounis, Benghazi, Libya, p. 131.

Amrouni, K.S., Pope, M.C., and Ahmed, S., 2013, Sedimentology and Sequence Stratigraphy of the Middle to Late Miocene, Al-Jabal Al-Khdar Uplift and Soluq Trough, Cyrenaican NE Libya: AAPG 2013 Annual Convention and Exhibition, Pittsburgh, Pennsylvania, May 19-22, p. 4.

Amthor, J.E., Mountjoy, E.W., and Machel, H.G., 1993, Subsurface dolomites in Upper Devonian Leduc Formation buildups, central part of Rimbey-Meadowbrook reef trend, Alberta, Canada: Bulletin of Canadian Petroleum Geology, v. 41, p. 164-

185.

Arenas, C., Casanova, J., and Pardo, G., 1997, Stable-isotope characterization of the Miocene lacustrine systems of Los Monegros (Ebro Basin, Spain): palaeogeographic and palaeoclimatic implications: Palaeogeography, Palaeoclimatology, Palaeoecology, v. 128, p. 133-155.

Banerjee, S., 1980, Stratigraphic Lexicon of Libya. Department of Geological Researches & Mining: Bulletin.

Banner, J.L., 1995, Application of the trace element and isotope geochemistry of strontium to studies of carbonate diagenesis: Sedimentology, v. 42, p. 805-824.

Banner, J.L., 1995, Application of the trace element and isotope geochemistry of strontium to studies of carbonate diagenesis: Sedimentology, v. 42, p. 805-824.

Banner, J.L., and Hanson, G.N., 1990, Calculation of simultaneous isotopic and trace element variations during water-rock interaction with applications to carbonate diagenesis: Geochimica et Cosmochimica Acta, v. 54, p. 3123-3137.

Barr, F., 1968, Upper Cretaceous stratigraphy of Jabal al Akhdar, Northern Cyrenaica, Geology and Archaeology of Northern Cyrenaica, Libya. Pet. Explor. Soc. Libya, 10th Annu. Field Conf, p. 131-142.

Barr, F., and Berggren, W.A., 1978, Lower Tertiary biostratigraphy and tectonics of northeastern Libya, Woods Hole Oceanographic Institution.

Barr, F., and Weegar, A., 1972, Stratigraphic Nomenclature of the Sirte Basin, Libya, The Petroleum Exploration Society of Libia.

Barron, J.A., and Keller, G., 1982, Widespread Miocene deep-sea hiatuses: Coincidence with periods of global cooling: Geology, v. 10, p. 577-581.

Barron, J.A., Keller, G., and Dunn, D.A., 1985, A multiple microfossil biochronology for the Miocene: Geological Society of America Memoirs, v. 163, p. 21-36.

Bathurst, R.G., 1972, Carbonate sediments and their diagenesis, Elsevier.

Bathurst, R.G., 1975, Carbonate sediments and their diagenesis: Amsterdam, Elsevier, 658 p.

Benson, D.J., and Mancini, E.A., 1984, Porosity development and reservoir

characteristics of the Smackover Formation in southwest Alabama, Geological Survey of Alabama.

Best, M.W., and Boekschoten, G., 1981, On the coral fauna in the Miocene reef at Baixo, Porto Santo (Eastern Atlantic): Netherlands Journal of Zoology, v. 32, p. 412-418.

Bosworth, W., El-Hawat, A.S., Helgeson, D.E., and Burke, K., 2008, Cyrenaican "shock absorber" and associated inversion strain shadow in the collision zone of northeast Africa: Geology, v. 36, p. 695-698.

Braithwaite, C., 1986, Mechanically induced stylolites and loss of porosity in dolomites: Journal of Petroleum Geology, v. 9, p. 343-348.

Braithwaite, C., 1993, Cement Sequence Stratigraphy in Carbonates: Perspective: Journal of Sedimentary Research, v. 63.

Brand, U., 2004, Carbon, oxygen and strontium isotopes in Paleozoic carbonate components: an evaluation of original seawater-chemistry proxies: Chemical Geology, v. 204, p. 23-44.

Brand, U., and Veizer, J., 1980, Chemical diagenesis of a multicomponent carbonate system--1: Trace elements: Journal of Sedimentary Research, v. 50.

Brand, U., and Veizer, J., 1980, Chemical diagenesis of a multicomponent carbonate system--1: Trace elements: Journal of Sedimentary Research, v. 50.

Brand, U., and Veizer, J., 1981, Chemical diagenesis of a multicomponent carbonate system-2: stable isotopes: Journal of Sedimentary Research, v. 51.

Brandano, M., Brilli, M., Corda, L., and Lustrino, M., 2010, Miocene C-isotope signature from the central Apennine successions (Italy): Monterey vs. regional controlling factors: Terra Nova, v. 22, p. 125-130.

Broecker, W.S., 1982, Glacial to interglacial changes in ocean chemistry: Progress in Oceanography, v. 11, p. 151-197.

Broecker, W.S., 1982, Glacial to interglacial changes in ocean chemistry: Progress in Oceanography, v. 11, p. 151-197.

Buchbinder, B., 1996, Middle and Upper Miocene reefs and carbonate platforms in

Israel.

Buchbinder, B., Martinotti, G., Siman-Tov, R., and Zilberman, E., 1993, Temporal and spatial relationships in Miocene reef carbonates in Israel: Palaeogeography, Palaeoclimatology, Palaeoecology, v. 101, p. 97-116.

Carannante, G., Esteban, M., Milliman, J., and Simone, L., 1988, Carbonate lithofacies as paleolatitude indicators: problems and limitations: Sedimentary Geology, v. 60, p. 333-346.

Carmignani, L., 1984, Geological Map of Libya, scale 1:250,000, Sheet Wadi al Hamim (NH 34-7), Explanatory Booklet Industiial Research Centre, Tripoli.

Carozzi, A.V., and Von Bergen, D., 1987, Stylolitic porosity in carbonates: a critical factor for deep hydrocarbon production: Journal of Petroleum Geology, v. 10, p. 267-282.

Chevalier, J.-P., 1961, Recherches sur les Madréporaires et les formations récifales miocènes de la Méditerranée occidentale, Société géologique de France, 562 p.

Chevalier, J.-P., 1961, Recherches sur les Madréporaires et les formations récifales miocènes de la Méditerranée occidentale, Société géologique de France.

Choquette, P.W., and Pray, L.C., 1970, Geologic nomenclature and classification of porosity in sedimentary carbonates: AAPG bulletin, v. 54, p. 207-250.

Conant, L., C. , and Goudarzi, G., H. , 1964, Geological map of the Kingdom of Libya. U.S. Geol Surv. Misc. Geo.l Inv. Map 1-350A, scale 1:2,000,000. Washington.

Conant, L.C., and Goudarzi, G.H., 1967, Stratigraphic and tectonic framework of Libya: AAPG bulletin, v. 51, p. 719-730.

Daghastani, N., S. , 1999, Field Lectures Notes, G.F.M Course. Garyounis University, Benghazi, Libya.

Demarcq, G., 1984, Importance des mégafaunes marines benthiques dans l'évolution paléothermique de la Méditerranée au Néogène, Annales géologiques des pays helléniques, Volume 32, Laboratoire de géologie de l'Université, p. 87-95.

Demarcq, J., 1985, Paleothermic evolution during the Neogene in Mediterranean through the marine megafauna: Abstracts (abs.): VII Congress: Regional

Commission on Mediterranean Neogene Stratigraphy (RCMNS), Budapest, p. 176-178.

Desio, A., 1929, Risultati scientifici della Missione alla oasi di Giarabub (1926–1927), Fasc. 2, La Geologia: R. Soc. Geogr. Ital, p. 83-163.

Desio, A., 1935 a, Missione Scientifica della Reale Accademia d'ltalia a Cufra. Vol. I—Studi geologici sulla Cirenaica, sul Deserto libico, sulla Tripolitania e sul Fezzan orientale: Realc Accademia d'ltalia. Roma.

Desio, A., 1935 b, Studi geologici sulla Cirenaica, sul Deserto Libico, sulla Tripolitania e sul Fezzan orientali.(Missione scientifica della Reale Accademia d'Italia a Cufra, 1931.)[With a map.].

Desio, A., 1939, Studi morfologici sulla Libia Orientale. Missione Scientifica della Reale, Accd. d'Italia a Cufra, v. II, p. 216.

Desio, A., 1968, History of geologic exploration in Cyrenaica, Geology and archaeology of Northern Cyrenaica, Libya. Petrol. Explor. Soc. Libya, 10th Annual Field Conference, Tripoli, p. 79-113.

Dickson, J., 1965, A modified staining technique for carbonates in thin section.

Dickson, J., 1966, Carbonate identification and genesis as revealed by staining: Journal of Sedimentary Research, v. 36.

Dunham, R.J., 1962, Classification of carbonate rocks according to depositional textures.

Dunn, D.A., and Moore, T., 1981, Late Miocene-Pliocene (Magnetic Epoch 9-Gilbert Magnetic Epoch) calcium-Carbonate Stratigraphy of the Equatorial Pacific Ocean: Geological Society of America Bulletin, v. 92, p. 408-451.

El Amawy, M.A., Muftah, A.M., El-Wahed, M.A., and Nassar, A., 2011, Wrench structural deformation in Ras Al Hilal-Al Athrun area, NE Libya: a new contribution in Northern Al Jabal Al Akhdar Belt: Arabian Journal of Geosciences, v. 4, p. 1067-1085.

El Arnauti, A., Lawrece, S., Mansouri, A., Sengor, A., Soulsby, A., and Hassan, H., 2008, Structural styles in NE Libya: Geology of the East Libya, v. 4, p. 153-178.

El-Arnauti, A., and Shelmani, M., 1985, Stratigraphic and structural setting: Journal of

Micropalaeontology, v. 4, p. 1-10.

EL-Defter, T., S , and Issawi, B., 1977, Geological Map of Libya, scale 1:250,000, Sheet Al Bardia (NH 35-1), Explanatory Booklet, Industrial Research Centre, Tripoli.

El Hawat, A., and Abdulsamad, E., 2004, The geology of Cyrenaica: a field seminar: Earth Sci Soc, Libya, Tripoli, v. 130, p. 501-520.

El Hawat, A., S. , Barghathi, H., and Obeidi, A., 2004, Cyrenaica - Transect VII. In W. Cavazza, W. Roure, F., Spakman, W., Stampfli, G., Ziegler, P (eds.), The TRANSMED Atlas: the Mediterranean Region from Crust to Mantel. CD Rom, Springer-Verlag. Web site: http://www2.unibas.it/transmed/index.htm

EL Hawat, A., S. , and Salem, M., J., 1985, Stratigraphic reappraisal of Ar Rajmah Fm. Miocene, Al Jabal Al Akhdar, NE Libya: A case of field sedimentological approach. V IIIth Cong. Reg. Cong. Med. Neogene. (Abs.) Hung. Geol. Survey, Budapest, p. 206-208.

El Hawat, A., and Salem, M., 1987, A case study of the stratigraphie subdivision of Ar-Rajmah Formation and its implication on the Miocene of Northern Libya: Ann. Inst. Geol. Publ. Hung., v. 70, p. 173-183.

El Hawat, A., and Salem, M., 1987, A case study of the stratigraphie subdivision of Ar-Rajmah Formation and its implication on the Miocene of Northern Libya: Ann. Inst. Geol. Publ. Hung., v. 70, p. 173-183.

El Hawat, A.S., 1980, Intertidal and storm sedimentation from Wadi al Qattarah Member, Ar-Rajmah Fm., Al Jabal al Akhdar: Geology of Libya. Academic Press, London, II, p. 449-462.

El Hawat, A.S., and Shelmani, M.A., 1993, Short notes and guidebook on the geology of Al Jabal al Akhdar, Cyrenaica, NE Libya, Earth Science Society of Libya.

El Hawat, A.S., and Shelmani, M.A., 1993, Short notes and guidebook on the geology of Al Jabal al Akhdar, Cyrenaica, NE Libya, Earth Science Society of Libya, p. 70.

El-Hawat, A., S., 2006, Afield seminar guide to the geology of Cyrenaica. Shell-Libya field trip 5-9 Nov. 2006, Unpublished, p. 66.

El-Hawat, A., S., 2007, A guidebook to the geology of Cyrenaica. Pb-Libya field trip

2007, Unpublished, p. 38.

El-Hawat, A., and Pawellek, T., 2005, A field guidebook to the geology of Cyrenaica, Libya, RWE Dea North Africa, p. 90.

El-Hawat, A.S., Jorry, S., Hammuda, O., Obeidi, A., Barghathi, H., and Caline, B., 2007, The Eocene Ramp Complex of Al Jabal al Akhdar, Cyrenaica, NE Libya-A Surface Analogue for Nummulite Reservoirs, 3rd North African/Mediterranean Petroleum & Geosciences Conference & Exhibition.

El Khoudary, R., 1980, Planktonic Foraminifera from the middle Eocene of the northern escarpment of Al Jabal al Akhdar, NE Libya: Geology of Libya, Academic Press, London, p. 193-204.

Elwerfalli, A., Muftah, A., El Hawat, A., and Shelmani, M., 2000, A guidebook on the geology of Al Jabal al Akhdar, Cyrenaica, NE Libya: Earth Sciences Society of Libya (ESSL), Tripoli.

Embry III, A.F., and Klovan, J.E., 1971, A Late Devonian reef tract on northeastern Banks Island, NWT: Bulletin of Canadian Petroleum Geology, v. 19, p. 730-781.

Emiliani, C., 1955, Pleistocene temperatures: The Journal of Geology, p. 538-578.

Erbacher, J., D , Mosher, J., Bauldauf , and Malone, M., 2002, Equatorial Cretaceous and Paleogene paleoceanographic transect, western Atlantic: Ocean Drilling Program Scientific Prospectus No. 107.

Esteban, M., 1996, An overview of Miocene reefs from Mediterranean areas: general trends and facies models.

Fanton, K., and Holmden, C., 2007, Sea-level forcing of carbon isotope excursions in epeiric seas: implications for chemostratigraphy: Canadian Journal of Earth Sciences, v. 44, p. 807-818.

Floridia, G., B., 1935, Contributo alla conoszenza strtigrafica del Neogen della Cirenaica: Atti Soc. Ital. Sci. Natur,Milano, v. 75 ser. G, no.2, p. 1-24.

Flügel, E., 2004, Microfacies of carbonate rocks: analysis, interpretation and application, Springer Science & Business Media.

Flügel, E., 2010, Carbonate Depositional Environments, Microfacies of Carbonate

Rocks, Springer, p. 7-52.

Folk, R., Andrews, P.B., and Lewis, D., 1970, Detrital sedimentary rock classification and nomenclature for use in New Zealand: New Zealand journal of geology and geophysics, v. 13, p. 937-968.

Folk, R.L., 1965, Some aspects of recrystallization in ancient limestones.

Föllmi, K.B., Godet, A., Bodin, S., and Linder, P., 2006, Interactions between environmental change and shallow water carbonate buildup along the northern Tethyan margin and their impact on the Early Cretaceous carbon isotope record: Paleoceanography, v. 21.

Föllmi, K.B., Weissert, H., Bisping, M., and Funk, H., 1994, Phosphogenesis, carbon-isotope stratigraphy, and carbonate-platform evolution along the Lower Cretaceous northern Tethyan margin: Geological Society of America Bulletin, v. 106, p. 729-746.

Francis, M., and Issawi, B., 1977, Geologic map of Libya; 1: 250,000. Sheet: Soluq NH 34-2. Explanatory Booklet, Industrial Research Centre, Tripoli.

Franseen, E., K., Esteban, M., Ward, W., C. , and Rouchy, J.-M., 1996, Models for Carbonate Stratigraphy From Miocene Reef Complexes of Mediterranean Regions: SEPM (Society for Sedimentary Geology), Concepts in Sedimentology and Paleontology v. 5, p. 391.

Giammarino, S., 1984, Geological Map of Libya, scale 1:250,000, Sheet Wadi al Khali (NH 34-8), Explanatory Booklet: Industrial Research Centre, Tripoli.

Giglia, G., 1984, Geological Map of Libya, scale 1:250,000, Sheet Ajdabiya (NH 34-6), Explanatory Booklet: Industrial Research Centre, Tripoli.

Gregory, J.W., 1911, Contributions to the geology of Cyrenaica Quart: J.Geol.Sco. London, v. 67, p. 572-615.

Grossman, E.L., 2012, Applying oxygen isotope paleothermometry in deep time, Paleontological Society Papers, Volume 18, Paleontological Society, p. 39-67.

Grossman, E.L., Yancey, T.E., Jones, T.E., Bruckschen, P., Chuvashov, B., Mazzullo, S., and Mii, H.-s., 2008, Glaciation, aridification, and carbon sequestration in the

Permo-Carboniferous: the isotopic record from low latitudes: Palaeogeography, Palaeoclimatology, Palaeoecology, v. 268, p. 222-233.

Grotzinger, J., Fike, D., and Fischer, W., 2011, Enigmatic origin of the largest-known carbon isotope excursion in Earth's history: Nature Geoscience, v. 4: doi, v. 10, p. 285-292.

Grotzinger, J.P., Fike, D.A., and Fischer, W.W., 2011, Enigmatic origin of the largest-known carbon isotope excursion in Earth's history: Nature Geoscience, v. 4, p. 285-292.

Hajikazemi, E., Al-Aasm, I., and Coniglio, M., 2012, Chemostratigraphy of Cenomanian–Turonian carbonates of the Sarvak Formation, Southern Iran: Journal of Petroleum Geology, v. 35, p. 187-205.

Hajikazemi, E., Al-Aasm, I., and Coniglio, M., 2012, Chemostratigraphy of Cenomanian–Turonian carbonates of the Sarvak Formation, Southern Iran: Journal of Petroleum Geology, v. 35, p. 187-205.

Halfar, J., and Mutti, M., 2005, Global dominance of coralline red-algal facies: a response to Miocene oceanographic events: Geology, v. 33, p. 481-484.

Hallam, A., 1981, Relative importance of plate movements, eustasy, and climate in controlling major biogeographical changes since the early Mesozoic: Eds, Nelson, G,, Rosen, D, E ed (s). Vicariance biogeography. A critique. Columbia Univ. Press: New York, p. 303-30.

Hallett, D., 2002, Petroleum geology of Libya, Elsevier.

Halverson, G.P., Hoffman, P.F., Schrag, D.P., Maloof, A.C., and Rice, A.H.N., 2005, Toward a Neoproterozoic composite carbon-isotope record: Geological Society of America Bulletin, v. 117, p. 1181-1207.

Haq, B.U., Hardenbol, J., and Vail, P.R., 1987, Chronology of fluctuating sea levels since the Triassic: Science, v. 235, p. 1156-1167.

Harzhauser, M., and Piller, W.E., 2007, Benchmark data of a changing sea—palaeogeography, palaeobiogeography and events in the Central Paratethys during the Miocene: Palaeogeography, Palaeoclimatology, Palaeoecology, v.

253, p. 8-31.

Holmden, C., Creaser, R., Muehlenbachs, K., Leslie, S., and Bergström, S., 1998, Isotopic evidence for geochemical decoupling between ancient epeiric seas and bordering oceans: implications for secular curves: Geology, v. 26, p. 567-570.

Humbolt, A., and Ahr, W.M., 2008, Genetic Pore Typing as a Means of Characterizing Reservoir Flow Units: San Andres, Sunflower Field, Terry County, Texas, Texas A&M University.

Immenhauser, A., Della Porta, G., Kenter, J.A., and Bahamonde, J.R., 2003, An alternative model for positive shifts in shallow-marine carbonate δ13C and δ18O: Sedimentology, v. 50, p. 953-959.

Immenhauser, A., Kenter, J.A., Ganssen, G., Bahamonde, J.R., Van Vliet, A., and Saher, M.H., 2002, Origin and significance of isotope shifts in Pennsylvanian carbonates (Asturias, NW Spain): Journal of Sedimentary Research, v. 72, p. 82-94.

Ivanov, D., Ashraf, A., Mosbrugger, V., and Palamarev, E., 2002, Palynological evidence for Miocene climate change in the Forecarpathian Basin (central Paratethys, NW Bulgaria): Palaeogeography, Palaeoclimatology, Palaeoecology, v. 178, p. 19-37.

Jacobs, E., Weissert, H., Shields, G., and Stille, P., 1996, The Monterey event in the Mediterranean: A record from shelf sediments of Malta: Paleoceanography, v. 11, p. 717-728.

Jacobsen, S.B., and Kaufman, A.J., 1999, The Sr, C and O isotopic evolution of Neoproterozoic seawater: Chemical Geology, v. 161, p. 37-57.

Jahren, A.H., Arens, N.C., Sarmiento, G., Guerrero, J., and Amundson, R., 2001, Terrestrial record of methane hydrate dissociation in the Early Cretaceous: Geology, v. 29, p. 159-162.

Janson, X., Van Buchem, F., Dromart, G., Eichenseer, H., Dellamonica, X., Boichard, R., Bonnaffe, F., and Eberli, G., 2010, Architecture and facies differentiation within a Middle Miocene carbonate platform, Ermenek, Mut Basin, southern

Turkey: Geological Society, London, Special Publications, v. 329, p. 265-290.

Jenkyns, H.C., 1995, Carbon-isotope stratigraphy and paleoceanographic significance of the Lower Cretaceous shallow-water carbonates of Resolution Guyot, Mid-Pacific Mountains, Proceedings of the Ocean Drilling Program, Scientific Results, Volume 143, Ocean Drilling Program College Station, p. 99-104.

John, C.M., Mutti, M., and Adatte, T., 2003, Mixed carbonate-siliciclastic record on the North African margin (Malta)—coupling of weathering processes and mid Miocene climate: Geological Society of America Bulletin, v. 115, p. 217-229.

Kaufman, A.J., and Knoll, A.H., 1995, Neoproterozoic variations in the C-isotopic composition of seawater: stratigraphic and biogeochemical implications: Precambrian Research, v. 73, p. 27-49.

Kleinsmiede, W., and Van Den Berg, N., 1968, Surface geology of the Jabal al Akhdar, northern Cyrenaica, Libya, Geology and archaeology of northern Cyrenaica, Libya. Petrol. Explor. Soc. Libya. 10th Annual Field Conference, Tripoli, p. 115-123.

Klen, L., 1974, Geological Map of Libya, scale 1:250,000, Sheet: Benghazi (NI 34-14), Explanatory Booklet, Industrial Research Centre, Tripoli.

Kocsis, L., Vennemann, T., Fontignie, D., Baumgartner, C., Montanari, A., and Jelen, B., 2008, Oceanographic and climatic evolution of the Miocene Mediterranean deduced from Nd, Sr, C, and O isotope compositions of marine fossils and sediments: Paleoceanography, v. 23.

Kump, L.R., and Arthur, M.A., 1999, Interpreting carbon-isotope excursions: carbonates and organic matter: Chemical Geology, v. 161, p. 181-198.

Kürschner, W.M., Kvaček, Z., and Dilcher, D.L., 2008, The impact of Miocene atmospheric carbon dioxide fluctuations on climate and the evolution of terrestrial ecosystems: Proceedings of the National Academy of Sciences, v. 105, p. 449-453.

Lees, A., and Buller, A.T., 1972, Modern temperate-water and warm-water shelf carbonate sediments contrasted: Marine Geology, v. 13, p. M67-M73.

Lietz, J., and Schwarzbach, M., 1970, Neue Fundpunkte von marinem Tertiär auf der Atlantik-Insel Porto Santo (Madeira-Archipel): N. Jb. Geol. Paläont. Mh. H, v. 5, p. 271-282.

Lohmann, K.C., 1988, Geochemical patterns of meteoric diagenetic systems and their application to studies of paleokarst, Paleokarst, Springer, p. 58-80.

Manetti, P., 1984, Geological Map of Libya, scale 1:250,000,Sheet Al Mufawwaz (NH 35-5), Explanatory Booklet: Industrial Research Centre, Tripoli.

Marchetti, M., 1934, Note illustrative per un abbozzo di carta geologica della Cirenaica, Stamperia moderna.

Marchetti, M., 1938, Idrologia cirenaica; Bibl. Agr. Col., Ist. Agr. Ital., Firenze.

Marinelli, O., 1920, Sulla morfologia della Cirenaica: Riv. Geogr. Ital, v. 27, p. 69-86.

Marshall, J.D., 1992, Climatic and oceanographic isotopic signals from the carbonate rock record and their preservation: Geological magazine, v. 129, p. 143-160.

Martin, M., Starkie, S., Yanilmaz, E., Huffman, D., P., Gutteridge, P., COLES, G., EL-Arnauti, A., and Keegan, J., B., 2008, Sequence Stratigraphy of the Precambrian to Middle Miocene of NE Libya: Geology of East Libya, v. 1, p. 267-304.

Mazhar, A., and Issawi, B., 1977, Geological Map of Libya, scale 1:250,000, Sheet: Zawiyat Msus (NH 34-3), Explanatory Booklet: Industrial Research Centre, Tripoli.

Megerisi, M., and Mamgain, V., 1980, The Upper Cretaceous-Tertiary formations of northern Libya: a synthesis, Bulletin No. 12. Industrial Research Centre, Tripoli, p . 85.

Moore, T., Pisias, N., and Dunn, D., 1982, Carbonate time series of the Quaternary and late Miocene sediments in the Pacific Ocean: a spectral comparison: Marine Geology, v. 46, p. 217-233.

Mutti, M., 1999, Lower and Middle Miocene carbonate facies in the central Mediterranean: the impact of paleoceanography on sequence stratigraphy.

Mutti, M., Bernoulli, D., and Stille, P., 1997, Temperate carbonate platform drowning linked to Miocene oceanographic events: Maiella platform margin, Italy: Terra

Nova, v. 9, p. 122-125.

Mutti, M., Droxler, A.W., and Cunningham, A.D., 2005, Evolution of the Northern Nicaragua Rise during the Oligocene–Miocene: drowning by environmental factors: Sedimentary Geology, v. 175, p. 237-258.

Mutti, M., John, C.M., and Knoerich, A.C., 2006, Chemostratigraphy in Miocene heterozoan carbonate settings: applications, limitations and perspectives: Geological Society, London, Special Publications, v. 255, p. 307-322.

Orszag-Sperber, F., and Pilot, M., 1976, Grands traits du Néogène de Corse: Bulletin de la Société géologique de France, p. 1183-1187.

Panchuk, K.M., Holmden, C.E., and Leslie, S.A., 2006, Local controls on carbon cycling in the Ordovician midcontinent region of North America, with implications for carbon isotope secular curves: Journal of Sedimentary Research, v. 76, p. 200-211.

Patterson, W.P., and Walter, L.M., 1994, Depletion of 13C in seawater ΣC02 on modern carbonate platforms: Significance for the carbon isotopic record of carbonates: Geology, v. 22, p. 885-888.

Patterson, W.P., and Walter, L.M., 1994, Depletion of 13C in seawater ΣC02 on modern carbonate platforms: Significance for the carbon isotopic record of carbonates: Geology, v. 22, p. 885-888.

Permanyer, A., and Esteban, M., 1973, El arrecife mioceno de Sant Pau d'Ordal (provincia de Barcelona): Revista del Instituto de Investigaciones Geológicas, v. 28, p. 45-72.

Pietersz, C.R., 1968, Proposed nomenclature for rock units in Northern Cyrenaica: Geology and Archeology of Northern Cyrenaica, Libya, p. 125-130.

Piller, W.E., Harzhauser, M., and Mandic, O., 2007, Miocene Central Paratethys stratigraphy—current status and future directions: Stratigraphy, v. 4, p. 71-88.

Pitman, W.C., and Talwani, M., 1972, Sea-floor spreading in the North Atlantic: Geological Society of America Bulletin, v. 83, p. 619-646.

Potter, P.E., and Szatmari, P., 2009, Global Miocene tectonics and the modern world:

Earth-Science Reviews, v. 96, p. 279-295.

Purser, B.H., 1996, Miocene reefs of the northwest Red Sea.

Randazzo, A.F., and Zachos, L.G., 1983/1984, Classification and description of dolomitic fabrics of rocks from the Floridan aquifer, USA: Sedimentary Geology, v. 37, p. 151-162.

Read, J.F., 1985, Carbonate platform facies models: AAPG bulletin, v. 69, p. 1-21.

Reuter, M., Piller, W.E., Brandano, M., and Harzhauser, M., 2013, Correlating Mediterranean shallow water deposits with global Oligocene–Miocene stratigraphy and oceanic events: Global and Planetary Change, v. 111, p. 226-236.

Rögl, F., Steininger, F., and Müller, C., 1978, Middle Miocene salinity crisis and paleogeography of the Paratethys (Middle and Eastern Europe): Initial Reports of the Deep Sea Drilling Project, v. 42, p. 985-90.

Rohlich, P., 1974, Geological Map of Libya, scale 1:250,000, Sheet: Al Bayda (NI 34-15), Explanatory Booklet: Industrial Research Centre, Tripoli, p. 70.

Röhlich, P., 1978, Geological development of Jabal al Akhdar, Libya: Geologische Rundschau, v. 67, p. 401-412.

Röhlich, P., 1980, Tectonic development of Jabal al Akhdar: The geology of Libya, v. 3, p. 923-931.

Rouchy, J., 1982b, La crise évaporitique messinienne de Méditerranée: nouvelles propositions pour une interprétation génétique: Bulletin du Museum National d'Histoire Naturelle, Paris (France). pp: 107, v. 136.

Rouchy, J.-M., 1982a, La genèse des évaPorites messiniennes de Méditerranée, Memoires du Museum National d'Histoire Naturelle, v. 50, 267 p, p. .

Sánchez-Almazo, I.M., Spiro, B., Braga, J.C., and Martín, J.M., 2001, Constraints of stable isotope signatures on the depositional palaeoenvironments of upper Miocene reef and temperate carbonates in the Sorbas Basin, SE Spain: Palaeogeography, Palaeoclimatology, Palaeoecology, v. 175, p. 153-172.

Schlager, W., 2005, Carbonate sedimentology and sequence stratigraphy, SEPM Soc for

Sed Geology.

Scholle, P.A., Bebout, D.G., and Moore, C.H., 1983, Carbonate Depositional Environments: AAPG Memoir 33, Aapg.

Scholle, P.A., and Ulmer-Scholle, D.S., 2003, A Color Guide to the Petrography of Carbonate Rocks: Grains, Textures, Porosity, Diagenesis, AAPG Memoir 77, AAPG.

Scott, R., and Govean, F., 1985, Early depositional history of a rift basin: Miocene in western Sinai: Palaeogeography, Palaeoclimatology, Palaeoecology, v. 52, p. 143-158.

Selley, R.C., 1968, Facies profile and other new methods of graphic data presentation: application in a quantitative study of Libyan Tertiary shoreline deposits: Journal of Sedimentary Research, v. 38.

Selley, R.C., 1996, Ancient sedimentary environments and their sub-surface diagnosis, Psychology Press.

Shackleton, N.J., and Opdyke, N.D., 1973, Oxygen isotope and palaeomagnetic stratigraphy of equatorial Pacific core V28-238: Oxygen isotope temperatures and ice volumes on a 10 5 year and 10 6 year scale: Quaternary research, v. 3, p. 39-55.

Shinn, E.A., 1983, Tidal flat environment, Carbonate depositional environments, Volume 33, p. 171-210.

Sibley, D.F., and Gregg, J.M., 1987, Classification of dolomite rock textures: Journal of Sedimentary Research, v. 57.

Silvestri, A., 1928, Di alcune facies litho-paleontologiche del Terziario di Derna, nella Cirenaica: Bolletino Società Geologica Italiana, v. 37, p. 109-113.

Simms, M.J., and Ruffell, A.H., 1990, Climatic and biotic change in the Late Triassic: Journal of the Geological Society, v. 147, p. 321-327.

Stefanini, G., 1923, Struttura geologica della Cirenaica e cenni descrittivi a corredo dello schizzo geologico dimostrativo della Cirenaica: La Cirenaica geografica economica, politica, p. 1-18.

Stefanini, G., 1935, Notizie generali sulla constituzione fisica della Grenaica: Soc. Geol. Ital., Boll., fasc. 1, Steffey, R. L., 1934, Stratigraphy., v. 54, p. 39-49.

Stoll, H.M., and Schrag, D.P., 2000, High-resolution stable isotope records from the Upper Cretaceous rocks of Italy and Spain: Glacial episodes in a greenhouse planet?: Geological Society of America Bulletin, v. 112, p. 308-319.

Swart, P.K., 2008, Global synchronous changes in the carbon isotopic composition of carbonate sediments unrelated to changes in the global carbon cycle: Proceedings of the National Academy of Sciences, v. 105, p. 13741-13745.

Swart, P.K., and Eberli, G., 2005, The nature of the δ 13 C of periplatform sediments: implications for stratigraphy and the global carbon cycle: Sedimentary Geology, v. 175, p. 115-129.

Swart, P.K., Reijmer, J., and Otto, R., 2009, A reevaluation of facies on Great Bahama Bank II: Variations in the δ13C, δ18O and mineralogy of surface sediments: Perspectives in Carbonate Geology: A Tribute to the Career of Robert Nathan Ginsburg, International Association of Sedimentologists Special Publication, p. 47-59.

Swedan, A., and Issawi, B., 1977, Geological Map of Libya, scale 1:250,000, Sheet: Bir Hacheim (NH 34-4), Explanatory Booklet: Industrial Research Centre, Tripoli.

Taylor, J.M., 1950, Pore-space reduction in sandstones: AAPG bulletin, v. 34, p. 701-716.

Thomas, E., 1986c, Deep sea benthic foraminifera in the Pacific lower to middle Miocene, in International Conference on Paleoceanography, 2nd, September 1986, Abstracts with Program: Woods Hole, Massachusetts, Woods Hole Oceanographic Institution, p. 40.

Thomas, E., and Vincent, E., 1987, Major changes in benthic foraminifera in the equatorial Pacific before the middle Miocene polar cooling: Geology, v. 15, p. 1035-1039.

Tonietto, S., N., and Pope, M., C., 2013, Diagenetic evolution and its ifnfluence on the Petrophysicsal properties of the Jurassic Smackover Formation thrombolite and

grainstone units of Little Cedar Creek Field, Alabama: GCAGS Journal, v. 2, p. 68-84.

Tucker, M., C., 1998, Sedimentary Rocks in the Field, Biddle Ltd, Guildford and King's Lynn, Manchester. 2nd edit, p. 153.

Tucker, M.E., 1988, Techniques in sedimentology, Blackwell Scientific Publications. p 394.

Tucker, M.E., 1996, Sedimentary petrology: an introduction to the origin of sedimentary rocks, BLACKWELL SCIENCE, 260 p.

Tucker, M.E., 2003, Sedimentary rocks in the field, John Wiley & Sons.

Tucker, M.E., 2009, Sedimentary petrology: an introduction to the origin of sedimentary rocks, John Wiley & Sons.

Veizer, J., 1983, Chemical diagenesis of carbonates: theory and application of trace element technique.

Veizer, J., 1983, Chemical diagenesis of carbonates: theory and application of trace element technique.

Veizer, J., Ala, D., Azmy, K., Bruckschen, P., Buhl, D., Bruhn, F., Carden, G.A., Diener, A., Ebneth, S., and Godderis, Y., 1999, 87Sr/86Sr, δ13C and δ18O evolution of Phanerozoic seawater: Chemical Geology, v. 161, p. 59-88.

Veizer, J., Ala, D., Azmy, K., Bruckschen, P., Buhl, D., Bruhn, F., Carden, G.A., Diener, A., Ebneth, S., and Godderis, Y., 1999, 87Sr/86Sr, δ13C and δ18O evolution of Phanerozoic seawater: Chemical Geology, v. 161, p. 59-88.

Vincent, E., and Berger, W.H., 1985, Carbon dioxide and polar cooling in the Miocene: The Monterey hypothesis: The Carbon Cycle and Atmospheric CO: Natural Variations Archean to Present, p. 455-468.

Vincent, E., Killingley, J.S., and Berger, W.H., 1985, Miocene oxygen and carbon isotope stratigraphy of the tropical Indian Ocean: Geological Society of America Memoirs, v. 163, p. 103-130.

Vincent, E., Shackleton, N., and Hall, M., 1991, Miocene oxygen and carbon isotope stratigraphy of planktonic foraminifers at Sites 709 and 758, Tropical Indian

Ocean, Proc. Ocean Drilling Program, Scientific Results, Volume 121, p. 241-252.

Weber, L.J., 1995, Sequence stratigraphy and reservoir delineation of the Middle Pennsylvanian (Desmoinesian), Paradox basin and Aneth field, southwestern USA.

Weissert, H., and Lini, A., 1991, Ice age interludes during the time of Cretaceous greenhouse climate: Controversies in modern geology, p. 173-191.

Weissert, H., Lini, A., Föllmi, K.B., and Kuhn, O., 1998, Correlation of Early Cretaceous carbon isotope stratigraphy and platform drowning events: a possible link?: Palaeogeography, Palaeoclimatology, Palaeoecology, v. 137, p. 189-203.

Xiong, B., and Heckel, P.H., 1996, Cementation patterns and diagenesis in the Stanton Limestone/cyclothem (Missourian, Upper Pennsylvanian) in the northern Midcontinent: Special Papers-Geological Society of America, p. 373-388.

Zachos, J., Pagani, M., Sloan, L., Thomas, E., and Billups, K., 2001, Trends, rhythms, and aberrations in global climate 65 Ma to present: Science, v. 292, p. 686-693.

Zert, B., 1974, Geological Map of Libya, scale 1:250,000, Sheet Darnah (NI 34-16), Explanatory Booklet: Industrial Research Centre, Tripoli.

Ziegler, P.A., 1988, Evolution of the Arctic-North Atlantic and the Western Tethys-- A visual presentation of a series of Paleogeographic-Paleotectonic Maps*: American Association of Petroleum Geologists Memoir, v. 43, p. 164-196.

APPENDIX